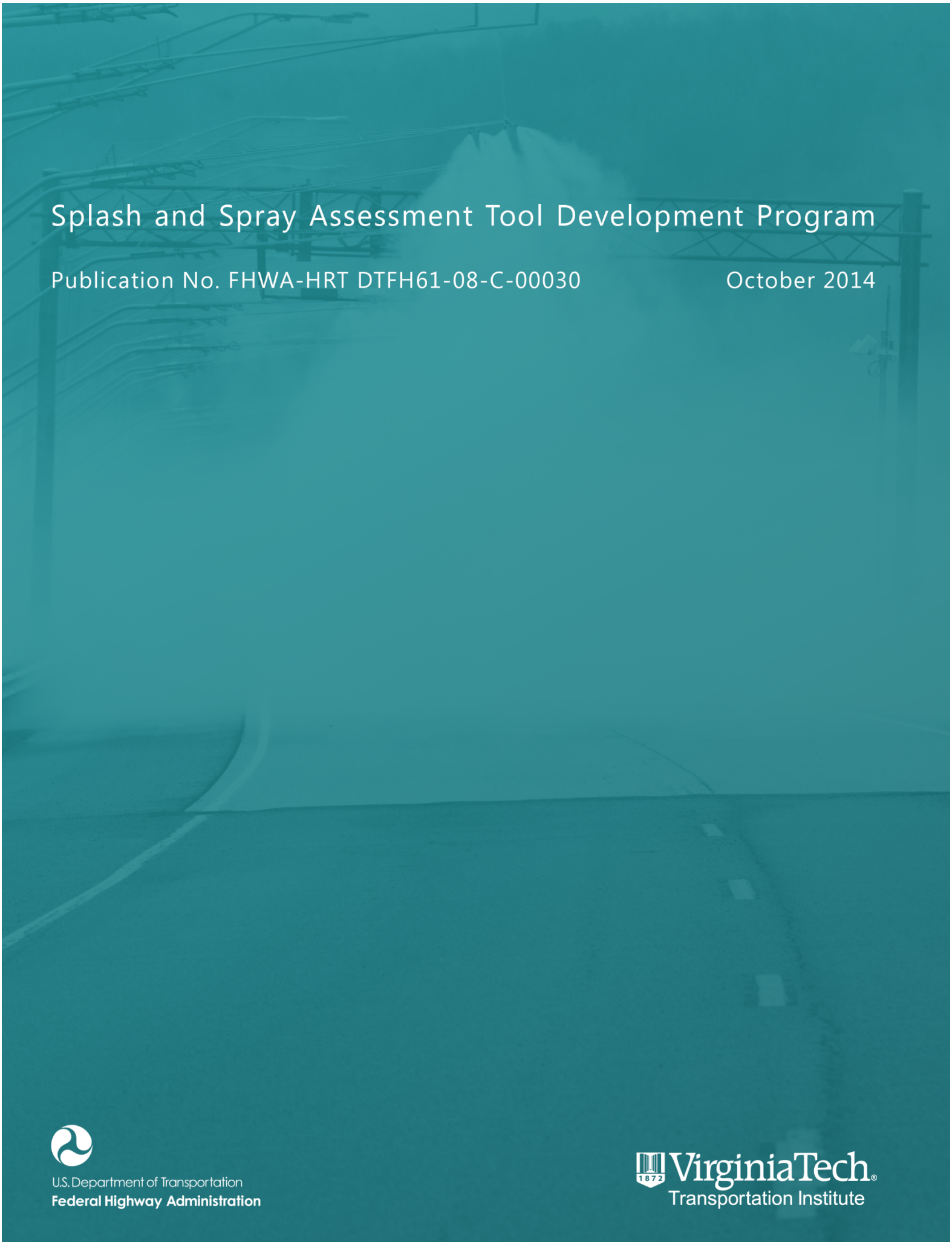

Splash and Spray Assessment Tool Development Program

Publication No. FHWA-HRT DTFH61-08-C-00030 October 2014

U.S. Department of Transportation
Federal Highway Administration

Virginia Tech
Transportation Institute

Splash and Spray Assessment Tool Development Program

Final Report – Revised Draft

DTFH61-08-C-00030

Submitted to FHWA for Review and Comment

Prepared by:

Gerardo W. Flintsch, Lijie Tang, Samer Katicha and Edgar de Leon, Center for Sustainable Transportation Infrastructure, Virginia Tech Transportation Institute.

Helen Viner, Alan Dunford, Kamal Nesnas, Fiona Coyle and Peter Sanders, TRL Ltd.

Ronal Gibbons and Brian Williams, Center for Infrastructure-based Safety Systems, Virginia Tech Transportation Institute.

David Hargreaves and Tony Parry, Nottingham Transportation Engineering Center, University of Nottingham.

Kevin McGhee, Virginia Center for Transportation Innovation and Research.

Roger M. Larson and Kelly Smith, Applied Pavement Technology, Inc.

October 2014

Table of Contents

List of Figures

List of Tables

Executive Summary

The effects of vehicle splash and spray are well known to motorists who have driven in wet weather conditions. Research suggests that splash and spray contribute to a small but measureable portion of road traffic accidents and are the source of considerable nuisance to motorists. Splash and spray from highway pavements also can carry a number of pollutants and contaminants. When deposited, these contaminants can be poisonous to plant life and accelerate the corrosion of roadway appurtenances.

Project Overview

The report describes the development of an assessment tool to characterize the propensity of highway sections to generate splash and spray during rainfall and the impact of splash and spray on road users. The project accomplished the following specific objectives:

1. Evaluation of prior work in the area of splash and spray mechanisms.
2. Development of a model to predict water film thickness and splash and spray occurrence on pavement surfaces that encompasses an appropriate range of conditions.
3. Evaluation of the impact of splash and spray on roadway users.
4. Validation and refinement of the developed model.
5. Documentation of the development efforts and preparation of technology transfer materials.

The project started with a review of prior work in the area of splash and spray mechanisms. It then developed the three sub-modules that compose the splash and spray assessment model:

1. A water film thickness model that predicts the water film thickness on pavement surfaces based on pavement surface properties and rain intensity.
2. An exposure model that estimates the amount of water that is going to be projected by the tire given the water film thickness, pavement characteristics, and vehicle speed.
3. A splash and spray model that predicts pavement surfaces' propensity for splash and spray occurrence based on the other two models.

Field tests under controlled rainfall conditions were conducted to assess the impact of different levels of splash and spray on user comfort and perceived safety. Based on the results of these tests, a new method of measuring splash and spray, by computing an *occlusion factor*, was proposed. The occlusion calculation measures the loss of visibility because of splash and spray and links it with various user perceptions. The models were implemented in simple prototype tools and validated through a series of additional field experiments and a pilot implementation using existing data. These experiments confirmed that the developed splash and spray assessment model was practical and can be used to support highway engineers' decisions regarding highway design and maintenance.

Main Findings

A review of available literature showed that there has been a considerable amount of research into the problem of splash and spray, but results have often been inconclusive and contradictory. This literature review allowed us to identify the main factors that affect splash and spray: water film thickness, vehicle speed, tire geometry, tire tread depth, vehicle aerodynamics, and vehicle spray suppression devices. It also showed that though several techniques have been used to measure splash and spray, there has been no commonly accepted and readily available method for routine measurement.

Laboratory fume experiments were used in the project to define a calibrated formula for computing the water film thickness as a function the texture of the surface, the length of the drainage path, the intensity

of the rainfall, and the slope of the drainage path. This formula showed that the water film thickness is higher with lower slopes and smoother surfaces, and, as expected, increases with longer drainage paths and rainfall intensities.

Nationwide rainfall data available from the National Climate Data Center (NCDC) was used to create an inventory of the expected percentage of time that the precipitation intensity will exceed different precipitation thresholds. Exposure distribution for all counties in the continental United States were developed to estimate the levels of user exposure thought the country.

Field tests were conducted under controlled precipitation conditions to assess the impact of splash and spray on road users. A large checkerboard was mounted on the rear of a lead vehicle that generated splash and spray. A camera mounted on a following vehicle captured the mean luminance of the checkerboard's black squares and the mean luminance of the white squares. The ratio of the mean luminance of the black and white squares defined a new measure of splash and spray: the occlusion factor. The experiment was also used to select the critical conditions to use for the modeling efforts and showed that the occlusion factor correlated well with the five subjective user perception variables studied (obstruction, concentration, risk, confidence, and control) and therefore can be used as a measure of nuisance from splash and spray.

The four prevailing splash and spray mechanisms identified in the literature—bow wave, side wave, tread pickup, and capillary adhesion—were modeled for different vehicle speeds and water film thicknesses by using a computational fluid dynamic (CFD) model of splash/spray generation. The most critical combination of maneuver and vehicle identified in the field experiments was simulated in a virtual wind tunnel. The outcomes of the various simulation runs were synthesized in a set of simple equations that model the mechanisms and combined into a simple equation to model pavement splash and spray. These were used to develop simple prototype tools to illustrate the practicality and ease of implementation of the developed approach. Pilot applications of the models showed that the values produced by the model approximately follow the trends observed in the field and that the approach can be easily implemented using available pavement surface data.

The Splash and Spray Assessment Model

The main product of this study is a model that can be used to predict splash and spray based on pavement surface characteristics and climatic conditions. The model can provide useful information for supporting highway design and maintenance business processes. The following steps summarize the process for calculating the amount of splash and spray according to the developed assessment tool:

1. Compute the water film thickness based on the rainfall intensity and pavement surface properties.
2. Compute the maximum amount of water available for splash and spray based on the computed water film thickness.
3. Compute the contribution of each splash and spray mechanism.
4. Compute the spray density corresponding to each mechanism based on the corresponding mass flow and the speed of the truck.
5. Compute the total spray density.
6. Convert the spray density level to a subjective nuisance index.

1 Background, Objective, and Scope

The effects of vehicle splash and spray are well known to motorists who have driven in wet weather conditions. Research suggests that splash and spray contribute to a small but measureable portion of road traffic accidents and are the source of considerable nuisance to motorists. Splash and spray from highway pavements also can carry a number of pollutants and contaminants. When deposited, these contaminants can be poisonous to plant life and accelerate the corrosion of roadway appurtenances.

Splash and spray are individually definable processes that are the product of a number of different factors. Many parties have gone to great lengths to reduce the splash and spray created by motor vehicles, especially that from heavy vehicles, by retrofitting devices that alter the vehicle's aerodynamics. Another possible solution to the problem is to change the characteristics of the highway pavement. Previous research shows that pavement geometry, drainage, texture, and porosity all contribute to splash and spray generation, but the exact mechanisms are largely unknown. A model capable of predicting the splash and spray propensity of pavements can be used by highway engineers to support decisions in highway maintenance and design.

1.1 Project Objective

The project objective was to develop a simple and practical assessment tool to characterize the propensity of highway sections to generate splash and spray during rainfall and the impact of splash and spray on road users. The project accomplished the following specific objectives:

1. Evaluation of prior work in the area of splash and spray mechanisms.
2. Development of a model to predict water film thickness and splash and spray occurrence on pavement surfaces, encompassing an appropriate range of conditions.
3. Evaluation of the impact of splash and spray on roadway users.
4. Validation and refinement of the developed model.
5. Documentation of the development efforts and preparation of technology transfer materials.

The developed model for predicting the propensity of pavements to produce splash and spray is a useful tool that can inform highway engineers' decisions regarding highway design and maintenance.

1.2 Scope

This report summarizes the development of the splash and spray model and its implementation in an easy-to-use, practical tool. The modeling of the pavements' splash and spray potential was broken down into the following steps:

1. Determining the water film thickness given the pavement characteristics and rainfall rate (Chapter 3 of this report).
2. Estimating the amount of water available for projection by the tire, given the water film thickness, pavement characteristics, and vehicle speed (Chapter 0 of this report).
3. Determining the user exposure to splash and spray by predicting the likelihood of a specified amount of spray being generated, given local meteorological conditions and the propensity of the pavement to generate splash and spray (Chapter 6 of this report).
4. Evaluating the impact of the splash and spray on user perception (Chapter 5 of this report).
5. Validating the models though field testing and pilot implementations (Chapter 7 of this report).

1.3 Report Overview

Chapter 1 introduces the objectives and scope of the project and outlines the structure of the report.

Chapter 2 reviews available literature. The review included models to determine the water film thickness, factors that impact splash and spray propensity, splash and spray measurement techniques, and gaps in the knowledge base.

Chapter 3 covers the methodology and results from laboratory-based experiments to develop the water film thickness model that was used to determine the volume of water present for splash/spray formation. It describes the experiments conducted on a flume and the statistical analysis conducted to develop a generic model, which considers surface drainage length and slope, pavement texture, and rainfall intensity.

Chapter 4 focuses on the determination of the rainfall expected for the location of the roadway section under consideration. It presents the development of an exposure model that is relevant for the prediction of splash and spray potential. The model computes the wet exposure as the percentage of a year that pavement receives a specified minimum amount of rainfall, using precipitation data for the entire United States (2000-2009) extracted from the National Climate Data Center (NCDC).

Chapter 5 describes the methodology and results from a set of field tests that assessed the impact of splash and spray on road users. The analysis of the results provided the essential links between the experimental data, the splash and spray model, and threshold values for the classification of model output. This information was used to quantify user responses (subjective ratings) to a range of different controlled conditions at the Virginia Smart Road.

Chapter 6 covers the final stages of development, which combined outcomes from the lab and field experiments with computational fluid dynamic (CFD) modeling of mechanisms of splash/spray generation to develop a simple and practical model to predict splash and spray based on surface properties (slope and texture), pavement drainage properties, and rainfall intensity or geographical location. It summarizes the CFD modeling techniques used and amalgamates the results to propose tools that can be used by highway engineers.

Chapter 7 presents a second set of field experiments conducted under controlled condition at the Virginia Smart Road to validate the splash/spray model, summarizes the results, and illustrates the application of the model using field data collected on an actual road segment.

Chapter 8 summarizes the overall research effort and highlights the main findings and conclusions of the study.

2 Literature Review[1]

Attempts have been made to reduce the amount of splash and spray generated by vehicles, but results on their effectiveness differ. Some researchers report a 60 percent improvement in visibility when using a spray suppression device on vehicles, but others testing similar devices report no significant improvement.

Another possible solution to the problem of splash and spray is to change the characteristics of the highway surface. Previous research shows that pavement geometry, drainage, texture, and porosity contribute to splash and spray. An unknown, however, is how each of these factors contributes to a pavement's splash and spray propensity. This chapter describes results of the literature review conducted to assess both the state of the art and the scope for the development of splash and spray modeling technology, described later in the report.

The modeling of the pavements' splash and spray potential can be broken down into three components:

1. Determining the water film thickness given the pavement characteristics and rainfall rate.
2. Estimating the amount of water available to be projected by the tire given the water film thickness, pavement characteristics, and vehicle speed.
3. Determining the user exposure to splash and spray by predicting the likelihood of a specified amount of spray being generated given local meteorological conditions and the propensity of the pavement to generate splash and spray.

In addition, the model may include threshold criteria to classify the impact of splash and spray on highway users.

2.1 Splash and Spray Mechanisms

The generation of splash and spray is an extremely complex process and is dependent upon a number of independent variables. The terms "splash" and "spray" refer to two separate processes. The definitions of splash and spray are usually given as a function of the droplet sizes produced or by the process by which they are created. Pilkington (1990) defines them as follows:

- **Splash** as "the mechanical action of a vehicle's tire forcing water out of its path. Splash is generally defined as water drops greater than 1.0 mm (0.04 inches) in diameter, which follow a ballistic path away from the tire."
- **Spray** as being formed "when water droplets, generally less that 0.5 mm (0.02 inches) in diameter and suspended in the air, are formed after water has impacted a smooth surface and been atomized."

Though splash and spray are separate processes, they are often referred to collectively because of the difficulty of monitoring and measuring them individually.

When traveling at high speeds on wet roads, the tires of a truck can displace many gallons of water per second by four well-established primary mechanisms: bow splash waves, side splash waves, tread pickup, and capillary adhesion (Weir et al., 1978). These mechanisms are illustrated in Figure 1.

1 This chapter is an updated version of the *First Interim Report: Revised Synthesis Report, Splash and Spray Assessment Tool Development Program*, prepared by P.D. Sanders, A. Dunford, and H. Viner, TRL Ltd.; G.W. Flintsch, Center for Sustainable Transportation Infrastructure, VTTI; and R.M. Larson, Applied Pavement Technology, Inc.

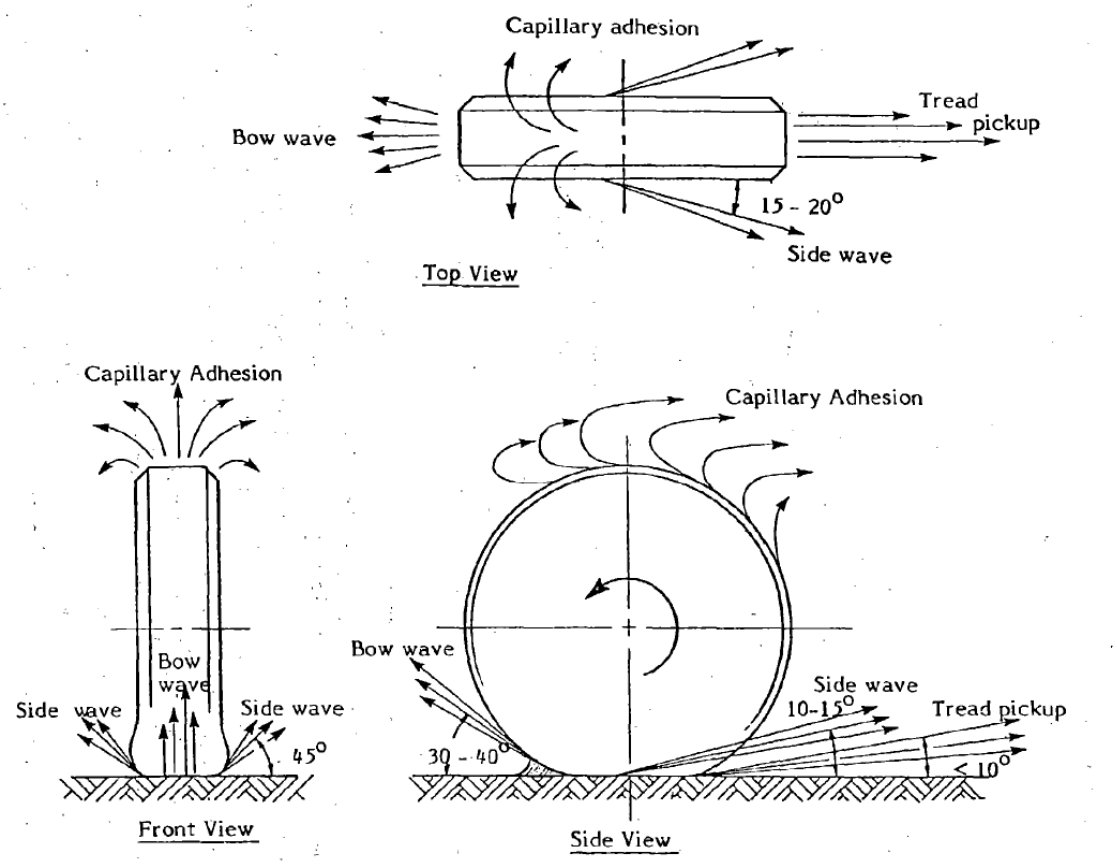

Figure 1. Diagram. Mechanisms of splash and spray (Weir et al., 1978).

The bow and side waves consist of relatively large drops (splash). Water passing through the tire tread grooves is either thrown up into the air immediately behind the wheel as tread pickup or is retained on the tire surface as a thin capillary film. Tread pickup shatters into smaller droplets (spray) through interaction with the turbulent airflow or by impacts with following tires or other parts of the vehicle structure. Water held in the capillary film creates additional spray as it is stripped off near the top of the tire by the incoming airflow.

To better understand the mechanisms, a tool designed to create spray under controlled conditions was devised by McCallen et al. (2005). Water was injected onto the interface of two counter-rotating tires (one smooth and one with a circumferential groove). The water would then be ejected from the interface and form spray. High-speed image capture was used to analyze the interaction. The study examined the tread pickup source, and results are summarized below:

1. Just beyond the tire contact patch, water completely fills the tire groove (depending on the necessary amount of free water available).
2. Slightly further downstream, the tires separate and are subjected to high accelerations. Some of the water remains within the tire grooves, and some is ejected from the interface as a water jet.
3. Further downstream, but within the tire extremities, some water still remains in the grooves, and the ejected jet is more clearly defined. The water remaining in the tire grooves is connected to the central jet by a thin web of water.
4. As the distance between the tires increases, the connecting web continually thins until reaching a breaking point, where water droplets are produced.

The amount of water thrown up depends on the presence and amount of water available on the road surface, the vehicle type and design, the tires fitted, the speed, and the nature of the road surface. These factors will be discussed in the following sections of this chapter.

2.2 Water Film Thickness

The greater the depth of water, the greater the amount of water there is available to be displaced by a vehicle's tires. There is no consensus of opinion in the literature about exact relationships between water film thickness and splash/spray, but there is evidence that it is an important consideration (e.g., Koppa et al., 1985), and this will be discussed in more detail in Section 2.3.1. Furthermore, the literature suggests that water film thickness is heavily dependent on rainfall intensity, pavement geometry, texture, porosity, and drainage. If the splash/spray assessment tool is to be useful during the design of highways, then the effect of these factors must be taken into account. Many models for calculating the water film thickness of road pavements currently exist, each with differing levels of complexity and, presumably, accuracy.

2.2.1 Pavement Geometry

Pavement geometry dictates the length and gradient of the flow path that water has to take before being removed from the pavement. The geometry is introduced into the pavement as a function of longitudinal gradient and pavement cross slope. These geometric features are an important aspect of highway design, and guidelines are published for minimum values. For example, in the United Kingdom, the Design Manual for Roads and Bridges (1999) specifies a minimum cross slope of 2.5 percent. In the United States, the AASHTO "Green Book" recommends a range of cross slope between 1.5 percent and 2 percent for high-type roads, but it indicates that a slope of 2.5 percent may be needed in areas of intense rainfall. It also recommends slopes of 2 percent to 6 percent for low-type surfaces (AASHTO 2004). A geometric function of longitudinal gradient, cross slope, and pavement width produces a drainage length as given in Equation 1:

$$L_f = \frac{LS_3}{S_1} \tag{1}$$

$$S_3 = \sqrt{S_1^2 + S_2^2} \tag{2}$$

where:

S_1 = cross slope gradient
S_2 = longitudinal gradient
S_3 = drainage path gradient
L = width of pavement
L_f = length of drainage path

Anderson (1995) indicated that L_f is the distance that water has to travel before it leaves the pavement. One of the simplest equations relating water film thickness to drainage length, rainfall intensity, and the slope of the drainage length was proposed by Ross and Russam (1968):

$$d = 0.015(L \times I)^{1/2} N^{1/5} \tag{3}$$

where:
d = water film thickness (cm)
L = drainage length (m)

I = rainfall intensity (cm/h)
1/N = slope of drainage length

This relationship shows that the water film thickness increases if the drainage length increases and decreases if the gradient of the drainage path increases.

Since that research was conducted, a number of other researchers, including Gallaway et al. (1971), Huebner et al. (1997), Roe et al. (1997), and Resendez et al. (2007), have attempted to calculate water film thickness from pavement geometry. However, research by Pruyost and Gothie (1998), which examined nine different models for predicting water film thickness, suggests that accurately calculating water film thickness may require a larger number of variables to be considered, in particular a variable for pavement surface texture. The various equations postulated here and those in the following paragraphs are analyzed together in Chapter 3 to identify common mechanisms and propose a generic water film thickness model.

Furthermore, pavement deterioration, such as rutting in hot-mix asphalt (HMA)-surfaced pavements and studded tire wear in Portland cement concrete (PCC) pavements, may contribute to longer drainage paths and higher water film thickness; however, the model does not explicitly consider these parameters.

2.2.2 Pavement Texture and Manning's Coefficient

Pavement texture provides a capacity for water to be held below the surface of the pavement and provides drainage for this water between the aggregate chippings of the road surface. Moore (1970) described a device called an "outflow meter" that was capable of measuring the capacity for pavement texture to aid in drainage. A commercial version of this device is the Hydrotimer.[2] In addition to contributing to drainage, the texture of the pavement is also likely to contribute to the turbulence of the flow of water on its surface.

Roe et al. (1997) and Gallaway et al. (1971) devised similar equations to calculate water film thicknesss, using drainage length, slope, rainfall intensity, and pavement texture. In these models, the texture variable was subtracted from the overall water film thickness to give the "free water film thickness." Roe et al. observed a difference between measured and predicted values when validating their model, and it was considered that this was due to the hydraulic roughness having an increased effect on the flow of the water and therefore increasing the water film thickness.

Anderson et al. (1998) provided details of models to predict water film thickness as part of the PAVDRN software used to predict the hydroplaning speed of highways. The models used as part of PAVDRN were based on the kinematic wave equation and include the Manning's roughness coefficient as a variable.

This equation is reproduced as Equation 4.

$$WFT = \left(\frac{n \times L \times i}{36.1 \times S^{0.5}} \right)^{0.6} - MTD \tag{4}$$

where:
WFT = water film thickness (in)
n = Manning's roughness coefficient
L = Drainage path length (in)
i = Rainfall rate (in/h)
S = Slope of drainage path (in/in)

[2] http://hydrotimer.com/ (accessed 06/09)

MTD = mean texture depth (inches)

In this equation, the Manning's coefficient is considered an inhibitor to water flow, and greater inhibition increases water film thickness. The coefficient is a measure of gravity-driven surface free-flow, and it can be empirically derived from several factors, including surface roughness. The common use of different surface materials means that specific equations can be written for different surface types. Anderson et al. (1998) describe the experimental procedure used for the calculation of the Manning's coefficients for PCC, dense-graded asphalt, and porous asphalt surfaces, as used in the PAVDRN software.

2.2.3 Pavement Porosity

In dense-graded pavement surfaces, pavement porosity is very low and can be considered negligible when calculating water film thicknesses. However, porous asphalt pavements contain a much higher percentage of air voids within the pavement structure. Because of this, porous asphalt pavements can aid in the removal of surface water by draining water through the pavement.

Researchers tend to agree that the use of porous pavements can reduce the amount of spray generated by a road surface. For example, Button et al. (2004) stated that "PA (porous asphalt) pavements are the most effective products on the market for addressing S&S (splash and spray)." Daines (1992) conducted experiments to relate the hydraulic conductivity to spray generation on porous asphalt surfaces on a highway in the United Kingdom. Daines found that the hydraulic conductivity of the pavement tested substantially reduced the water film thickness and the spray propagation of the pavement. "Measurements of spray levels on new porous asphalt show almost no spray raised at speeds up to 110km/h (70mph) even in heavy rainfall." Daines developed the following equation that gave the average percentage of spray reduction when compared with hot rolled asphalt (i.e., dense-graded asphalt):

$$S = 270(HC) + 25(SP) \tag{5}$$

where:
S = average percentage spray reduction when compared with hot rolled asphalt
HC = relative hydraulic conductivity
SP = sand-patch texture depth

The properties of porous asphalt pavements were also observed by Anderson et al. (1998). Anderson's team amended their water film thickness equation, Equation 4, to include these effects. The amended equation is shown in Equation 6.

$$WFT = \left(\frac{n \times L \times I}{36.1 \times S^{0.5}} \right)^{0.6} - MTD \tag{6}$$

where the rainfall rate, I, has been replaced by
I = Excess rainfall rate (in/h) = rainfall rate – infiltration rate/permeability of pavement

Pavement porosity can have some negative effects, however. Several researchers (Anderson et al., 1998, Daines, 1992, and Button et al., 2004) have found that the high void content of these pavements speeds ice development on the surface as compared to traditional materials. There are also concerns regarding the durability of the porous mixtures. Problems such as delamination from the underlying layers, higher rates of deformation, and raveling have been reported.

2.2.4 Pavement Drainage

Another way to remove surface water is through the use of pavement drainage systems. Drainage removes surface water in a controlled manner and can be used to reduce the drainage length of a pavement. Button et al. (2004) showed how the use of longitudinally installed drainage systems placed between lanes can reduce the drainage length of a pavement.

For a drainage system to be effective, its capacity must exceed the demand placed on it. In the United Kingdom, the Design Manual for Roads and Bridges (2000) defines the design capacities of curb stormwater inlets and manhole covers using the following equations:

Flow collection efficiency of manhole covers,

$$\eta = 100 - G_d\left(Q/H\right) \tag{7}$$

Flow collection efficiency of curb inlets,

$$\eta = 100 - \frac{36.1Q}{L_i H^{1.5}} \tag{8}$$

where:
η = flow collection efficiency (percent)
G_d = grating parameter defined by the type of grating (specified in the manual)
Q = flow rate (m^3/s)
H = water film thickness against the curb (mm)
L_i = length of the opening in the line of the curb provided by the inlet (m)

The manual also considers the demand placed on a drainage system by suggesting the use of a design rainfall intensity for a storm with a return period of N years. It also gives a series of equations to calculate the flow rate of water that approaches a drainage system.

It is also noted that in the U.S. both the Federal Highway Administration (FHWA) and the National Cooperative Highway research Program (NCHRP) have initiated research to improve the durability of porous pavements and will develop construction and maintenance guidance to encourage wider use.

2.2.5 Measurement of Water film thickness

The measurement of water film thickness is necessary for validating a splash and spray model. Many measurement techniques have been used by different researchers. Ross and Russam (1968) manually read water film thickness on a steel bar placed on the road surface with studs set at intervals and increasing in height. Gallaway et al. (1971) used a manually operated Leupold & Stevens point-gauge to take measurements of the water film thickness from a datum line. This device provided measurements with an accuracy of 0.2 mm.

Kulakowski and Douglas (1990) developed a tool for measuring the water film thickness and claimed an accuracy better than 0.025 mm. The device is shown in Figure 2, and it consists of a motor attached to a micrometer on the end of which was attached an electric probe. When the probe is lowered and contacts water, a circuit is closed, stopping the electric motor and allowing a micrometer reading to be taken. By lowering the probe further until it strikes the pavement surface, a second reading can be taken, and the water film thickness can be calculated. A similar principle is deployed by a device called a limnimeter, as used by Coiret (2005) for calibration when researching spectroscopy of pavement wetting states. The device uses a pair of metal needles lowered automatically until the water surface closes the circuit between them (shown in Figure 3).

More indirect methods of measurement include use of the water's conductivity or absorptivity. Roe et al. (1997) used a twin metal wire probe developed by HR Wallingford.[3] After calibration (for the particular water and its impurities) the resistance measured between the two probe wires, which were at a fixed distance apart, could be used to calculate the water film thickness. As water film thickness increases, a greater amount of current is able to pass between the electrodes.

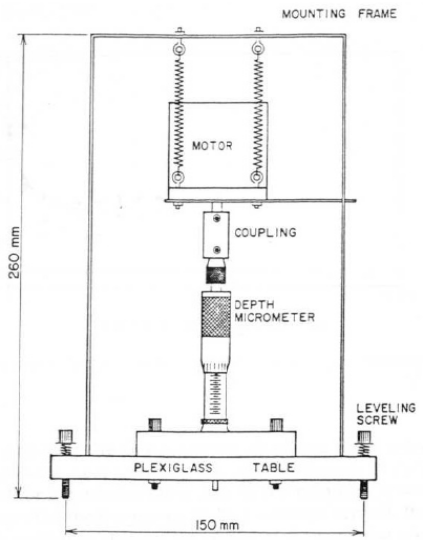

Figure 2. Schematic. Water film measurement device developed by Kulakowski and Douglas (1990).

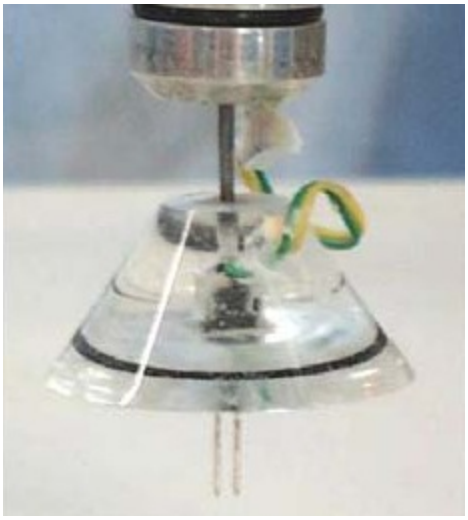

Figure 3. Photo. Limnimeter probe used by Coiret (2005).

Coiret (2005) investigated the specific absorption properties of water for radiation in the near-infrared. In Coiret's technique, a light ray is directed onto a wet pavement and analyzed after having been altered in the liquid medium and retro-reflected by the road surface. It was noted that the technique was sensitive to the pavement texture at lower water film thicknesses, but it was possible to reliably measure water levels between 1 and 5 mm.

The Vaisala remote road surface state sensor is a commercial system that uses reflection-based water detection principles to measure the presence of water or ice on a pavement. The manufacture claims that it

[3] http://www.hrwallingford.co.uk/ (accessed 06/09)

can measure water film thickness from 0 to 2 mm (0 to 0.08 inches).[4] This sensor can be installed as an addition to an existing weather station, on a pole adjacent to the road, or on a vehicle to enable the measurement anywhere without interrupting traffic (Figure 4).

Figure 4. Photo. Vaisala Condition Patrol DSP310.

2.3 Splash and Spray

The main factors affecting the generation of splash and spray are well documented. They are listed by Resendez et al. (2007) as:

- Water film thickness (function of pavement porosity, geometry, drainage capability, texture, and rainfall intensity).
- Vehicle speed.
- Tire geometry and inflation and tread design and condition.
- Vehicle aerodynamics.
- Vehicle spray suppression devices.
- Wind vector.

There are also limitations to the amount of splash and spray generated. For example, under certain conditions, if the water film thickness and speed are such that a layer of water completely separates the tire from the road, providing negligible skid resistance (hydroplaning), then not only will the mechanisms of splash and spray generation change, it is also less likely to be a primary concern to the driver.

2.3.1 Water Film Thickness

Though water film thickness must be considered a major factor of the generation of splash and spray, specific relationships between it and splash and spray generation have not been widely studied.

As a secondary study to their evaluation of splash and spray suppression devices, Koppa et al. (1985) used laser transmitters to measure splash and spray generation by a truck traversing three different water film thicknesss: approximately 0.5 mm, 1.3 mm, and 2.5 mm. They found that "water film thickness on the pavement appears to have a reasonably linear relationship to spray production." However, it was also found that as water film thickness increases further, the increase in splash and spray production may be

[4] http://www.vaisala.com/en/roads/products/mobileweathersystems/Pages/default.aspx (accessed 8/13)

lower, and the depths at which this may occur will be close to those necessary for hydroplaning. Conversely, in a separate study, Koppa et al. (1990) found no significant differences in spray generated from water film thicknesss of 0.5 mm and 1.3 mm.

Weir et al. (1978) discussed the effect of water film thickness greater than or less than 3 mm. This threshold determines whether or not tire tread grooves are filled and influences the proportion of splash versus spray.

Other studies not directly related to this subject have also found similar results. Chatfield et al. (1979) conducted research into the efficiency of several spray reduction devices. One conclusion was about the water film thickness of spray production: "The third way of reducing spray is to ensure that water rapidly drains from the road surface." The researchers also concluded that at very large water film thicknesss no spray reduction device would be expected to produce a significant improvement in spray generation.

2.3.2 Vehicle Contributions

A large amount of work has been carried out to assess the effect of vehicles on the generation of splash and spray. Early research concentrated primarily on the design or assessment of retrofit splash and spray suppression devices. As the research progressed and the available technology improved, the effect of vehicle aerodynamics on splash and spray was also analyzed. To this end, much is known about how and where spray is generated around vehicles, but none of the literature found was able to provide mathematical models linking all vehicular factors. Research has also been undertaken to assess the effect of factors influencing hydroplaning. What is universally agreed on is that the largest vehicle-related factor that influences the generation of splash and spray is vehicle speed.

2.3.2.1 Vehicle Speed

The effect of speed on spray generation was observed by Maycock (1966), who noticed that at speeds below approximately 50 km/h (31 mi/h), spray density was very small, but above this speed, spray density increases rapidly with the following relationship:

$$SprayDensity = Const.(Speed)^{2.8} \tag{9}$$

Pilkington (1990) gave almost identical limits and relationships to spray production with speed and stated, "Spray is generally not measurable until speed reaches 50 km/h (31 mph) and doesn't become undesirable until the speed is 80 km/h (50 mph)" and that "the density of spray increases at approximately three times the speed increase." Similar results were also found by Chatfield et al. (1979): "Spray density increases approximately with the cube of the speed in the range 64-96 km/h (40-60 mph)." This cube relationship between spray intensity and the vehicle speed was also reported in Resendez et al. (2007).

A different relationship between spray production and speed on dense-graded asphalt surfaces was found by Daines (1992), who presented a positive linear relationship (Equation 10). However, this relationship was found as a secondary result and was not the main focus of research.

$$Spray = 5.07 \times Speed - 54.7 \tag{10}$$

where *Speed* is measured in km/h

The research mentioned previously would suggest that the minimum speed before measureable spray is generated is in the range of 48 to 64 km/h (30 to 40 mi/h), which provides a lower speed limit for spray production. An upper limit to spray production could be defined as the speed required for full dynamic hydroplaning to occur (hydroplaning speed). The work carried out by Huebner et al. (1997) on water film thickness models produced a series of models relating water film thickness to hydroplaning speed:

$$HPS = 26.04 \times WFT^{-0.259} \text{ for WFT} < 2.4 \text{ mm (0.09 inches)} \quad (11)$$

$$HPS = \left(\frac{10.409}{WFT^{0.06}} + 3.507 \right) \text{ or}$$

$$HPS = \left(\frac{28.952}{WFT^{0.06}} - 7.817 \right) \times MTD^{0.14} \text{ for WFT} > 2.4 \text{ mm (0.09 inches)} \quad (12)$$

where:
HPS = hydroplaning speed (mi/h)
WFT = water film thickness (inches)
MTD = mean texture depth (inches)

2.3.2.2 Tire Properties

The mechanisms for splash and spray generation described in Section 2.1 rely heavily on the presence of water in the tire tread or on the tire surface. Maycock (1966) researched the effect of tread pattern and condition on splash and spray production. Three tread patterns were tested: worn, zig-zag rib, and heavy duty block, and the findings showed that the worn tire produced a larger amount of splash than the other tire types, though no significant change in spray production was found. He also observed that the worn tires threw more water out sideways. An experiment that collected splash water behind a vehicle fitted with either patterned tires or with smooth tires showed that the distribution of water across the width of the vehicle was skewed to the side.

Many researchers believe that tire geometry (particularly footprint aspect ratio and inflation pressure) are important factors in calculating the minimum vehicle hydroplaning speed. Research conducted by Horne at al. (1986) set out to ascertain a relationship between tire inflation pressure and footprint aspect ratio (width of footprint / length of footprint) to hydroplaning speed for a given water film thickness. The relationship for aspect ratios between 0.4 and 1.4 was found to be:

$$V_p = 51.8 - 17.5FAR + 0.72p \quad (13)$$

where:
V_p = hydroplaning speed (mi/h)
FAR = footprint aspect ratio
p = inflation pressure (lb/inch^2)

Similar experiments at the Texas Transportation Institute, summarized by Yager et al. (2009), concluded the following relationship:

$$VEL = 23.3(P)^{0.21}\left(\frac{1.4}{W/l} \right)^{0.5} \quad (14)$$

where:
VEL = minimum hydroplaning speed (mi/h)
P = tire pressure (lb/inch^2)
W = width of tire contact patch
l = length of tire contact patch

A computational model to predict hydroplaning potential was developed by Ong and Fwa (2007). This model used an analytical method to predict hydroplaning speed. First, the footprint is calculated based on inflation pressure and wheel load. The model then simulates the wheel sliding over a pavement with a

given depth of water at a given speed. The speed is increased incrementally until a state is reached whereby the calculated fluid uplift is equal to or exceeds the wheel load. At this point, the wheel is considered to be hydroplaning. The accuracy of this method is limited by the incremental increase in speed and is only intended to produce a rough estimate of hydroplaning speed.

2.3.2.3 Tire/Road Interaction

It is the interaction between the tire and the road that generates splash and spray, so it will be important to consider how the factors already encountered (e.g., pavement texture, tire properties) also affect the interaction between the tire and the road. Though this is an extensive and complex topic, and most research in the field has investigated the effect of tire/road contact on friction (rolling and sliding) and noise generation, it must be borne in mind that, for example, the effect of changing road texture will influence more than the volume of water present on the surface.

It is thought that a tire rolling or sliding over a wet road surface has three distinct zones of contact (Gough, 1974 and Moore, 1975). The tire squeezes water out in front of it, and the front part of the tire in zone 1 (Figure 5) floats on an unbroken, thin film of water. Farther back, in zone 2, the tire is able to drape over the larger asperities of the road surface and will begin to make actual contact with the smaller asperities. In zone 3, only a thin film of water may remain, and in this area the tire makes contact with the surface through the film. The relative size of these three zones depends on speed, and above a critical speed there may be no contact with the pavement, which leads to hydroplaning, as noted above.

During research to investigate the tire/road interaction and its effect on skid resistance, Parry (1999) concluded that, ignoring the influence of the tire, the geometry of the contact surface determines the level of contact and the pressure distribution between the tire and the surface. The degree of contact between a tire and the surface can be predicted from numerical models derived from pavement profile measurements, and it is possible to estimate the distribution of contact pressures in the tire.

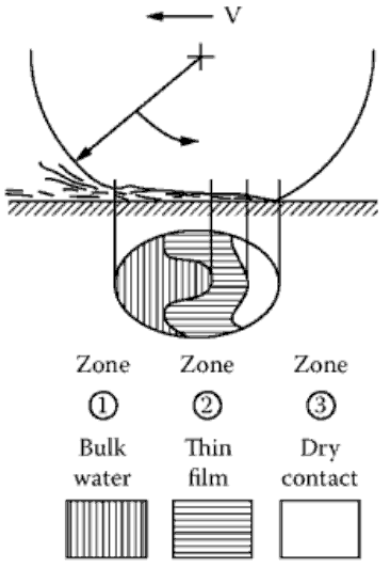

Figure 5. Diagram. Three-zone contact concept (Smith, 2008).

2.3.2.4 Vehicle Loading

Data gathered as part of an accident study conducted by Horne et al. (1986) suggests that there is a correlation between truck loading values and the ratio between wet and dry single-vehicle accidents. The

same paper shows that a variation in vehicle loading can change the tire footprint aspect ratio, which, as described above, influences the hydroplaning of the vehicle. Similar work on truck hydroplaning reported by Forrest et al. (2009) produced similar findings: "It was found that empty rigs were three times more likely to be involved in losses of control than were loaded rigs."

There is also the possibility that a change in vehicle loading could change the stress distribution across the tire footprint and that this could have an influence on hydroplaning speed. However, this is not mentioned in any of the reviewed literature.

2.3.2.5 Vehicle Aerodynamics

Although vehicle aerodynamics do not contribute directly to the amount of spray produced, the turbulence and areas of varying pressure produced by large vehicles allow the spray particles to be suspended within the airstream. This has an effect on the size and shape of the spray cloud produced.

A full-scale comparison between two tractor units was undertaken by Manser et al. (2003). One tractor unit was a 1985 Freightliner, and the second tractor unit was a 1997 Freightliner Century Class S/T. Though their aerodynamic qualities were not quantified, the 1997 tractor unit was deemed to have improved aerodynamic performance over the 1985 tractor unit. Using a laser transmittance and video measuring technique, a series of tests compared the spray generated by both tractor units. The results gathered showed that the 1997 tractor unit produced 13.8 percent less spray than the 1985 tractor unit. The researchers concluded that this reduction in spray was due to the improved aerodynamic qualities of the later model tractor.

Work conducted by the FHWA and cited by Pilkington (1990) suggested that the critical areas of induced aerodynamic disturbance were the front of the tractor unit, the gap between tractor and trailer, the areas around the driving wheels, and the rear of the trailer. If there are additional trailer units, then the gaps between the trailers also become critical areas (Figure 6).

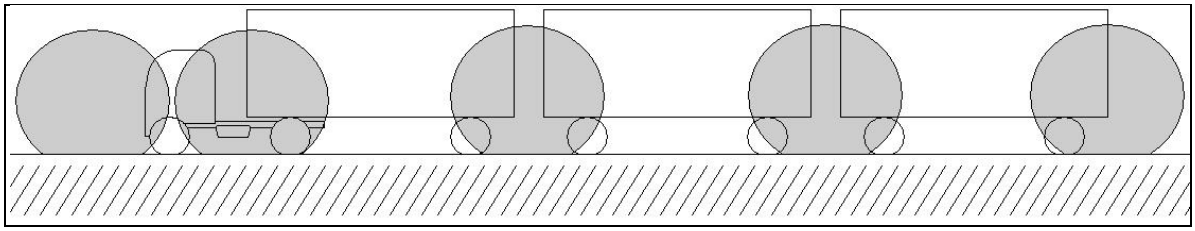

Figure 6. Diagram. Critical areas of vehicle-induced aerodynamic effects (Pilkington, 1990).

One-tenth scale wind-tunnel experiments conducted by Pilkington (1990), which partially agreed with the FHWA results, showed that the front of the tractor unit and the "drive tandem wakes" produced the highest turbulence. However, no mention was made of the gap between trailer and cab or the rear of the trailer.

A computational study of large-vehicle aerodynamics was conducted by McCallen et al. (2005) for assessing various aerodynamic improvement devices. This study showed that areas of high aerodynamic disturbance could be found between the tractor and trailer units and behind the trailer as shown in Figure 7.

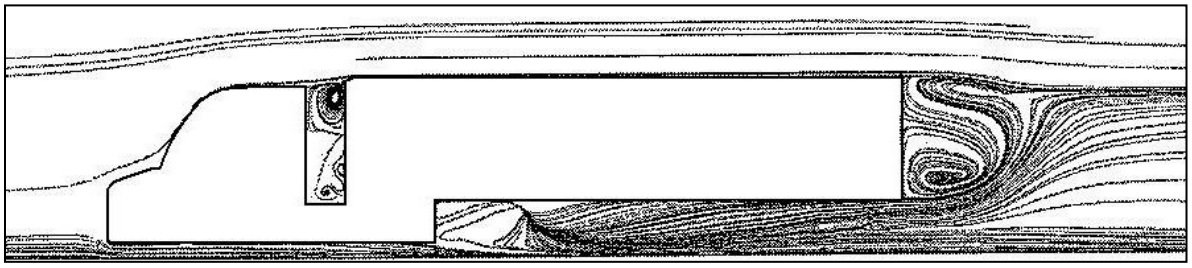

Figure 7. Illustration. Velocity streamlines at the centerplane of the baseline Generic Conventional Model (McCallen et al., 2005).

These findings are in agreement with those of FHWA, though in McCallen et al. the area in front of the tractor unit seems to be fairly aerodynamically efficient; however, this could be due to the type of tractor unit assessed. The FHWA results were based on a European-style COE (cab over engine) tractor, which presents the airflow with a large surface area, whereas McCallen et al. considered a more aerodynamically efficient American-style CBE (cab behind engine) tractor unit. An additional aspect of this work was to assess the effect of aerodynamic improvement devices on spray cloud generation. A key finding of this study was that the aerodynamic improvements made by the particular devices tested produced a "quantitatively more concentrated" spray cloud that would have a negative effect on motorists' visibility. The increase in spray density was attributed to a focusing effect on the spray droplets.

A later study by Consano et al. (2007), again looking at drag reduction devices, confirms the critical areas of aerodynamic drag as the tractor-trailer gap, the underbody, and the bluff shape of the rear of the tractor.

While the majority of vehicle aerodynamic studies concentrate on the straight line aerodynamics of vehicles, recent work by Hargreaves and Morvan (2008) has shown that traveling into a crosswind significantly modifies vehicle wake. In particular, the transverse extent of the wake is increased because the vehicle presents a large cross-sectional area to the incoming flow resulting from both the vehicle's movement and the crosswind. The gap between the tractor and trailer actually channels the flow of the crosswind, producing a very distinct jet on the leeward side of the vehicle. Both the widened wake and this jet will have an effect on the transportation of any spray generated.

Vehicle overtaking is another important aspect of vehicle aerodynamics. Corin et al. (2008) used two-dimensional computational fluid dynamics (CFD) models to look at the forces acting on both the lead vehicle and overtaking vehicles as they pass at motorway speeds. Crosswind effects were also investigated, and the conclusion was that existing quasi-static models do not capture the peak forces accurately. The CFD techniques used are relevant to the present work because overtaking is one of is one of the critical maneuvers investigated by this study.

2.3.2.6 Spray Suppression Devices

Spray suppression is well documented and the subject of much research. The number of documents pertaining to this topic is so great that it would have been infeasible for this literature review to review the entire body of work. Instead, the review summarizes the most influential and relevant papers.

NHTSA (2000) describes the most commonly used spray suppression devices as:

- Mud flaps: A flat, rectangular device usually grooved or coated with durable grass-like material that is placed behind the wheels. The aim of such a device is to catch the spray generated, separate the water from air, and channel the water to the road surface.
- Side-skirt/valance: Fitted to the vehicle body just above the wheel, this device is designed to contain any spray within the wheel well. Like mud flaps, these may be flat panels with a grass-like or grooved coating.

- Fenders: This is a rigid structure placed around part of the wheels. As with a side-skirt, the aim of these devices is to contain the spray within a defined area and channel it toward the road surface.

The literature finds mixed results as to the effectiveness of spray suppression devices. Some researchers measured no difference in spray production, but others reported as much as a 60 percent improvement in visibility.

As a result of early experiments in the 1960s, Maycock (1966) found that the use of a circumferential fender spray suppression device had the effect of reducing spray density 10 m behind the vehicle at 80 km/h by a factor of between 3 and 4, and that spray between the tire and mudguard was "largely eliminated" by the use of a side valance. Pilkington (1990) also assessed the effectiveness of spray suppression devices. This work concluded that, within the trial, the most effective system to suppress spray was a combination of the "Reddaway" system (now known as clear pass) and a drag shield (details of a "drag shield" were not given though a safe assumption would be that this is some kind of aerodynamic device). Pilkington reported that this combination improved visibility by 60 percent and that the least effective system improved visibility by 18 percent when compared with an untreated vehicle.

However, several researchers have found evidence that seems to contradict Pilkington's results. Chatfield et al. (1979), Koppa et al. (1985), and Manser et al. (2003) all tested the effect of a number of mudguard/fender geometries or splash and spray suppression devices. Chatfield measured a reduction in spray due to mudguard/fender geometry but saw no visual improvement. Koppa found only "trivial" reductions in spray due to suppression devices. And Manser concluded that "no significant differences were found between the amount of spray produced with the spray-reducing devices and the baseline configuration."

2.3.3 Measurement of Splash and Spray

To validate any splash and spray model, it must be accurately compared to empirical evidence. This requires an accurate means of measuring the splash and spray generated by heavy vehicles. A number of techniques have been developed to quantify the amount of splash and/or spray generated by a vehicle. The different methods used can be separated into the following categories.

2.3.3.1 Collection

This technique consists of fitting devices to the measured vehicle itself or to a following vehicle. Maycock (1966) attached a number of disposable collectors consisting of several layers of absorbent paper to the bonnet of a following vehicle. During testing, the absorbent paper would collect any spray that impacted the collectors. The collectors could then be weighed, and the difference in mass before and after testing would provide a measure of the amount of spray generated.

A similar system was used by Pilkington (1990), whereby a spray cloud would be "fingerprinted" by means of capturing droplets in an absorbent screen for a specified length of time. The droplet size, droplet frequency, and spray density could then be calculated.

Maycock (1966) also used a system for collecting splash. A series of polythene bottles were mounted in a line, close to the rear wheels of the measured vehicle. Splash thrown up by the wheels would then be caught in the bottles, and the amount could be calculated.

Figure 8 shows a spray collection device developed by Ritter (1974). This device was fitted to the side of the measured vehicle close to the wheels. A proportion of the spray generated by the vehicle would enter the device, which would allow the air to exit and collect the water. The water could then be quantified and could provide an indication of the amount of spray generated.

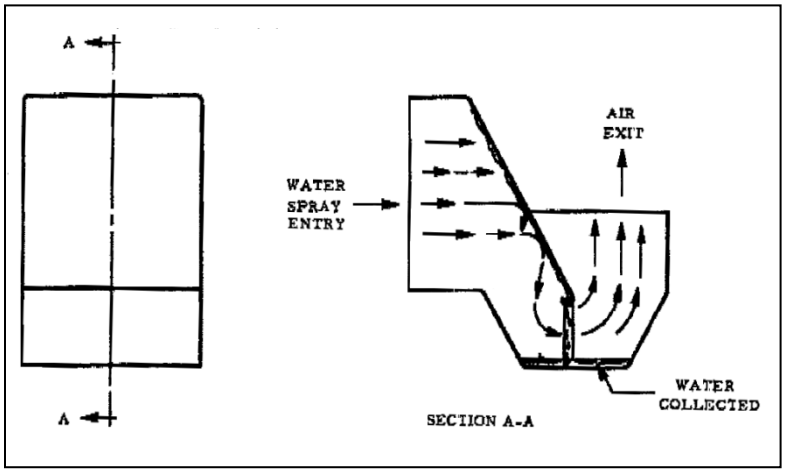

Figure 8. Diagram. Spray collector (Ritter, 1974).

2.3.3.2 Contrast Change

The small droplets of water that compose vehicle spray have the effect of scattering light as it passes through the spray cloud. If an image is viewed through a spray cloud, the contrast of the image is reduced as a function of the light refraction occurring within the spray particles. If a simple image, such as a black board or checkerboard, is viewed before and during spray, the difference in intensity values will provide a measure of the light scatter and the amount of spray. This technique has been used by Ritter (1974), Baughan and Hart (1988), Manser et al. (2003), and Knight et al. (2005), and it has produced results similar to that of the standard transmittance analysis method detailed in Section 2.3.3.3.

Knight et al. (2005) devised a continual measurement system that used this principle. A black screen would be fixed to the rear of the measured vehicle, and a second vehicle would follow at a fixed distance. A video camera mounted in the following vehicle filmed the screen on the back of the measured vehicle. The images could then be analyzed and the changes in contrast calculated. This device was used on public roads, and it was found that this technique was very susceptible to environmental conditions such as the direction of the sun or changes in light due to cloud cover.

2.3.3.3 Light Attenuation

As mentioned previously, a spray cloud scatters the light traveling through it. In addition to reducing the image contrast, this scattering of light reduces the strength of the light passing through the spray cloud. Many methods use light scattering to evaluate the amount of splash and spray, though the most widely used is known as the transmittance analysis method.

Early development of the transmittance analysis method was undertaken by Ritter (1974). A 12-V automobile headlamp light source was directed longitudinally down the test section at a photometer. The photometer was linked to a recording device, and light intensity measurements were taken through the spray cloud as a vehicle traveled along the test section. This method worked well, but the use of a visible-light source allowed environmental lighting conditions to affect the result.

This technique was developed further by Koppa et al. (1985), who replaced the automobile headlamp with low-power laser light sources. The researchers also used four laser and detector couplings placed on both sides of the test section at varying distances. This configuration allowed the researchers to characterize the effect of wind on spray position. This improvement on the original design has served as the standard method for this technique and is recommended in the Society of Automotive Engineers (SAE)

standard practice for splash and spray evaluation, J2245. Manser et al. (2003) compared the laser and video-based methods and concluded that the two methods provided very similar results.

2.3.3.4 Subjective Observation

Using photographs, video, or direct observations of splash and spray testing can provide subjective evaluations of spray-cloud properties. Figure 9 and Figure 10 compare spray and splash images collected by running a truck at 32 km/h (20 mi/h) and 80 km/h (50 mi/h) (Chatfield et al., 1979).

Figure 9. Photo. Image of spray emission at 32km/h (Chatfield et al., 1979).

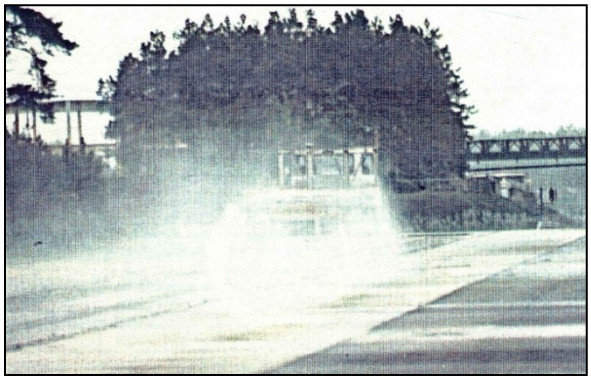

Figure 10. Photo. Image of spray emission at 80km/h (Chatfield et al., 1979).

Though this method has very poor repeatability, it can be a useful technique for confirming results gained by other means. Pilkington (1990) and Baughan and Byard (1997) used observers to rate the reduction in visibility caused by a spray cloud in conjunction with a laser transmittance technique. Good correlation was found between the two techniques, which provides extra confidence in the results and demonstrates that the nuisance caused by spray can be inferred from the transmission technique. This technique also provides an advantage in that the nuisance of splash and spray can be directly measured and contributing factors such as speed can be directly observed.

2.3.3.5 Other Techniques

Kalantari and Tropea (2006) used the Doppler technique and a high-speed charge-coupled device (CCD) camera to measure the amount of splash and spray produced. The Doppler technique determines the number flux, size distribution, and the velocity of the water droplets. The CCD camera is used to characterize the droplets and to measure the film thickness caused by the spray.

Salles and Poesen (1999) describe an "optical spectro pluviometer (OSP)," an infrared optical device used to measure raindrop size, fall velocity, and intensity. The OSP works on the principle of measuring an optical shadow, and it enables independent measurement of drop size and drop velocity in real time. Use of the OSP seems limited to the work of Salles and Poesen, but it may be applicable to the measurement of splash and spray, certainly in the far-field, away from the truck when the droplets have assumed near-vertical trajectories.

Pérez-Jiménez et al. (2011) developed a prototype laser-based system that can measure splash and spray in the field. The system measures the amount of splash produced by a tire as it travels over a wet pavement. The prototype consists of a water tank that releases a constant stream of water in front of the tire and a high-resolution, high-speed camera that captures images of the water as it crosses a measurement plane illuminated by a laser light source. The splash and spray is estimated by processing the images captured during the test, quantifying the number and size of the water droplets observed using a visual recognition algorithm, and reporting the mean area (pixels) occupied by water.

2.3.4 Modeling Splash and Spray

It appears from the literature that there is currently no model capable of displaying or calculating the splash and spray created by a vehicle based on fundamental inputs such as rainfall rate, pavement geometry, and vehicle geometry. Resendez et al. (2007) express this lack explicitly, but they do not postulate how such a model may be built. The researchers hypothesize that a splash and spray model would exist as a function of water film thickness and air/rubber ratio in the vehicle's tires. Resendez et al. provide the following example (2007):

> *To illustrate this it might be assumed that there are four truck tires running two-by-two in the wheel tracks (ruts) of a pavement, each being 0.82 ft (0.25 m) wide expressed as a contact patch width. A calculation could be made about how much water is accommodated within the tread of the tires. For example, if the tread is assumed to be 0.4 in (10 mm) and the air/rubber ratio in the tread is 30 percent, this would correspond to an average water depth on the pavement of 0.12 in (3 mm), which is equivalent to a volume of 0.24 gallons/ft (3 litres/m) of pavement before the tread is saturated. Thus, at up to 0.12 in (3 mm) of water depth, one could assume that one may find a reasonably linear relationship between water depth and spray. Splash, on the other hand, would dominate above 0.12 in (3 mm) of water depth (for the example indicated).*

The existing models for splash and spray are derivatives of aerodynamic models and are based on CFD systems, not fundamental inputs. These models calculate the air flow around a vehicle (usually a simplified computer-generated vehicle model) using commercially available computer software that contains pre-defined fluid mechanics sub-models for fluid flow droplet breakup, fluid temperature, pressure, and other characteristics. To model splash and spray, droplets of water are injected into the model at strategic points (usually just behind the wheels). These water droplets are given an initial velocity and size, and the simulation then calculates the flow path of each droplet and changes in size from impaction. This then creates a representative model of the spray generated by aerodynamic turbulence, which can be used in comparative testing.

McCallen et al. (2005) used this technique to assess spray cloud generation by heavy vehicles with aerodynamic improvements. Paschkewitz (2006) used the technique to study the spray dispersion around a simplified trailer wheel assembly. Both papers showed that the use of CFD to calculate splash and spray generation was indeed technologically and financially viable. This is a fairly good technique for aerodynamic properties. However, as stated in Paschkewitz (2006), the injection locations, directions, velocities, and size distribution of the water droplets are largely unknown. This has implications for the comparison of different systems influencing splash and spray such as wheel and pavement geometry and rainfall rates. However, if a relationship between water film thicknesss (a parameter for which there are

existing models) and the properties of water droplets created due to tire-road contact could be found, then a CFD-based system could be used to accurately model splash and spray generation for many different inputs.

2.3.4.1 Modeling Rain

While not directly relevant to the modeling of splash or spray, some recent work has modeled rain using CFD and can inform the present study. In the transportation field, Abdul Ghani et al. (2001) performed wind tunnel experiments and CFD simulations of rain falling on a car. The study's most relevant issue for the present project is a discussion of the fate of water droplets as they impact on a solid surface, either a following vehicle or the ground. Abdul Ghani et al. also classified the size of raindrops (unfortunately without reference) according to the type of rainfall event. Best (1950) was one of the earliest works to categorize rain by size and velocity, and some of the statistical techniques Best used can be applied to the analysis of spray and the subsequent definition of a droplet diameter distribution in a CFD model.

An excellent review of wind-driven rain in the built environment by Blocken and Carmeliet (2004) contains a number of interesting points. It appears that only the smallest raindrops are influenced by high levels of turbulence in the flow; the medium-sized droplets follow streamlines, and the largest droplets tend to follow inertia-dominated trajectories.

In the CFD field, Choi (1997) has led the way in the modeling of rain using CFD. He has coined the Local Effect Factor (LEF), which is the proportion of droplets launched from an area upstream of the building that actually impacts the building. Such a concept could be applied to a following vehicle in the present work.

2.4 Exposure to Splash and Spray

Splash and spray cause a significant nuisance to motorists, and, under some conditions, can cause a momentary loss of visibility. Accident studies on this topic agree that there is a small but measureable increase in accident risk related to splash and spray. However, the amount of research conducted thus far does not provide the accurate number of accidents caused by splash and spray (NHTSA, 2000 and Botes, 2002). The NHTSA report concludes that "the number of recorded splash/spray crashes is extremely small," accounting for less than 0.02 percent of accidents. The Fatality Analysis Reporting System (FARS) reported that 0.0011 percent of accidents were caused by splash and spray. The type of vehicle, however, was unable to be determined, so these crashes and accidents cannot be attributed specifically to trucks. The National Automotive Sampling System (NASS) General Estimates System (GES) reported 0.0036 percent of crashes have been caused by splash and spray. However, the small size of these percentages could partly be due to most records not considering splash or spray as a possible cause of accidents, meaning that the involvement of splash and spray in many crashes may have gone unrecorded. The same report also concludes that "it is unlikely that there is any crash file with better data than FARS or GES. It is unlikely that any state file can provide meaningful data on the question." These figures could therefore be higher, but it is still unlikely that splash and spray are a significant accident risk. However, improved control of splash and spray could improve comfort and reduce nuisance experienced by motorists.

2.4.1 Human Factors

Fuller (2005) describes how driving can be conceptualized by comparing the demand of the task to the capability of the driver. When task demand exceeds capability, a loss of control will occur. Task demand is determined by many factors in the driver's environment, although some are within the driver's control, such as speed. The gap between task demand and capability is the driver's safety margin, and momentary

changes in the environment, including splash or spray, will raise task demand and reduce a driver's safety margin significantly. While a driver could reduce speed to increase the safety margin in such an event, reducing speed is contrary to the process of overtaking. It is likely that most of the time, a driver's safety margin when driving through splash or spray is much reduced, increasing a driver's feelings of risk and anxiety.

There have been a limited number of studies relating to the human interaction with splash and spray; however, work carried out in Baughan et al. (1983) showed that spray from heavy goods vehicles was the highest rated "problem" that heavy vehicles cause to motorists. Pilkington (1990) and NHTSA (2000) presented a series of possible consequences relating to splash and spray, which have been combined and condensed in Table 1.

Table 1. Potential consequences of splash and spray.

Category	Motorist affected	Potential problem
Short term	Lead vehicle	Spray obscures following vehicles
	Following vehicle	Visibility – spray from lead vehicle obscures lead vehicle, signs, edge lines, other traffic at intersections, traffic signals
		Visibility – doused during passing, lane change
	Approaching vehicle	Visibility – spray obscures vision beyond oncoming vehicle
		Visibility – dousing during encounter may cause sudden braking and loss of control or collision with other motorists
	Motorcyclists, cyclists, pedestrians	Numerous visibility problems
		Knowing they cannot be seen produces a change in behavior
		Doused when vehicle passes
Long term	Lead vehicle	Dirt deposited on windscreen, mirrors, rear window, lights, and edge lines obscures view
	Following vehicle	Dirt deposited on lights obscures lead vehicle
		Dirt deposited on lead vehicle reduces vehicle visibility
	All road users	Dirt deposited on signage and street lighting reduces their visibility

The potential problems listed in Table 1 can be separated into three categories: gradual loss of vision, sudden loss of vision, and shock. The only work that was found pertaining to any of these topics was NHTSA (2000). This report contains a table showing the number of times that drivers divert their vision from the road when performing a number of activities, such as head turns prior to lane changes or when viewing mirrors. The table suggests that an acceptable limit for a loss of vision could be as high as 1.5 s. The study, however, does not assess acceptable times for an unexpected loss of vision, and when overtaking a spray-producing truck, it is possible for vision to be obscured for as long as 10 s (NHTSA, 2000). This shows that spray-based vision loss can persist for a considerable amount of time when compared with human tolerance limits.

2.4.2 Rainfall Exposure

Rainfall exposure is an important input for a splash and spray exposure model, and rainfall times should be considered because prolonged rainfall will increase the exposure time to splash and spray. Harwood et al. (1987a and b) include information that can be used for this effect. Furthermore, the Enhanced Integrated Climatic Model developed for the Mechanistic-Empirical Pavement Design Guide (MEPDG) could be used to obtain climatic data for specific sites.

In a project for CalTrans, Huang et al. (2008) updated the California Wet Percentage Time table of 1972. Wet percentage time refers to the proportion of time during which the pavement is damp enough to cause traffic accidents, and the table defines factors that can be applied to a corresponding list of high-accident-risk locations to develop a list of high-wet-accident-risk locations. At the time of the CalTrans project, the wet percentage time factors had not been updated in more than 30 years. Historical hourly precipitation data in California reported by rain gauges were obtained from five network data sources, and a subset for the preceding 11 years was analyzed using the following process: *Reprocessing*, *Quality Control*, and *Missing Data In-filling*. Data handling was a significant issue, and it was found that the data was often incomplete or of poor quality.

The National Oceanographic and Atmospheric Administration (NOAA) provides precipitation frequency estimates based on a partial duration series for most weather stations in the United States. As an example, Table 2 presents the frequency estimated for various durations and average recurrence intervals (ARI).

Table 2. Example of point precipitation frequency estimates (mm/hr) from NOAA Atlas 14 for Blacksburg, Va.[5]

ARI* (years)	5 min	10 min	15 min	30 min	60 min	120 min	3 h	6 h	12 h	24 h	48 h	4 day	...	60 day
1	90	72	60	41	26	15	11	7	4	2	1	1		0
2	108	86	72	50	31	18	13	8	5	3	2	1		0
5	129	103	87	62	40	23	16	10	6	4	2	1		0
10	144	115	97	70	46	27	19	11	7	4	3	1		0
25	163	130	110	81	54	32	23	14	8	5	3	2		1
50	176	140	118	89	60	36	25	15	9	6	3	2		1
100	188	150	126	97	66	40	28	17	11	7	4	2		1
200	200	158	133	104	73	43	31	19	12	8	4	2		1
500	213	168	141	112	81	49	35	22	14	9	5	3		1
1000	223	175	147	119	87	52	38	24	16	10	6	3		1

NOTES: The NOAA Atlas 14 Document provides more information. Formatting forces estimates near zero to appear as zero.

2.4.3 Light

Knight et al. (2005) noticed an interesting phenomenon while undertaking contrast change testing of splash and spray. Their methodology was to film a checkerboard as a spray-emitting vehicle passed it. The transmittance value of light reflected from the checkerboard would then be calculated to indicate the amount of generated spray. Under certain lighting conditions, it was noticed that the video image could totally "whiteout." It was thought that, under specific lighting conditions, bright sunlight could be reflected by the spray droplets directly into the camera lens. This effect was not quantified or studied further, but it is possible that the phenomenon could surprise a motorist and pose a safety hazard.

2.4.4 Wind

Wind can have a very strong influence on the position of a spray cloud. This was noted by Koppa et al. (1985), who developed a model to correct for wind effects on the direction of the spray cloud. This model was known as "Rule 4" and assumed that the vector of the spray cloud could be corrected by using a

[5] http://hdsc.nws.noaa.gov/hdsc/pfds/index.html (accessed June 2009)

geometric or arithmetic mean of several sensor readings. A diagram illustrating Rule 4 is shown in Figure 11, where the numbers indicate the sensors used.

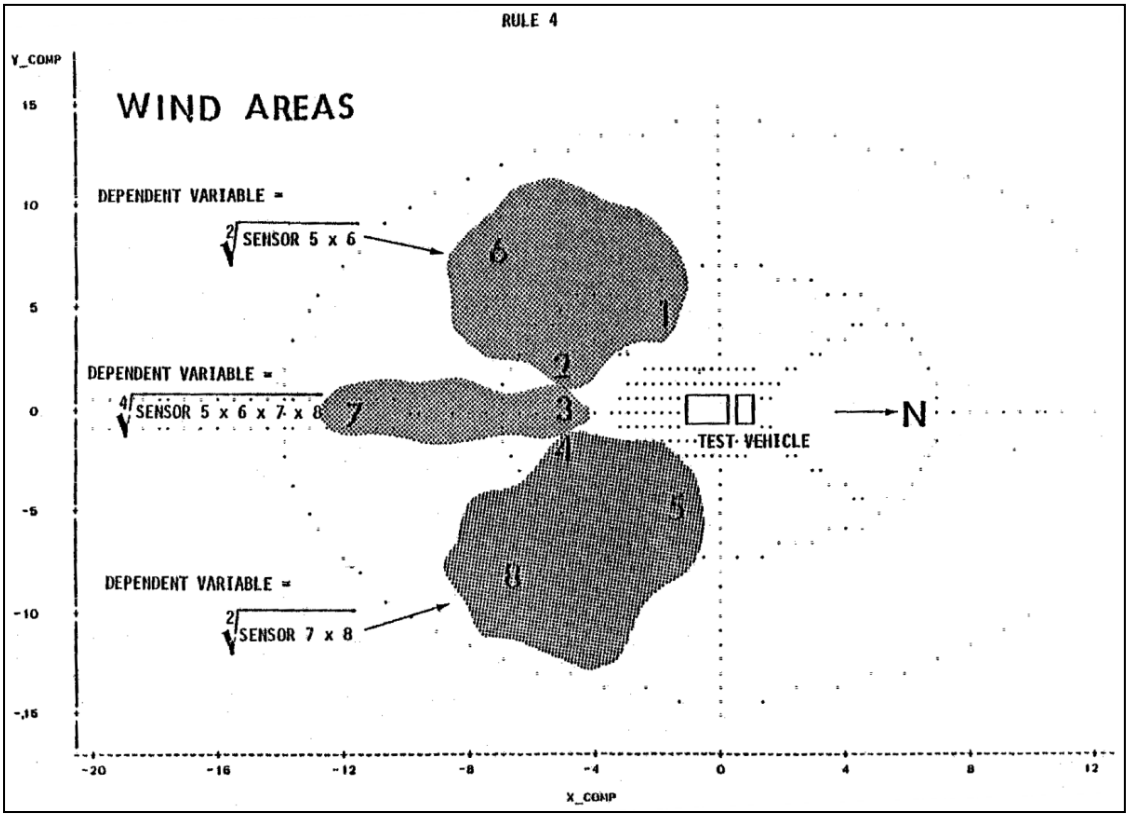

Figure 11. Diagram. Depiction of Rule 4 (dependent variable refers to the amount of spray produced) (Koppa et al., 1985).

Pendleton et al. (1988) describe specific research into the effect of wind on spray. They state that a linear relationship (like that of Koppa et al., 1985) cannot be reasonably assumed, and they present three alternatives based on empirical evidence. The model that showed the smallest mean squared error and best fit is shown below in Equation 15. This model is a piece-wise least squares regression model and was developed using empirical data gathered from a laser transmittance experimental methodology. In this setup, each of four pairs of lasers and sensors were positioned longitudinally down a straight test route and symmetrically at different distances from the center of the test route.

$$S_i = a_0 + a_1 S_j + a_2 \left(S_j - a_3\right) S_0 \tag{15}$$

where:

S_i and S_j are paired sensor readings

$S_0 = 1$ if $S_j \leq a_3$ and $S_0 = 0$ if $S_j > a_3$

2.5 Summary of the Literature Review

A review of available literature has shown that there has been a considerable amount of research into the problem of splash and spray, but the results of this research are often inconclusive and contradictory.

Considering the mechanisms of splash and spray generation shows that it would be important to consider a number of factors when modeling splash and spray.

On the basis that the volume of water present on the pavement surface will be critical to the model, a review of literature specifically concerned with water film thickness or water film thickness was carried out first. Further literature specifically treating the nuisance caused by water on the road surface was found to concentrate largely on measurement methods and empirical techniques for reducing the various phenomena. Additional literature concerning the modeling of the water displaced and projected at the tire-pavement contact and the estimation of factors that might affect splash and spray (rainfall, wind, etc.) was also reviewed. Some of the important points are summarized below:

- **Water film thickness:** There are several models for the calculation of water film thickness that are based on geometric, environmental, and surface properties. Though these models share some common features, they are not all the same. The main factors considered include drainage path length and slope of drainage (affected by cross slope and gradient), rainfall rate (or excess rainfall rate), and pavement texture depth.
- **Splash and spray:** The literature describes the main contributing factors to splash and/or spray as:
    - Water film thickness.
    - Vehicle speed.
    - Tire geometry.
    - Tire tread design and condition.
    - Vehicle aerodynamics.
    - Vehicle spray suppression devices.
- **Measurement techniques:** The techniques most commonly used to measure splash and spray include:
    - Collection – A proportion of the generated splash and spray is collected within a container and assessed after testing to provide a representative sample of the splash and spray generated.
    - Contrast change – Images of a standardized target before and during spray are analyzed using image analysis technology, and the differences are used to estimate the amount of spray.
    - Light attenuation – A light source is directed through a spray cloud at a photocell a fixed distance away. The light becomes scattered through the spray, and the amount of light collected by the photocell gives an indication of the quantity of spray.
    - Subjective observation – Images of, or the direct observation of, spray testing is undertaken by a number of people. Each image or test run is scored, and a subjective quantity of spray is obtained.
- **Limitations:** No conclusive link has been demonstrated between water film thickness and splash and spray generation, and there is little knowledge of the effect of splash and spray on motorists' safety and comfort. These factors must be considered explicitly during experiments carried out in the remainder of this project before a useful model can be achieved.

3 Water Film Thickness Model[6]

This chapter describes the methodology and results of laboratory experiments to develop the water film thickness model that was used as part of the model to determine the volume of water present for splash/spray formation.

3.1 Flume Experiments

This section describes the flume experiments carried out at the University of Nottingham. A description of the apparatus used, the experimental procedure, and the basic theory behind the test is included.

3.1.1 Apparatus

The flume, shown from the downstream end in Figure 12, has a length of 4 m (13 ft), of which about 2.5 m (6 ft) could be termed the *working section*. The working section is 0.6 m (2 ft) wide and 0.3 m (1 ft) high. At the upstream end, water is pumped vertically down into a sump, which gradually fills up with water until it enters the working section. The water is cycled around the flume at a rate Q governed by the speed of the pump and measured using the rotameter shown in Figure 13. Also visible in Figure 12 is the pump below the flume and, to the right of the flume, the wave gauge signal box and computer. At the far end are the pipes, which supply water to the flume.

Figure 12. Photo. Image of the flume from the downstream end.

[6] This chapter is a revised version of the Task Report *Water Film Thickness Model*, prepared by D. Hargreaves, F. Coyle, and T. Parry

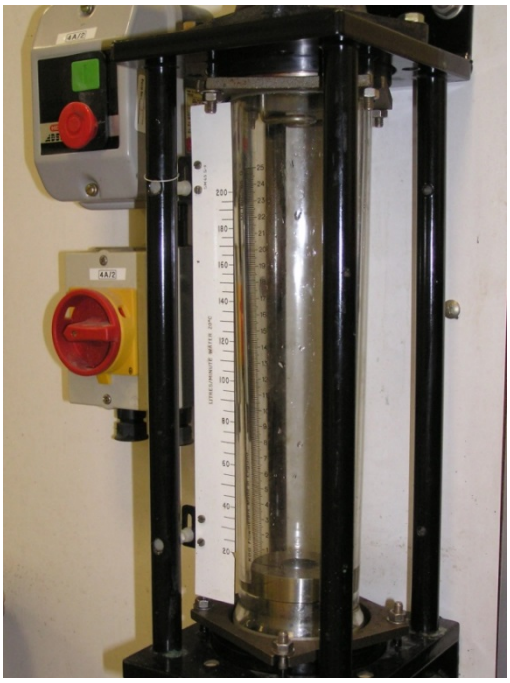

Figure 13. Photo. Image of the rotameter.

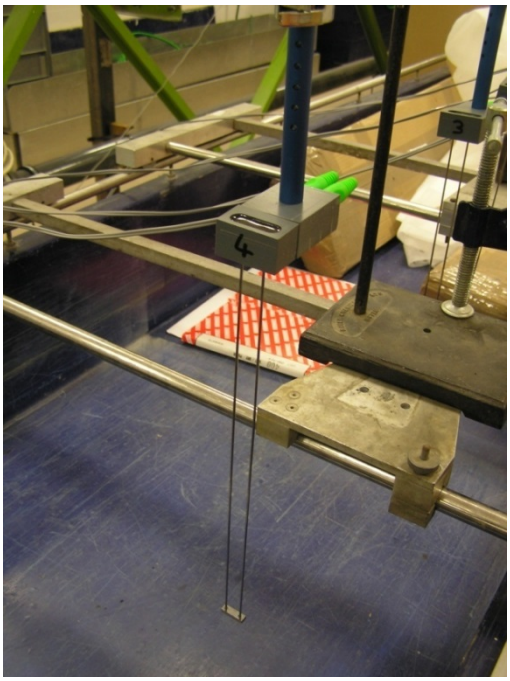

Figure 14. Photo. Image of a wave gauge.

The experiment tested six different road surfaces, listed in Table 3. These surfaces were mounted in the flume toward its upstream end (Figure 12). The simulated pavement was prepared in eight squares [length approximately 0.3 m (1 ft)] of road surface material. Three appropriately angled boards (at 0.5 percent, 2 percent, and 6 percent slope) were constructed, and the surface squares were mounted onto them. Sealant was then used to fill in the gaps around the mounting board and between the road surface squares. The sealant was then allowed to set for 24 hours before testing.

Table 3. Surface types used in the tests.

Number	Description
1	Stone mastic asphalt
2	Dense-graded asphaltic concrete
3	Porous asphalt
4	Smooth concrete
5	Tined concrete[7]
6	Perspex[8]

The water film thickness was measured using four wave gauges. These are produced by HR Wallingford and consist of two parallel stainless steel rods of length 300 mm (12 inches) and are kept parallel by a plastic head and foot. The plastic head, shown with a number "4" written on it in Figure 14, is connected to a stem from which two wires are taken to the rear of a four-channel signal processing box (the front of which is shown in Figure 15).

Figure 15. Photo. Image of the front of the signal processing box.

Wave gauges are simple and reliable devices for measuring water levels; they operate by measuring the current that flows between the two wires, which is then converted to an output voltage directly proportional to the immersed depth. The wave gauge is connected to a circuit inside the signal processing box that both energizes and senses the output from the wave gauge. There is also circuitry designed to compensate for the (very long) cable that takes the signal from the wave gauge to the circuitry. On the signal processing box, there are controls for adjusting the gain; in the present application, the depths are so low that the gain is turned up to the maximum to give a good voltage response for the gauge.

[7] The tined grooves ran perpendicular to the water flow.

[8] The Perspex surface was a single sheet, which was placed on the angled boards.

The signal processing box is then connected to a PC using a plug-and-play USB cable. The analog-to-digital processing is done within the signal processing box, and the digitized voltage from each of the four wave gauges can be stored using the *TracerDAQ* software that comes supplied with the wave gauges. This allows the voltages from all four gauges to be stored in text files, which also contain the time. The frequency of the sampling can be set by the software; 5 Hz was used here.

3.1.2 Methods

3.1.2.1 Calibration

Before each run, it was necessary to calibrate the wave gauges; this was done simply by immersing the wave gauge to a known depth in still water. The depths chosen were 0, 1, 2, 3, 4, 5, 10, 20, and 50 mm. The stem that holds the gauge was connected to a Vernier scale so that changes in the height of water could be determined very accurately. While it was trivial to determine a reference voltage at a depth of 0 mm, determining a reference voltage at an accurately measured depth of 1 mm (0.04 inch) was more problematic. Wave gauges are typically designed to work in much deeper water than the present application—it is possible to get wave gauges that are 2 m (6 ft) long. For the 1-mm (0.04-inch) water film thickness, the surface tension of the water and the resulting meniscus made the determination difficult, but a consistent method was applied throughout.

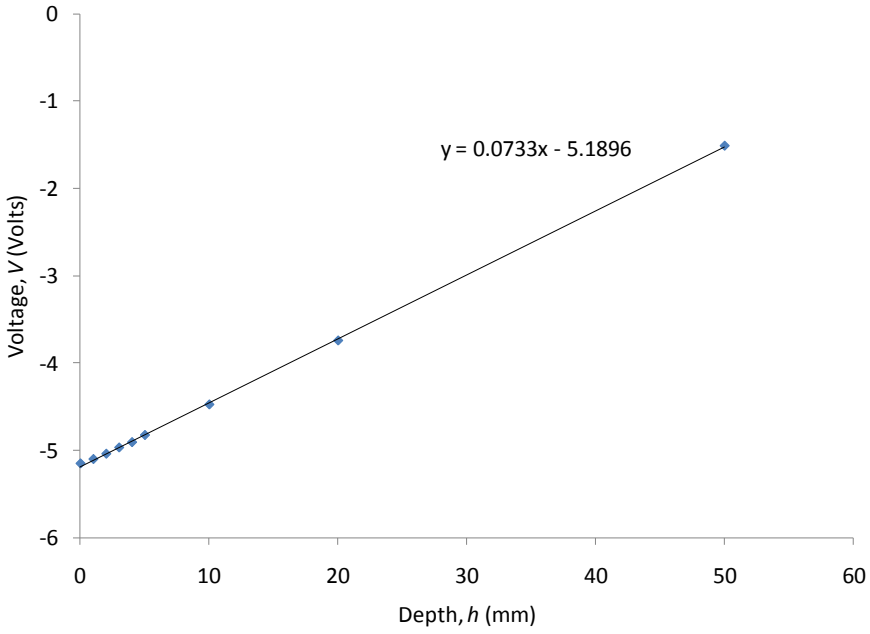

Figure 16. Graph. Sample calibration data for a wave gauge.

For each calibration depth, the readings were allowed to settle before the voltage data was sampled. The mean voltage, V, was plotted against the depth, h, and the straight line relationship shown in Figure 16 was found for each gauge with Equation 16:

$$V = mh + V_0 \quad (16)$$

where m is the gradient and V_0 is the offset voltage. In the example shown in Figure 16, these take values of 0.0733 V/m and -5.1896 V, respectively.

Once calibrated, the depth can be calculated from Equation 17:

$$h = 0.001\frac{V-V_0}{m} \tag{17}$$

where the factor 0.001 represents a change in units from millimeters to meters.

3.1.2.2 Depth Measurements

The experimental campaign consisted of 18 tests: testing of six surfaces at three angles each. Within each test, the flow rate, Q, was varied from 20 lt/min (5 gl/min) to 140 lt/min (35 gl/min) in increments of 20 lt/min (5 gl/min). The flow rates at the higher end of this range are not representative of surface water on roads, but they were included to determine whether the trend in the relationship between water film thickness and flow rate would extrapolate down to the lower flow rates. In all cases, it appeared to do so.

At the center of each of the eight road surface squares, a small rectangular notch was removed, so that the plastic foot of the wave gauge could fit flush with the road surface. Clearly, this is another source of experimental error, especially for the rougher surfaces where a mean surface "top" is difficult to ascertain.

Because only four wave gauges were available for the project, two sets of data were gathered for each combination of surface, slope, and flow rate with the gauges mounted on the left-hand side (LHS) and right-hand side (RHS) of the flume (looking from the downstream end). The four channels of voltage could be sampled simultaneously, and once the discharge rate was set, the flow was allowed to settle before voltages were gathered for 30 seconds.

3.1.3 Analysis

For each road surface, a single Microsoft Excel spreadsheet was created to hold all the calibration data, the voltage data for each flow rate, and the analysis of these data. The measured values were arranged in column format; the first half of a typical set is shown in Table 4. For each discharge rate, the voltage readings for both the RHS and LHS gauges are shown. Each of these voltage readings is the time-average of the 30 s of data sampled during the test. Next to each set of voltages are the depths, which were calculated from Equation 17. The columns headed P1 to P4 refer to the position of the probes, with P4 at the top (upstream) end of the road surface and P1 at the bottom end (downstream) of the slope.

The depth measurements for the RHS and LHS were then averaged to remove any problems with the road surface having any appreciable slope in the cross-flow direction; see the first set of columns in Table 5. The next set of columns calculate the cross-sectional area of the flow, A, given by (refer to Figure 17):

$$A = hb \tag{18}$$

where b is the width of the flume and h is the water film thickness. The wetted perimeter, P, is then:

$$P = 2h + b \tag{19}$$

The ratio of the area to wetted perimeter is called the hydraulic radius, R, with

$$R = A/P \tag{20}$$

which corresponds to the fourth set of columns in Table 5.

Table 4. Sample content of a data analysis spreadsheet (part 1).

		RHS								LHS							
Discharge		Voltage				Depth				Voltage				Depth			
		P1	P2	P3	P4	P1	P2	P3	P4	P1	P2	P3	P4	P1	P2	P3	P4
(l/min)	m3/s	(V)				(m)				(V)				(m)			
20.00	0.0003	-4.89	-4.65	-4.63	-4.58	0.0054	0.0085	0.0068	0.0063	-4.84	-4.69	-4.65	-4.65	0.0060	0.0079	0.0066	0.0055
40.00	0.0007	-4.70	-4.45	-4.37	-4.38	0.0077	0.0108	0.0098	0.0086	-4.69	-4.51	-4.46	-4.45	0.0079	0.0101	0.0088	0.0077
60.00	0.0010	-4.49	-4.30	-4.20	-4.19	0.0103	0.0125	0.0118	0.0107	-4.54	-4.35	-4.28	-4.27	0.0097	0.0120	0.0109	0.0098
80.00	0.0013	-4.35	-4.16	-4.06	-4.04	0.0120	0.0142	0.0135	0.0123	-4.42	-4.21	-4.19	-4.12	0.0112	0.0136	0.0120	0.0114
100.00	0.0017	-4.22	-4.03	-3.91	-3.90	0.0136	0.0158	0.0152	0.0140	-4.27	-4.06	-3.98	-3.96	0.0130	0.0154	0.0144	0.0133
120.00	0.0020	-4.11	-3.90	-3.78	-3.76	0.0150	0.0173	0.0167	0.0156	-4.15	-3.93	-3.85	-3.84	0.0144	0.0169	0.0159	0.0147
140.00	0.0023	-3.996	-3.771	-3.641	-3.612	0.0163	0.0188	0.0183	0.0172	-4.0305	-3.7919	-3.6965	-3.6919	0.0159	0.0186	0.0177	0.0163

Table 5. Sample content of a data analysis spreadsheet (part 2).

Depth				Area				Wetted perimeter				Hydraulic radius				Mannings n			
P1	P2	P3	P4	P1	P2	P3	P4	P1	P2	P3	P4	P1	P2	P3	P4	P1	P2	P3	P4
(m)				(m2)				(m)				(m)				()			
0.0057	0.0082	0.0067	0.0059	0.0034	0.0049	0.0040	0.0035	0.61141	0.6164	0.61341	0.6118	0.0056	0.00798	0.00656	0.00579	0.0229	0.0417	0.0299	0.0242
0.0078	0.0104	0.0093	0.0082	0.0047	0.0063	0.0056	0.0049	0.61556	0.62085	0.61866	0.6163	0.00758	0.01007	0.00905	0.00794	0.0191	0.0309	0.0258	0.0206
0.0100	0.0123	0.0113	0.0103	0.0060	0.0074	0.0068	0.0062	0.62002	0.62456	0.62268	0.62051	0.00969	0.0118	0.01093	0.00991	0.0193	0.0270	0.0237	0.0201
0.0116	0.0139	0.0127	0.0119	0.0070	0.0083	0.0076	0.0071	0.62318	0.6278	0.62544	0.62378	0.01116	0.01329	0.0122	0.01144	0.0184	0.0248	0.0215	0.0192
0.0133	0.0156	0.0148	0.0136	0.0080	0.0094	0.0089	0.0082	0.62652	0.63121	0.62957	0.62726	0.0127	0.01483	0.01409	0.01304	0.0184	0.0240	0.0220	0.0192
0.0147	0.0171	0.0163	0.0151	0.0088	0.0103	0.0098	0.0091	0.62937	0.6342	0.63261	0.63026	0.014	0.01618	0.01546	0.0144	0.0181	0.0232	0.0215	0.0190
0.0161	0.0187	0.0180	0.0168	0.0097	0.0112	0.0108	0.0101	0.63223	0.63736	0.636	0.63355	0.0153	0.01758	0.01698	0.01589	0.0181	0.0230	0.0216	0.0193

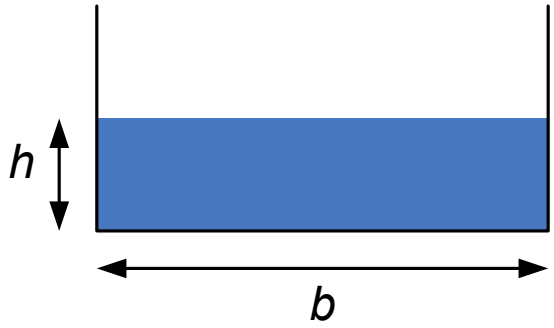

Figure 17. Illustration. Schematic of the flow in the flume above the roadway, on a vertical plane perpendicular to the flow direction.

Manning's Equation is often used to predict discharge rates in river channels:

$$Q = \frac{AR^{2/3}S^{1/2}}{n} \tag{21}$$

where Q is the flow, S is the slope of the channel, and n is the Manning's coefficient, which is a measure of the roughness of the river channel, but it varies with the flow depth and discharge in a complicated manner.

3.1.4 Results

Figure 18 shows a typical result of the analysis, with flow depth plotted against the discharge rate. The expected increase in depth with flow rate can be seen as well as a distinct variation between the gauges (referred to in the figure as *probes*).

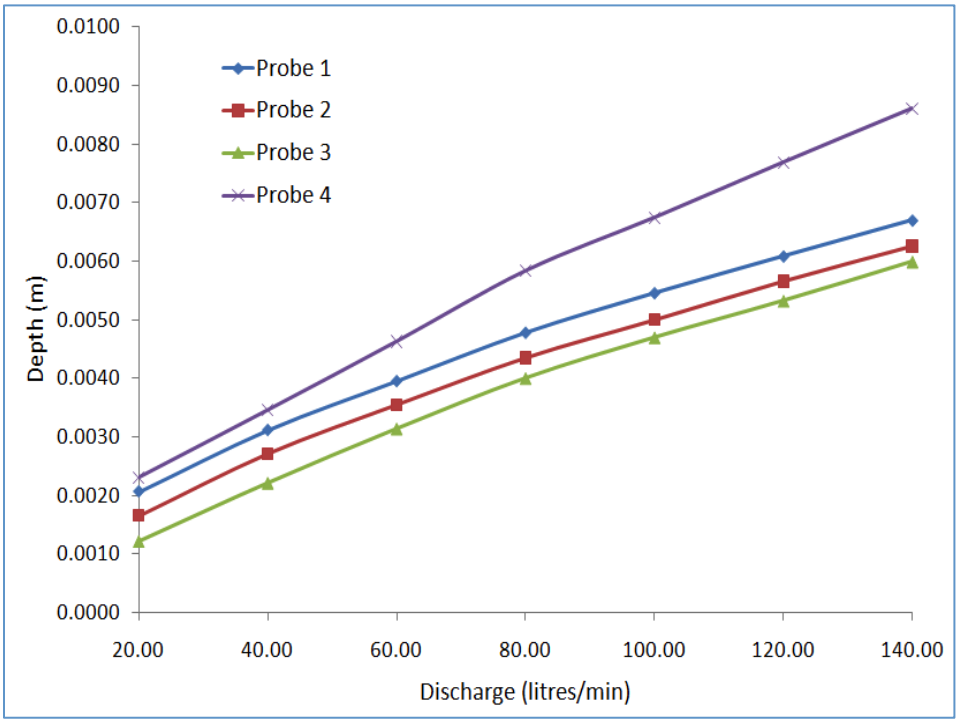

Figure 18. Graph. Sample of depth against discharge rate for one of the tests.

3.2 Water film thickness Model

3.2.1 Initial Comparison with Published Relationships

The literature reviewed in Chapter 2 revealed a number of formulas for calculating water film thickness given a number of parameters. Five of the formulas were published with full derivations, and these are listed below. They have been labeled d_1 through d_5 and have been harmonized in appearance so that d is water film thickness, T is texture depth, L is the length of the flow path (drainage length), I is rainfall rate (intensity), S is slope, and n is Manning's coefficient. The formulas used different units for the variables, but all values were converted to SI units before graphs were drawn or analysis was carried out.

(Gallaway et al., 1971)
$$d_1 = 3.38\times10^{-3}\, T^{0.11}\, L^{0.43}\, I^{0.59}\, S^{-0.42} \quad (22)$$

(Anderson et al., 1998)
$$d_2 = 3.76\times10^{-3}\, T^{0.125}\, L^{0.519}\, I^{0.562}\, S^{-0.364} \quad (23)$$

(Anderson et al., 1998)
$$d_3 = n^{0.6}\, 36.1^{-0.6}\, L^{0.6}\, I^{0.6}\, S^{-0.3} \quad (24)$$

(Roe et al., 1997)
$$d_4 = 8.68\times10^{-2}\, T^{0.5}\, L^{0.383}\, I^{0.383}\, S^{-0.333} \quad (25)$$

(Ross and Russam, 1968)
$$d_5 = 0.005\, L^{0.5}\, I^{0.5}\, S^{-0.2} \quad (26)$$

To evaluate the behavior of the formulas with respect to each of the variables, water film thicknesss d_1 through d_5 were calculated for an arbitrary range of values, one variable at a time: water film thickness was plotted against rainfall rate (Figure 19); drainage length (Figure 20); slope (Figure 21); and texture,

when present in the formula (Figure 22). The other variables in the formulas were given fixed values (listed below each graph).

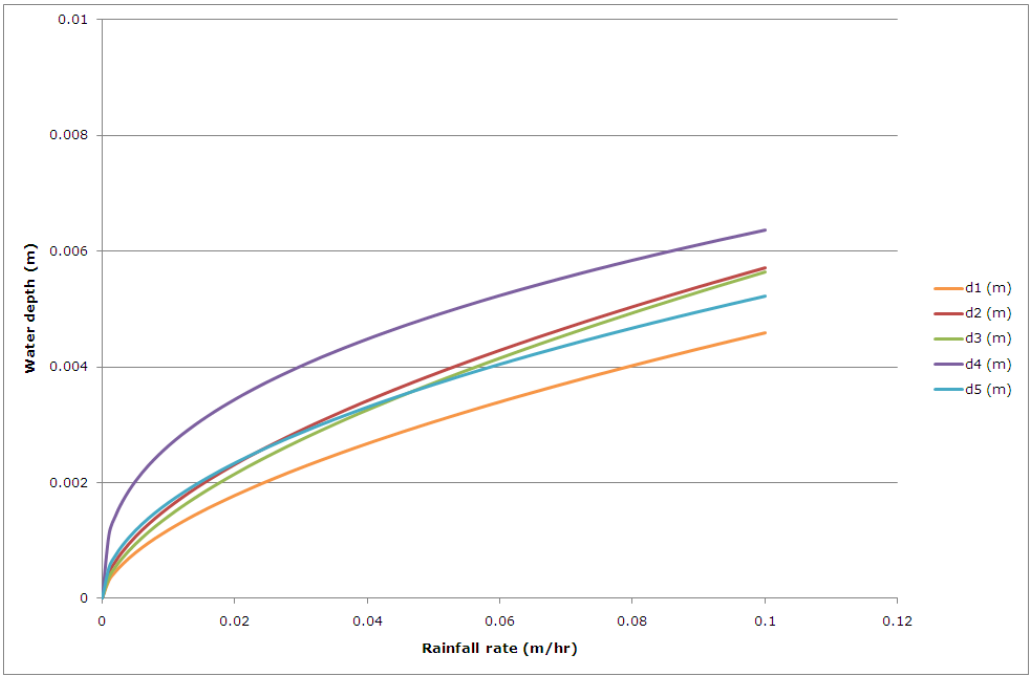

Figure 19. Graph. Calculated water film thickness (d) plotted against rainfall rate (I).
Flow length (L) fixed at 30 m, slope (S) fixed at 2.5 percent, and texture (T) fixed at 1 mm.

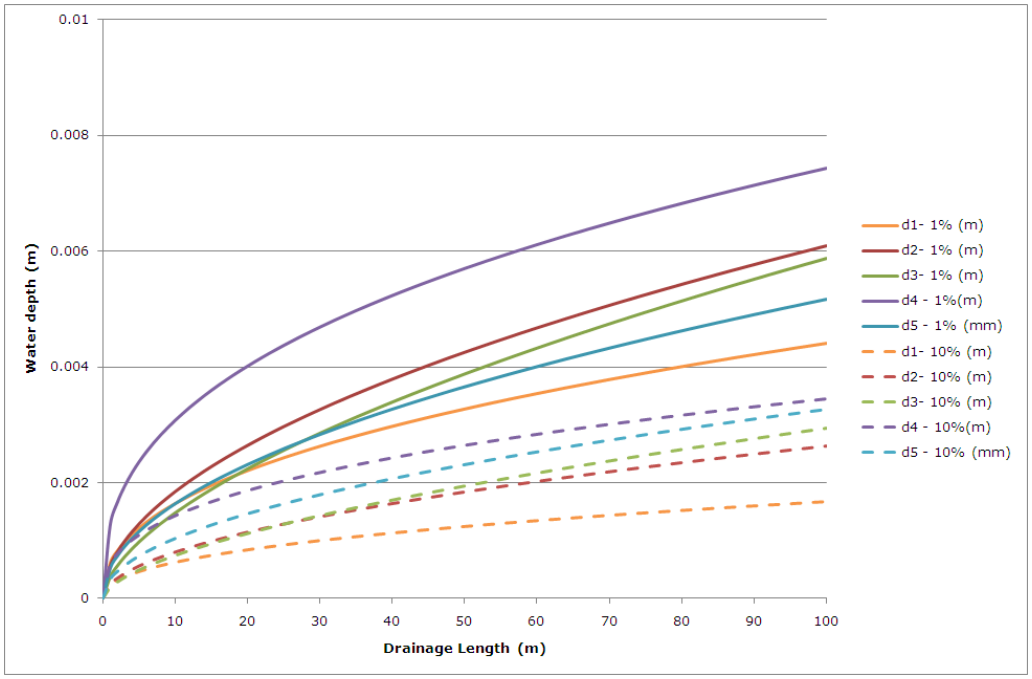

Figure 20. Graph. Calculated water film thickness (d) plotted against drainage length (L).
Rainfall rate (I) fixed at 0.02 m/hr, slope (S) fixed at 1 percent and 10 percent, and texture (T) fixed at 1 mm.

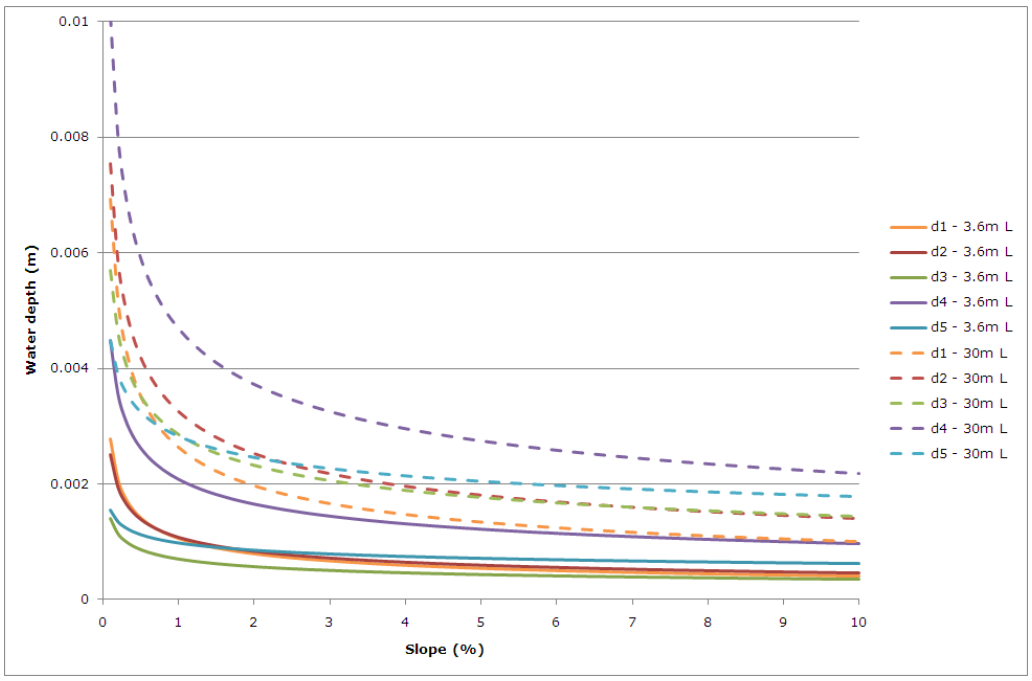

Figure 21. Graph. Calculated water film thickness (d) plotted against slope (S).
Rainfall rate (I) fixed at 0.02 m/hr, drainage length (L) fixed at 3.6 m and 30 m, and texture (T) fixed at 1 mm.

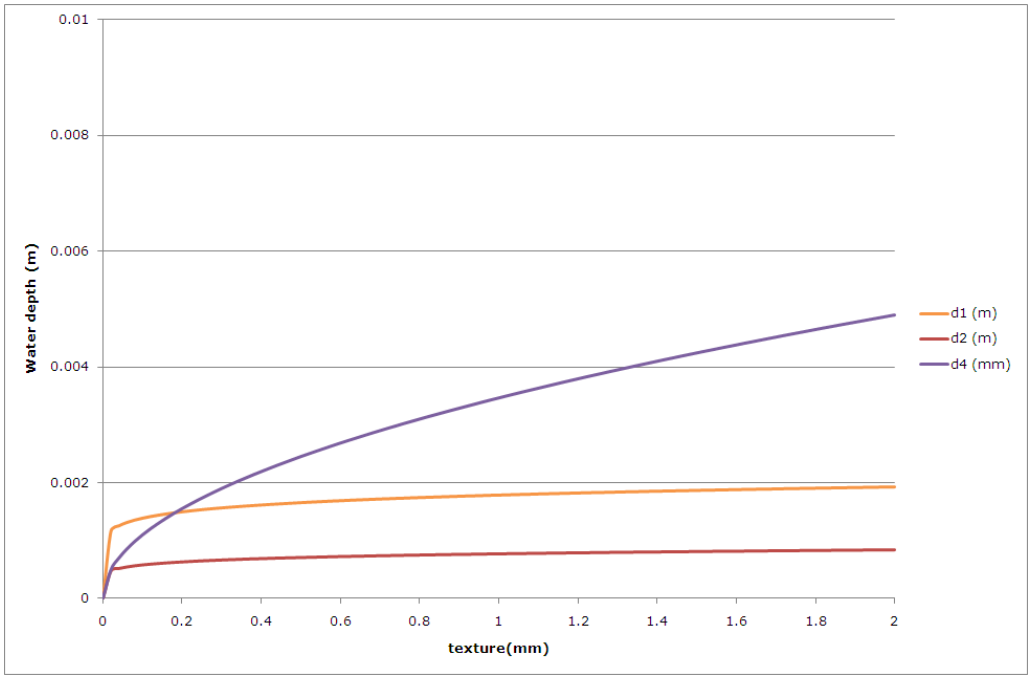

Figure 22. Graph. Calculated water film thickness (d) plotted against texture (T).
Rainfall rate (I) fixed at 0.02 m/hr, drainage length (L) fixed at 30 m, and slope (S) fixed at 2.5 percent..

The graphs in Figure 19 to Figure 22 show that all the formulas have the same general shape and that using any of them would produce similar outcomes. Flume measurements in Figure 23 and Figure 24 are from the first experiment carried out when the SMA surface was in place with a 0.5 percent slope. The water film thicknesses measured in the flume were plotted against the rainfall rate and drainage length along with the depths calculated from d_1 through d_5.

The volume of water in the flume is much higher than would be expected in a rain shower. However, when values in the range of the quantities rein the flume are used in the formulas (Equations 22–26), the calculated values and the initial flume measurements conform to the same general shape when plotted, as can be seen in Figure 23 and Figure 24.

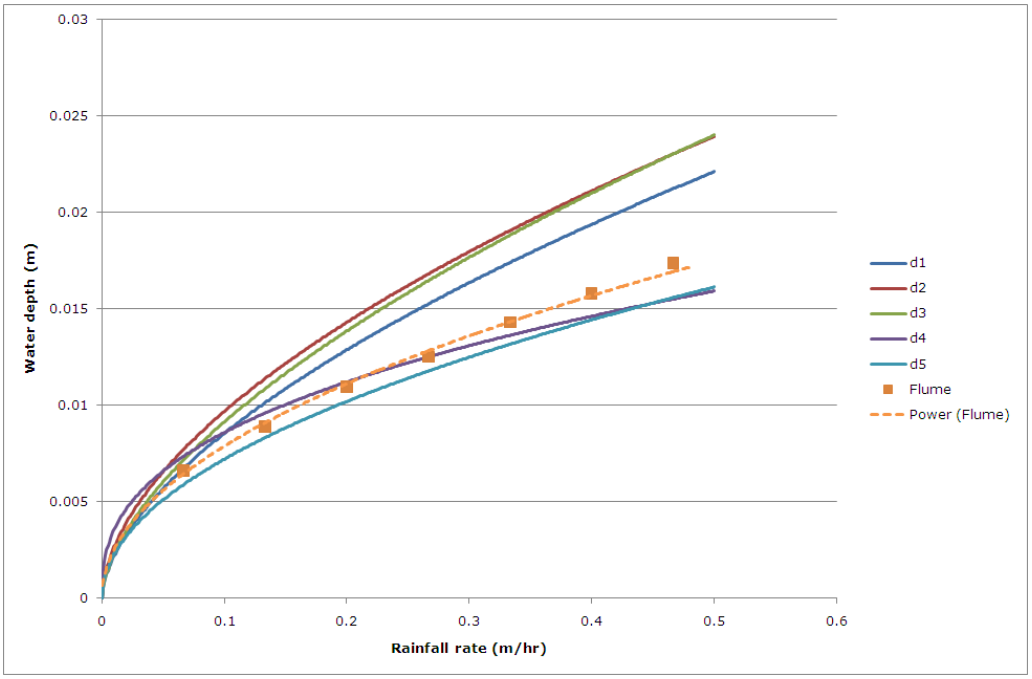

Figure 23. Graph. Measured water film thickness (Flume) and calculated water film thickness (d_1 through d_5) plotted against rainfall rate (I).

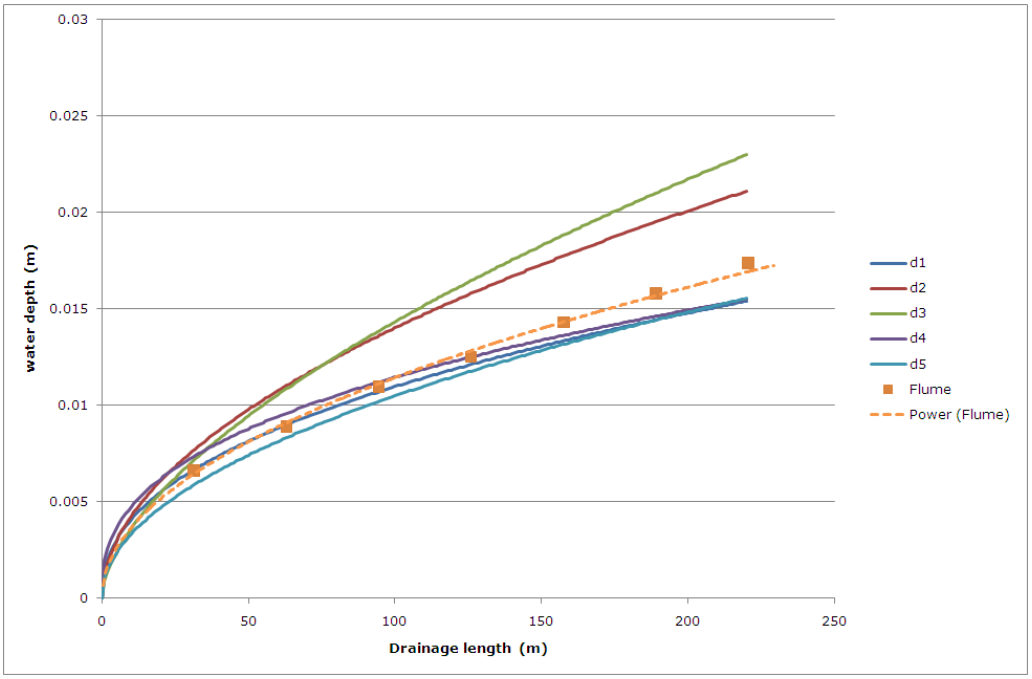

Figure 24. Graph. Measured water film thickness (Flume) and calculated water film thickness (d_1 through d_5) plotted against drainage length (L).

3.2.2 Generic Model

3.2.2.1 Form of the Equation

The main difference between the formulas was the powers to which the variables were raised. Based on the equations from the literature review, a generic formula was written:

$$d = k\ T^{w}\ L^{x}\ I^{y}\ S^{z} \quad (27)$$

where:
d = water film thickness (m)
T = texture (mm)
L = drainage length (m)
I = rainfall intensity (m/h)
S = slope (ratio)
k = constant that incorporates Manning's coefficient
w = constant in the range 0.11 to 0.5
x and y = constants in the range 0.383 to 0.6
z = constant in the range -0.42 to -0.2

3.2.2.2 Finding Values for Powers

To find a value for *w*, texture depth on each of the surfaces was measured using a circular texture meter. Table 6 shows the average depth for each surface. The flume measures the discharge of water leaving the end of the flow, which is the volume of water leaving the flume over time (m^3/hr). The discharge from the flume divided by the width of the flume (m^2/hr) is equivalent to rainfall intensity (m/hr) times the drainage length (m). Therefore, rainfall intensity (I) and drainage length (L) can be combined and raised to the same power, which is the case for three of the five formulas found in the literature. The generic formula is therefore rewritten as:

$$d = k\ T^{w}(L\,I)^{y} S^{z} \quad (28)$$

Table 6. Texture depths of surfaces used in flume.

Material	Texture (mm)
Stone mastic asphalt	0.549
Dense-graded asphalt	0.633
Porous asphalt	1.644
Tined concrete	1.011
Smooth concrete	0.208
Perspex	0.001[9]

[9] The texture depth of the Perspex is an estimate, as the clear surface was not suitable for measurement with the circular texture meter.

The generic formula was manipulated into a linear relationship by taking the natural log of both sides:

$$\ln(d) = \ln(k) + w\ln(T) + y\ln(LI) + z\ln(S) \quad (29)$$

Then using the texture depths and slopes of each of the surfaces, the average water film thicknesses during the experiments, and the discharge rate divided by the width of the flume, the constant k and the power terms w, y, and z were found using multiple linear regression, resulting in Equation 30:

$$d = 6x10^{-4}\, T^{0.09}\, (LI)^{0.6}\, S^{-0.33} \quad (30)$$

Figure 25 through Figure 30 compare the results from the flume for each of the surfaces to the results calculated from the water film thickness formula in Equation 17. In each graph, the flume experiment results are plotted with large diamonds, squares and triangles for 0.5 percent, 2 percent and 6 percent slopes, respectively. The smaller points show values calculated from the generic formula over the same range.

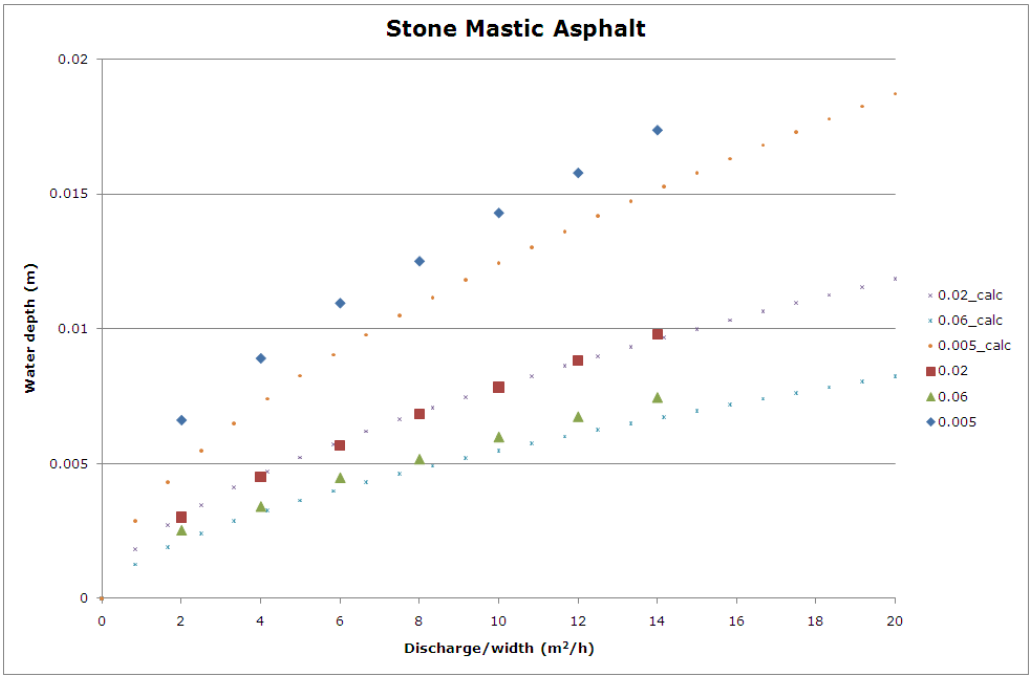

Figure 25. Graph. Comparison of flume results with results calculated from water depth formula for the stone mastic asphalt surface.

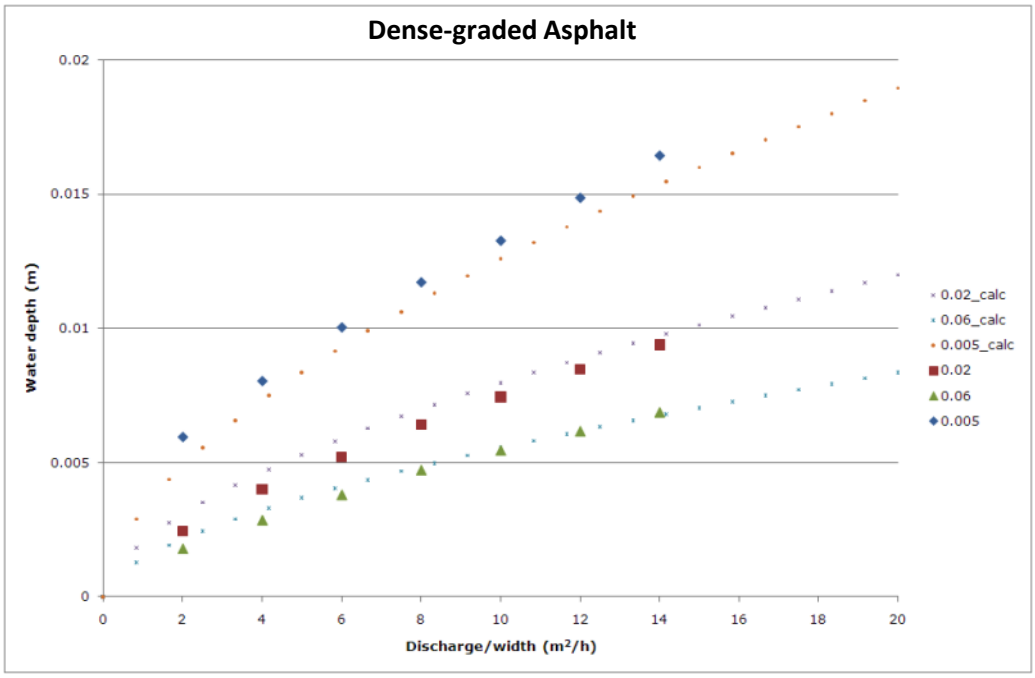

Figure 26. Graph. Comparison of flume results with results calculated from water depth formula for the asphaltic concrete surface.

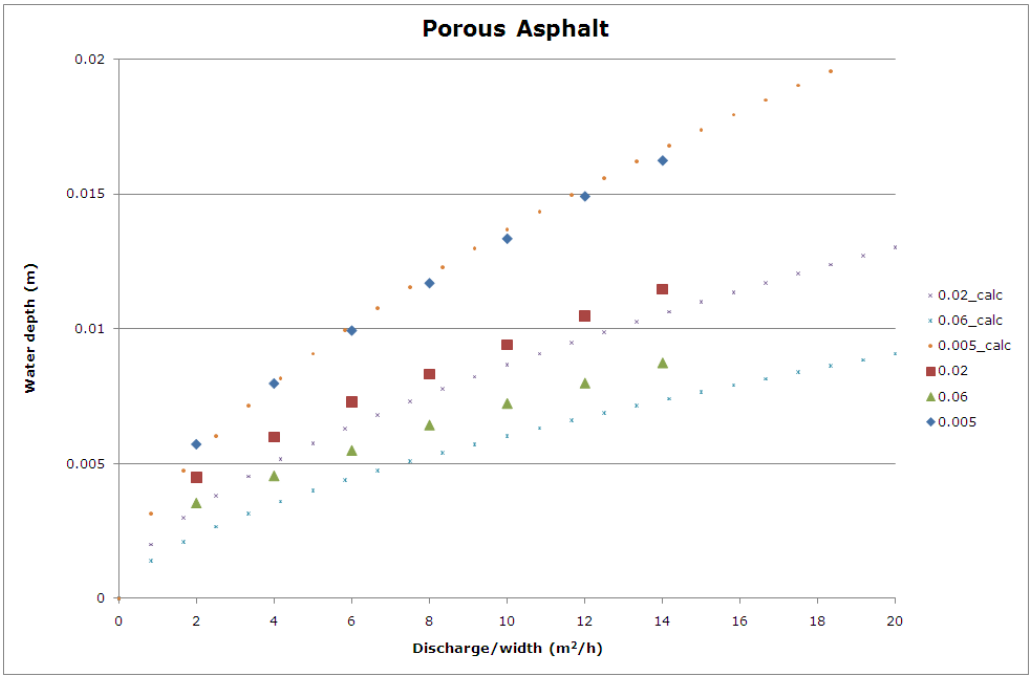

Figure 27. Graph. Comparison of flume results with results calculated from water depth formula for the porous asphalt surface.

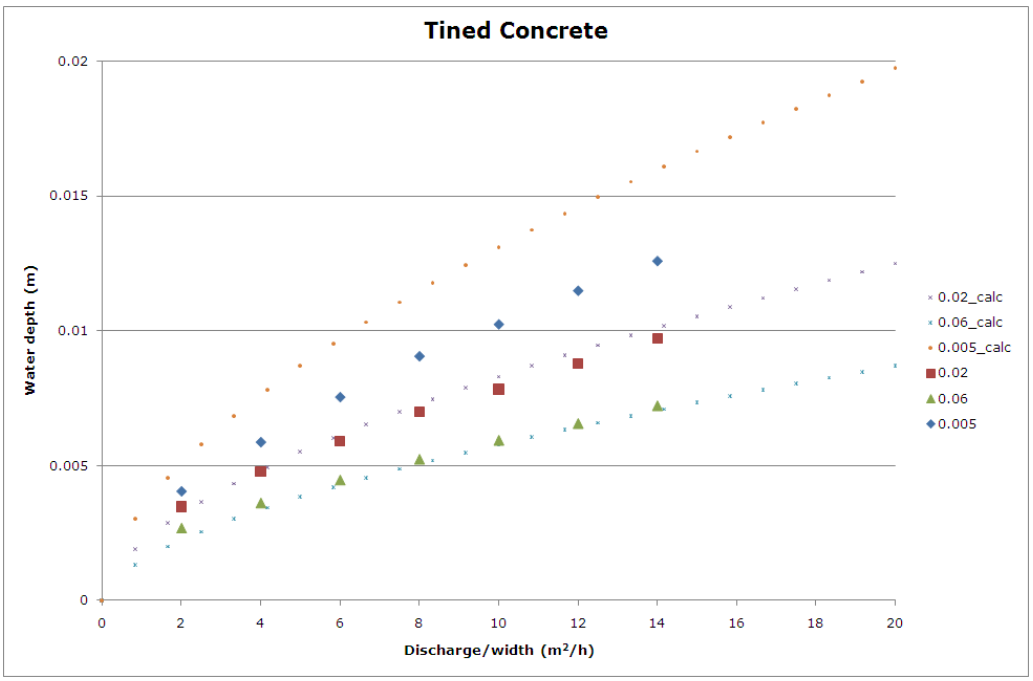

Figure 28. Graph. Comparison of flume results with results calculated from water depth formula for the tined concrete surface.

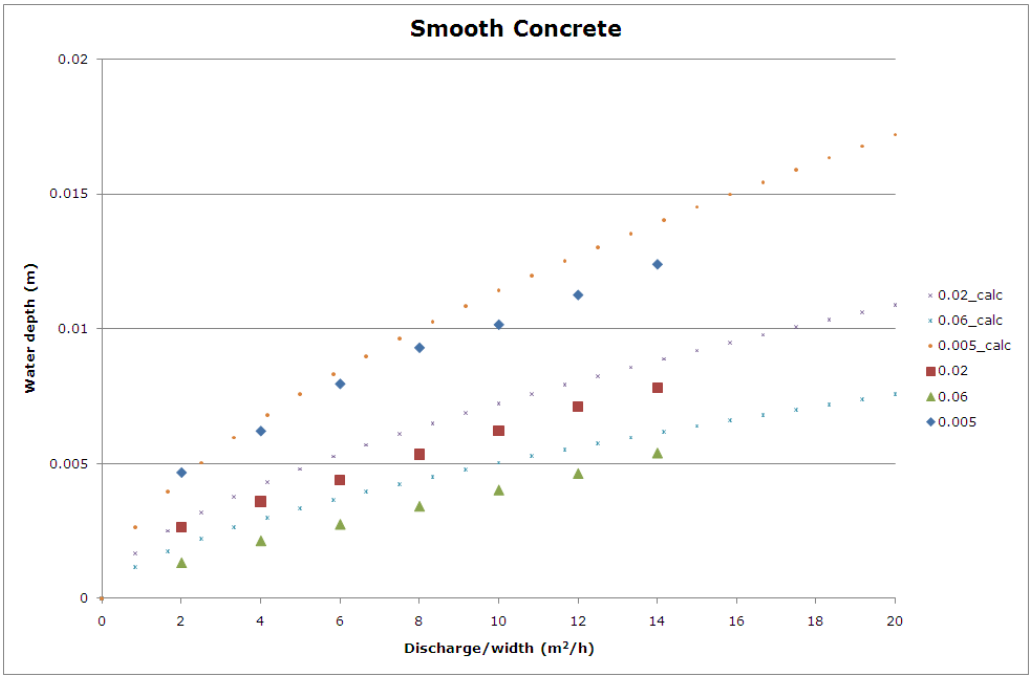

Figure 29. Graph. Comparison of flume results with results calculated from water depth formula for the smooth concrete surface.

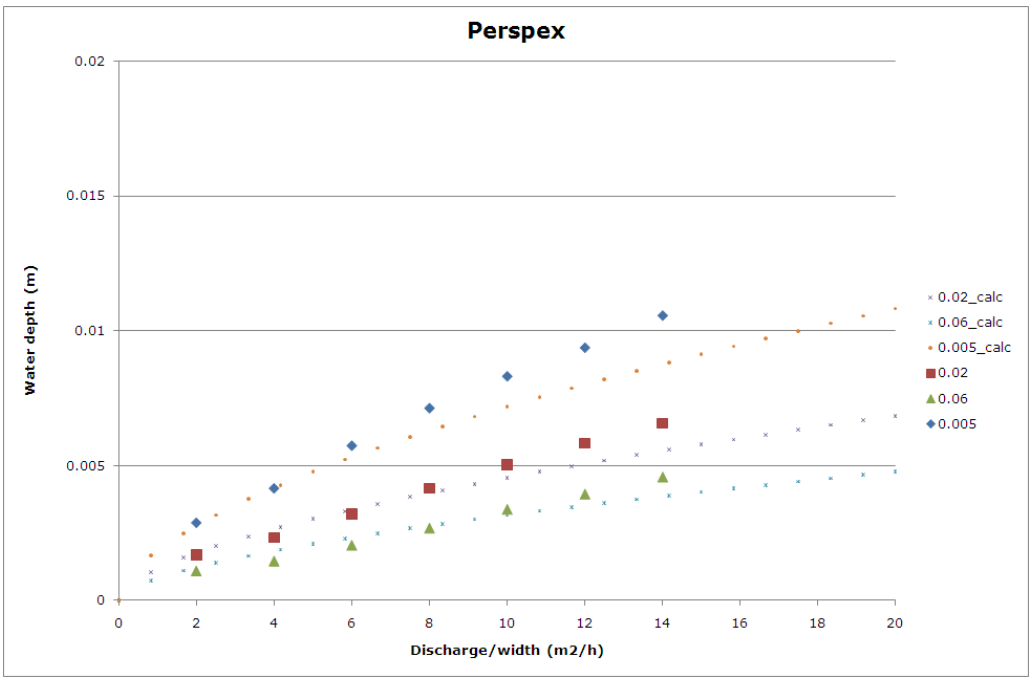

Figure 30. Graph. Comparison of flume results with results calculated from water depth formula for the Perspex surface.

3.3 Discussion

In general, water film thickness formulas proposed in the literature have the same structure with varying parameters (coefficients). Using the results of the flume experiment, the parameters were calibrated and the final proposed formula is presented in Equation 30.

The results calculated from this new formula were plotted alongside the results from the flume for each of the surfaces, and the following observations were made: (1) the water depth increases as the slope decreases; and (2) The water depth is lower for smooth surfaces.

The calculated water depths fit the experimental data better for some surfaces (asphaltic concrete and porous asphalt) than others (smooth concrete and Perspex). When the multi-linear regression was carried out on the results from the flume to find the values of the constants in Equation 30, the coefficient of determination for the regression was 93.4 percent. It should be noted that the quantity of water in the flume is much higher than the amount of water expected on the pavement.

4 Water Exposure Model[10]

The second component of the splash and spray model consists of determining the rainfall expected for the location of the roadway section under consideration. Previous research on wet exposure has considered various criteria. For example, Harwood et al. (1988) developed a method to calculate wet exposure based on recorded minimum rainfall, because the recorded minimum rainfall (0.01 inch/hr) makes "pavement damp enough to cause accident." In a project for the California Department of Transportation (CalTrans), Wang et al. (2008) updated the California Wet Percentage Time table. Wet percentage time refers to the amount of time during which there is precipitation, including rain or snow, on the given area. In the CalTrans study, the pavement condition was classified as wet when at least a measurable amount (0.01 inches) of precipitation occurred. The study combined this wet percentage table with the wet accident record to find the area of highest wet-accident risk in California.

This chapter presents the development of an exposure model that is relevant for the prediction of splash and spray potential. The model considers wet exposure as the percentage of a year that pavement receives a specified minimum amount of rainfall. A roadway's capability of generating splash and spray is then decided by both precipitation intensity and pavement surface propensity, as discussed in Chapter 6. The precipitation data for the entire United States (2000–2009) were extracted from the National Climate Data Center (NCDC). The approach is similar to the previous wet exposure research by Harwood (1988), but it provides more comprehensive precipitation exposure characterization by further enabling the consideration of pavement surfaces' splash and spray propensity.

4.1 Methodology and Data Sources

As previously mentioned, the wet exposure needed for the splash and spray model is the percentage of a year that enough water exists on the pavement surface to potentially generate splash and spray during tire-pavement interaction. This research considers precipitation to be the only source of pavement surface water. Thus, the wet exposure is determined by the precipitation and the pavement surface properties (e.g., surface texture, geometry, and drainage).

Two kinds of boundaries in the calculation of wet exposure are considered in this chapter:

- Minimum precipitation: Minimum precipitation refers to the minimum precipitation intensity needed for a pavement to produce splash and spray from passing vehicles. This minimum precipitation is dependent upon pavement surface properties (permeability, slope, etc.) and the duration of the precipitation event (e.g., 15 minutes, 1 hour). The wet exposure based on the minimum precipitation can be recognized as splash and spray capable exposure.

- Critical precipitation: A pavement's capability to produce splash and spray does not necessarily mean that the generated splash and spray is disturbing to road users. Adding vehicle speed and type to the wet exposure calculation yields the critical precipitation, or the minimum intensity of precipitation that puts enough water on the pavement to cause disturbing splash and spray. The wet exposure based on the critical precipitation can be recognized as splash-and-spray risk exposure, which is more significant than the splash-and-spray-capable exposure from minimum precipitation.

Finding the minimum and critical precipitations for different pavement surfaces is one of the main tasks of the FHWA splash and spray project. However, these two values are still not available for most of the pavement types. Instead of considering two boundaries, the wet exposure model considers all levels of

[10] This chapter is an expanded version of the paper "Exposure Model for Predicting Splash and Spray," by L. Tang, G.W. Flintsch, and H. Viner, presented at the *7th International Symposium on Pavement Surface Characteristics* (SURF 2012), Sep. 18-21, 2012, Norfolk, Va.

precipitation intensity in a given time period to present a wet exposure versus intensity curve. With this curve, one can easily find the corresponding wet exposure for a particular pavement surface, if the pavement surface property is known.

The wet exposure (WE) calculation requires large data sources. Table 7 presents an example: for a single weather station, the wet time depends on the recorded precipitation depth over a given time interval of 1 hour and chosen minimum precipitation intensities. The wet exposure is the wet time in hours over a year period divided by the total number of hours in a year. It is important to note that the wet hours calculated are always higher than the actual total precipitation time.

Table 7. Example of single-station calculation.

<table>
<tr><th colspan="2">Precipitation Records</th><th colspan="2">Minimum Precipitation
(0.01 inches)</th><th colspan="2">Critical Precipitation
(0.03 inches)</th></tr>
<tr><td>Date (hour)</td><td>Depth (inches)</td><td>Wet Hours</td><td>Wet Exposure (WE)</td><td>Wet Hours</td><td>Wet Exposure</td></tr>
<tr><td>01/01/2001 1:</td><td>0.03</td><td rowspan="5">The total number of hours having 0.01 inches or more depth of precipitation:
N = 350</td><td rowspan="5">WE = 350/(365×24)
= 4.00 percent</td><td rowspan="5">The total number of hours having 0.03 inches or more depth of precipitation:
N = 120</td><td rowspan="5">WE = 120/(365×24)
= 1.37 percent</td></tr>
<tr><td>01/01/2001 2:</td><td>0.01</td></tr>
<tr><td>…</td><td></td></tr>
<tr><td>12/31/2001 23:</td><td>0.08</td></tr>
<tr><td>12/31/2001 24:</td><td>0.00</td></tr>
</table>

The project used as a data source the 1-hour precipitation records of the NCDC. The 10-year hourly precipitation data from January 1, 2000, to December 31, 2009, for 2,885 stations were extracted from the NCDC database and subjected to a quality control process. Figure 31 presents a map showing the density and distribution of feasible data stations. The map shows that the available stations cover all of the United States. However, the density of stations is not enough to cover every single county, which is the minimum level of coverage desired in this research. A geographic information system (GIS) was used as the base platform to store and process the precipitation data and visualize the results. The ArcGIS spatial interpolation tool was used to generate the wet exposure parameters for each county.

Figure 32 summarizes the process for preparing the single-station data tables. The process started with the extraction of the hourly precipitation data from the NCDC online database. The data then underwent a quality control check, and the accepted data were integrated into the existing database and GIS shapefile. Then, by using the wet exposure calculation program and GIS spatial interpolation tool, the databases delivered part of the final product, which is point wet exposure results and an exposure raster map. Finally, the zonal tool was used to calculate the county-level wet exposure data based on the county map and raster map.

The single-station and the county-wide wet exposure data can provide the approximate wet exposure for any roadway section in the continental United States. Users can choose the single county-wide factor to do a quick wet exposure, or they can look into the yearly series and nearby stations to find a better fit for their specific condition.

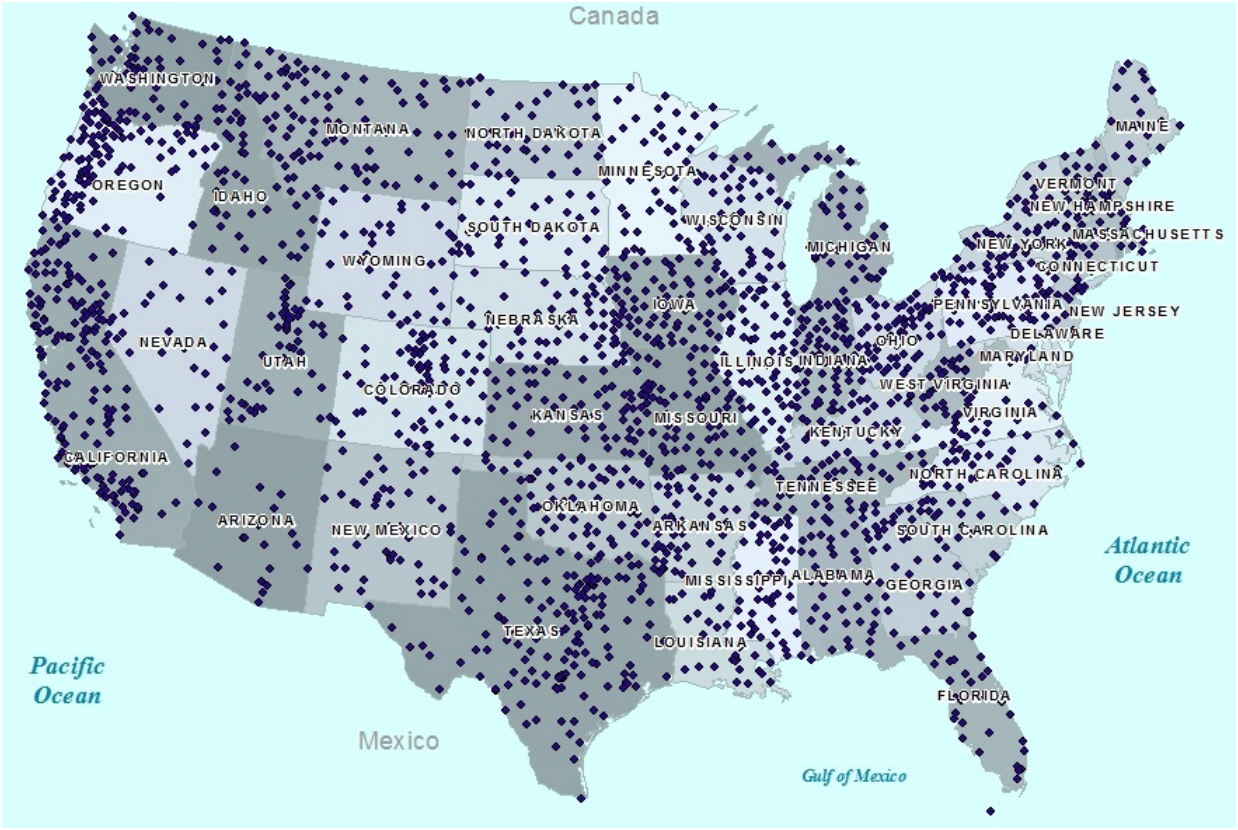

Figure 31. Map. Precipitation stations in the continental United States.

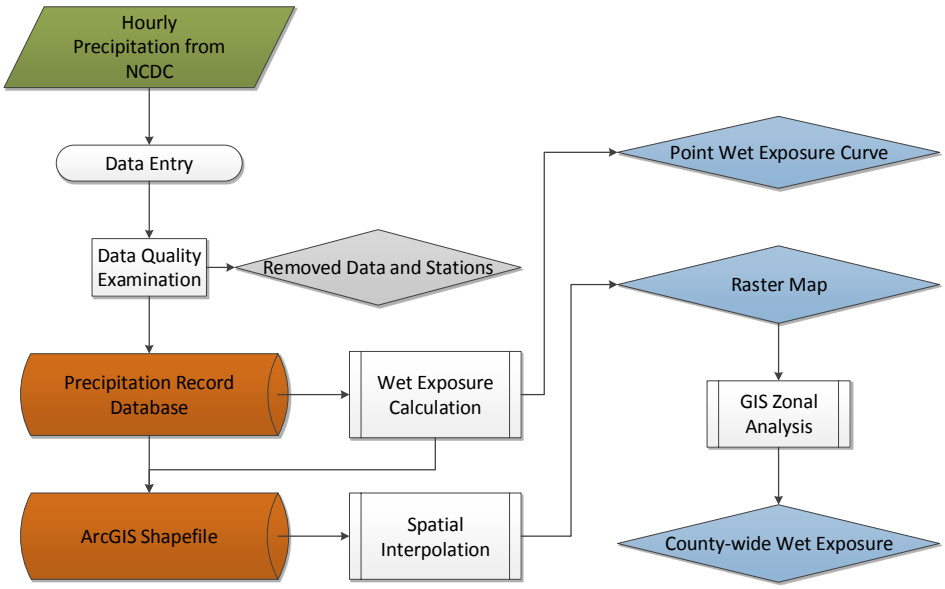

Figure 32. Flow chart. Data process.

4.2 Results

The wet exposure model integrated into the splash and spray assessment tool to calculate the splash and spray potential in the continental United States includes two databases, one containing the information for all stations and another that contains the average data for each county in the United States.

4.2.1 Single-Station Database

For each available weather station, the research team computed the wet hours and wet percentage for different levels of precipitation and developed wet exposure curves using the 10-year wet exposure data. Table 8 shows an example of the wet exposure data available for a given single station in a given year. For each year, the table shows wet hours (WH) and exposures (WE) for different precipitation thresholds, varying from 1 inch. The data inventory included the 10-year time series for about 3,000 stations.

Table 8. Example of wet hours and wet percentage by station.

Station	Year	Lower Boundary of Precipitation (inches)						
		1		0.8, 0.6, 0.4, 0.2, 0.1, 0.05	0.02		0.01	
		WH1	WE1 (percent)	…	WH0.02	WE0.02	WH0.01	WE0.01
Anniston	2000	1	0.01		109	1.24	377	4.3
Anniston	2002	1	0.01		127	1.45	443	5.1

The wet exposure routine calculates the wet exposure for different levels of precipitation and presents them in a curve, which summarizes wet exposure for a single station. Figure 33 and Figure 34 show an example of wet hour curves for one station. Once the user specifies boundaries for minimum and critical splash and spray levels, the model can find the corresponding wet exposure. This curve can also be used to find the exposure for other water-related pavement phenomenon, such as hydroplaning.

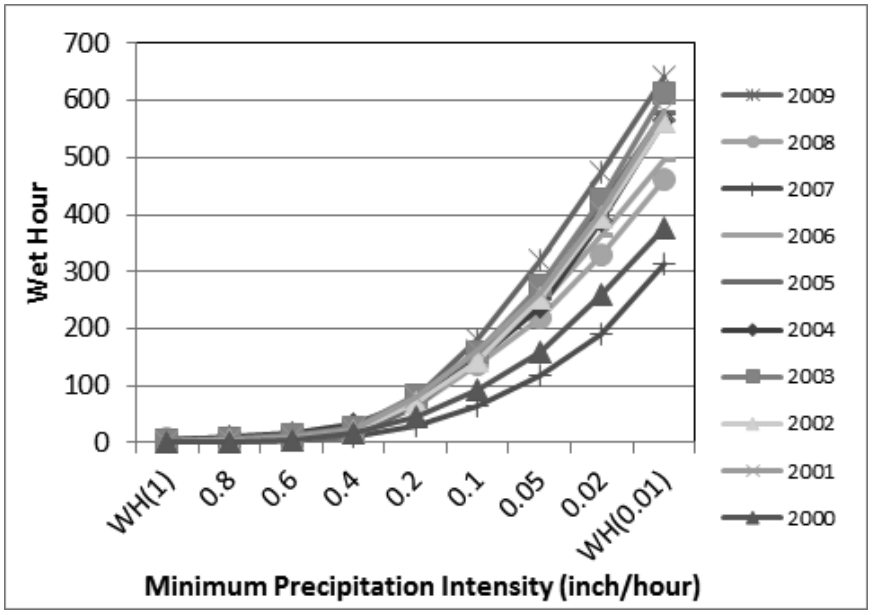

Figure 33. Graph. Example of a single station's wet hour curve (Anniston ARPT ASOS).

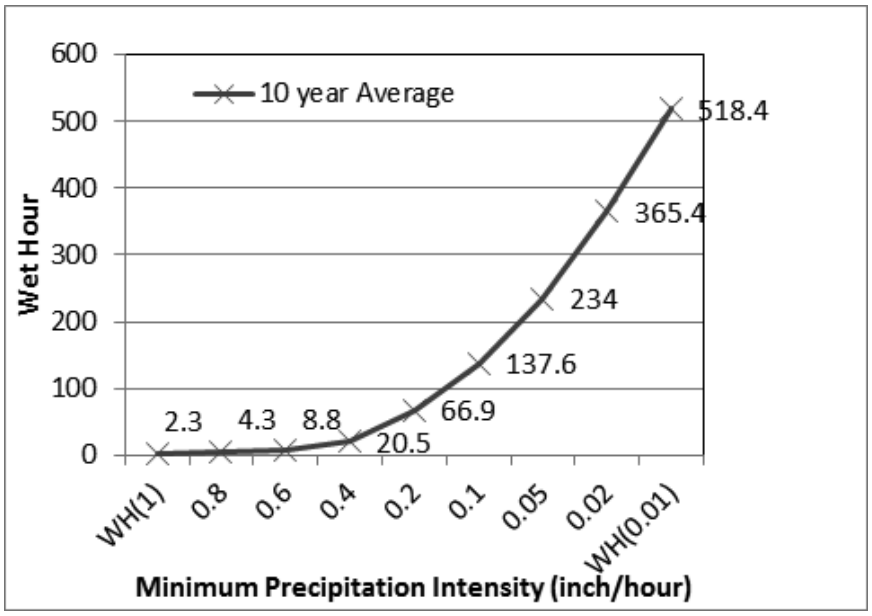

Figure 34. Graph. Example of a single station's 10-year average wet hour curve (Anniston ARPT ASOS).

Figure 35 shows the 10-year series of wet percentage values and their average for the same station. The results of these graphs can indicate the variability of wet exposure from year to year. Because the objective of this research is to mitigate the adverse effect of splash and spray in the future, the average value was considered the most appropriate.

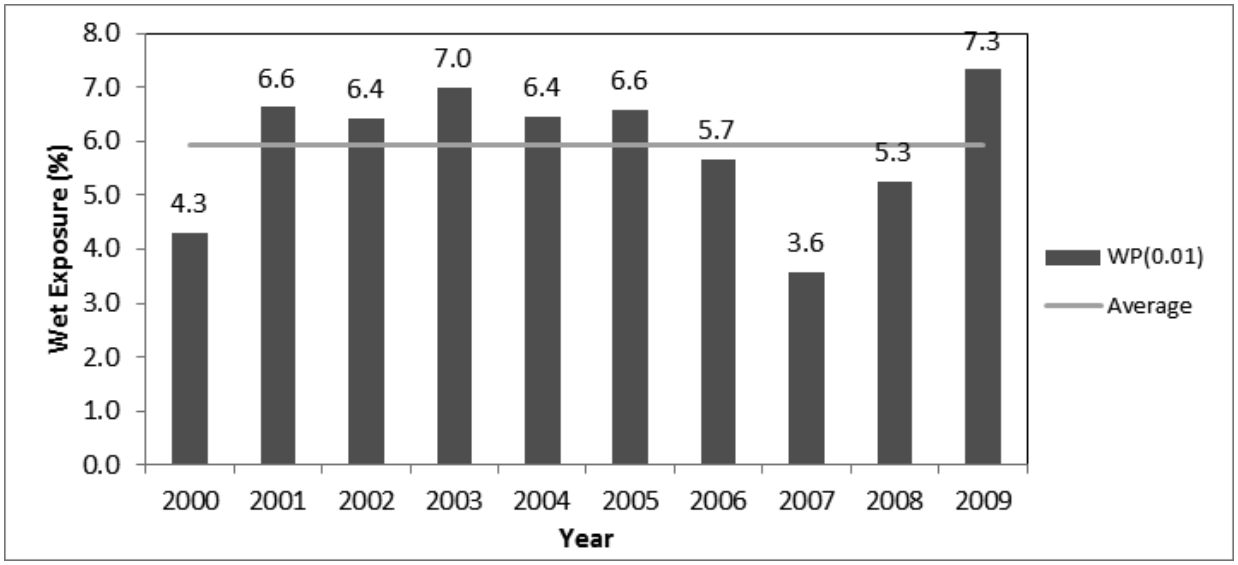

Figure 35. Graph. Example of a single station's wet percentage (Anniston ARPT ASON).

4.2.2 County-Wide Wet Exposure

To obtain wet exposure information for all counties of the United States, spatial interpolation was used to estimate an exposure value for the areas where stations are not currently available. The spatial interpolation method used was the inverse distance weighted (IDW) method, which bases the wet exposure value of areas without stations on the values of nearby stations and their distances to the area in question. The ArcGIS documentation gives the following explanation of this method:

> *IDW interpolation explicitly implements the assumption that things that are close to one another are more alike than those that are farther apart. To predict a value for any unmeasured location, IDW will use the measured values surrounding the prediction location. Those measured values closest to the prediction location will have more influence on the predicted value than those farther away. Thus, IDW assumes that each measured point has a local influence that diminishes with distance. It weights the points closer to the prediction location greater than those farther away, hence the name inverse distance weighted.*

Figure 36 shows a raster map with the available weather stations and the interpolation result for the wet exposure data. The resulting data can be used to compute the average wet exposures (percentage) for each county in the United States. Figure 37 shows the average wet exposure for each county. By using this map, the splash and spray assessment tool can get the wet exposure data for the particular county where the pavement section being studied is located. The research team used this procedure to compute the wet exposure map and data for each county for 10 years and each county's average.

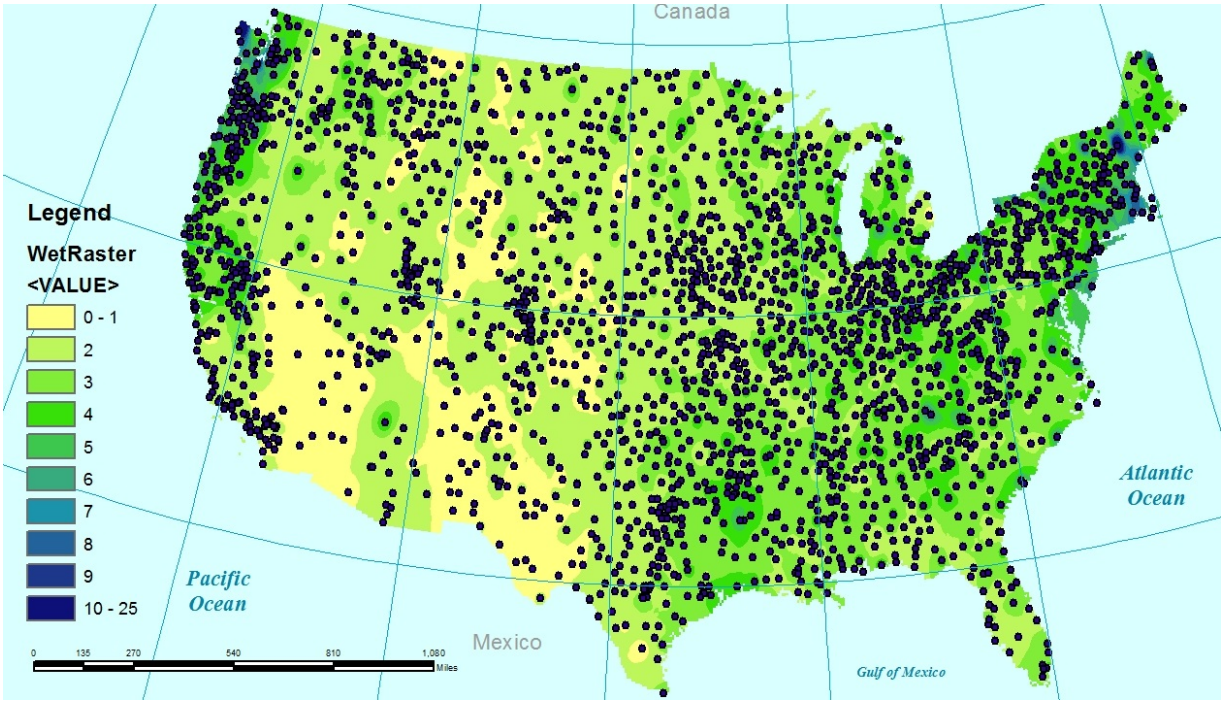

Figure 36. Map. Wet exposure (percentage) interpolation raster map for the year 2000.

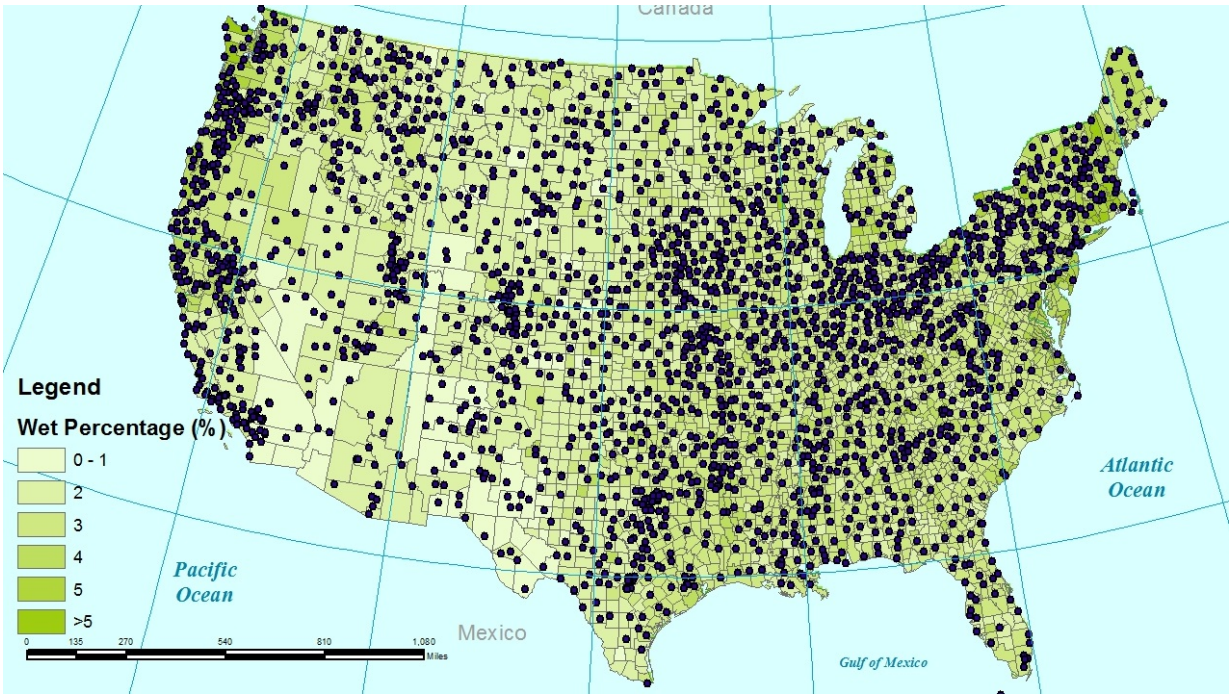

Figure 37. Map. Counties' wet percentage map.

4.3 Discussion

In addition to providing the foundation for the exposure component of the splash and spray model, the precipitation data analysis allowed the researchers to study other issues related to modeling exposure for vehicle-road interaction. The following sections discuss the major finding of this analysis.

4.3.1 Wet Pavement Exposure Impact on the User

The type of precipitation characterization parameters needed for modeling tire-pavement interactions is different from the precipitation parameters used for agriculture or river hydrology purposes. For agriculture, the total precipitation amount is more important than the amount of rain falling within a period of time. For example, long-duration, low-intensity rain can keep pavement wet for a long time and increase the potential of accident by increasing the exposure of vehicles to lower skid resistance and lower visibility (because of splash and spray), as well as increase the fatigue of drivers. As a result, for wet exposure calculation, a wide range of rain intensity should be considered. The wet times corresponding to several intensities are needed for weather-related pavement design and management.

4.3.2 Relationship between the Total Precipitation and Wet Exposure

Figure 38 compares the 10-year average precipitation to the 10-year average wet percentage as used in this project. The data points fall into a cone-shaped area. The linear regression trend line for these two data sets gives a low coefficient of determination, which suggests that it would not be appropriate to use total precipitation alone as a surrogate for the percentage wet exposure.

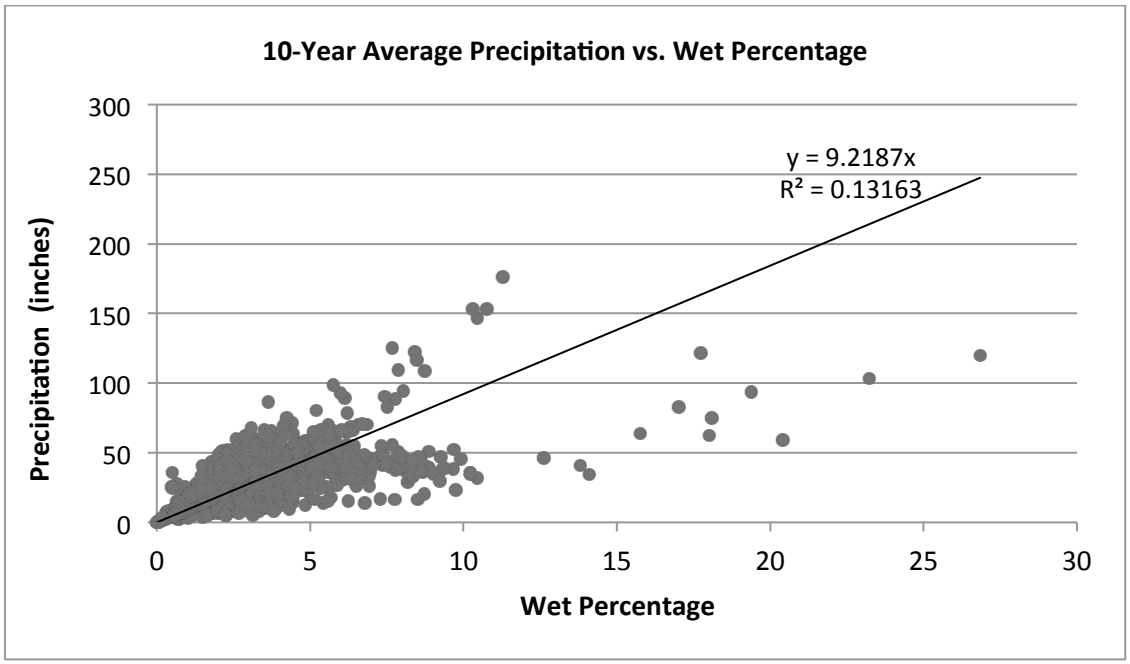

Figure 38. Graph. Correlation of wet percentage with precipitation.

4.3.3 Data Quality

The accuracy of wet exposure estimates depends on the accuracy of the hourly precipitation data collected by the stations. The total number of hours of missing data per year varied from 0 to the total recorded hours (ID: 10116, 552/552); Table 9 shows some sample data. To mitigate the bias that missing hours may have introduced to the wet exposure estimates, stations missing more than 10 percent of their total recorded hours were excluded from the analysis.

Table 9. Sample of available stations' data.

Station	Year	State	County	Lat	Longi	ELE	**Missing hours**	**Recorded Hour**
Abbeville	2009	Alabama	Henry	31.57	-85.25	456	**62**	**2472**
Addison	2009	Alabama	Winston	34.26	-87.18	818	**34**	**1128**
Alabaster Shelby Co AP	2009	Alabama	Shelby	33.18	-86.78	565	**552**	**552**
Alberta	2009	Alabama	Wilcox	32.23	-87.41	175	**71**	**2712**
Andalusia 3 W	2009	Alabama	Covington	31.31	-86.52	250	**0**	**2088**
Anniston ARPT ASOS	2009	Alabama	Calhoun	33.59	-85.86	594	**0**	**3576**

4.4 Conclusions

This chapter presented the development of a wet exposure model, one of the components of the splash and spray model. The wet exposure model can also be useful for supporting the modeling of other interactions between vehicles and wet pavement, such as wet friction. The model uses data from the NCDC to compute nationwide wet exposure data and create an inventory of the expected percentage of time that precipitation intensity will exceed different precipitation thresholds. A GIS-based spatial

interpolation process was developed to estimate wet exposure for the counties without an available precipitation station and to compute the average wet exposure for counties in which more than one station was available.

The primary limitation in the calculation process is the quality of the raw data. Many recorded hours are missing, and this impacts the accuracy of the predictions. However, the inventory of wet hours does provide enough information to predict user exposure to different levels of potential splash and spray.

5 Assessment of the Impact of Splash and Spray on Road Users – Controlled Experiment Results[11]

This chapter describes the methodology and results from a set of field tests assessing the impact of splash and spray on road users. These tests linked the experimental data, the splash and spray model, and threshold values for the classification of the model output. This information was used to quantify user responses (subjective ratings) to a range of different conditions under controlled conditions at the Virginia Smart Road.

Splash and spray causes a significant nuisance to motorists and, under some conditions, can cause a momentary loss of vision. There is a small but measureable increase in accident risk related to splash and spray, according to accident studies. The existing body of research does not provide the accurate number of accidents caused by splash and spray, and estimates of the small proportion of accidents caused directly by splash/spray include 0.011 percent (the Fatality Analysis Reporting System, FARS) and 0.0036 percent (the National Automotive Sampling System, NASS, and the General Estimates System, GES); both these statistics are reported by NHTSA (2000). However, the small size of these percentages could partly be due to most records not considering splash or spray as a possible cause in accidents, meaning many crashes related to splash and spray may have gone unrecorded. It is unlikely that splash and spray are a significant accident risk, but improved control of splash and spray could improve comfort and reduce nuisance experienced by motorists.

The gap between task demand and capability is the driver's safety margin; momentary changes in the environment, including the presence of splash or spray, will raise task demand and reduce a driver's safety margin significantly (Fuller, 2005). It is likely that, most of the time, a driver's safety margin when driving through splash or spray is much reduced, increasing the driver's feelings of risk and anxiety.

There have been a limited number of studies related to the human interaction with splash and spray; however, work carried out by Baughan et al. (1983) showed that spray from heavy vehicles was the highest rated "problem" that heavy vehicles cause to motorists. Pilkington (1990) and NHTSA (2004) presented a series of splash and spray's possible consequences, which can be separated into three categories: gradual loss of vision, sudden loss of vision, and shock.

To capture user perceptions for this study, the research team asked participants to view drivers'-eye videos of splash and spray under different conditions (described in Section 5.1.1) and to rate a series of dependent variables:

- **Obstruction**: As a measure of how splash and spray affected visibility, participants were asked to rate how obstructed their view of the roadway was. Participants answered using a seven-point scale, where 1 meant their view was obstructed "very little" and 7 meant it was obstructed "very much."
- **Concentration**: Participants were asked to rate how much concentration would be required for each driving condition. Participants answered using a seven-point scale, where 1 meant it would require "very little" concentration and 7 meant it would require "a lot" of concentration.
- **Confidence:** Participants were asked to rate how confident they would feel driving in each condition. Participants answered using a seven-point scale, where 1 meant "not confident" and 7 meant "very confident."

[11] This chapter is an expanded version of the paper "Assessment of the Impact of Splash and Spray on Road Users - Controlled Experiment Results," by G. Flintsch, B. Williams, R, Gibbons, and H. Viner, published by the *Journal of the Transportation Research Board*, 2012, Vol 2306, pp. 151-160.

- **Control**: Participants were asked to rate how much control they feel they would have in each driving condition. Participants answered using a seven-point scale, where 1 meant they would have "very little" control and 7 meant they would have "a lot" of control.
- **Risk**: Participants were asked to rate how risky each driving condition would be. Participants answered using a seven-point scale, where 1 meant "not risky" and 7 meant "very risky."

Occlusion Factor: In addition to the subjective perception variables, the experiment defined and measured a more objective parameter. The occlusion factor is a measure of how much splash and spray obstructed the view of the following/passing (driver) vehicle. This number was a ratio in which a value of 0 would indicate no occlusion and a value of 1 would indicate total occlusion. A detailed description of the methods used to determine this value is included in the data analysis section.

5.1 Experimental Methods

5.1.1 Experimental Design

This experiment sought to measure user perception by having participants watch pre-recorded videos of different scenarios involving splash and spray and subjectively rate several factors based on what they saw. The experimental design used for assessing the impact of splash and spray on road users consists of a 2x2x2x2x2 full-factorial design (Table 10). The controlled factors and the levels were the following:

- Between-Subjects Variables:
    - Gender (2 levels): Female, Male. The gender independent variable was chosen to generalize the results of this study to a broad user population. This factor was used for balance only; it was not used in the data analysis.
- Within-Subjects Variables:
    - Driver Vehicle (2 levels): Sedan, SUV. Two types of driver vehicle were selected for their differences in eye height of the driver.
    - Spray Vehicle (2 levels): Dump Truck, Tractor Trailer. Two types of spray vehicle were used to assess the differences in splash and spray between common types of commercial vehicles.
    - Maneuver (2 levels): Following, Passing. Two maneuvers were used to determine the effect of splash and spray in two common scenarios.
    - Rain Rate (2 levels): Heavy (64 mm/hr [2.5 inches/hr]), Moderate (20 mm/hr [0.8 inches/hr]). Two levels of rainfall were used to better understand how the amount of water on the road surface affects splash and spray.
    - Speed (2 levels): 45 mi/h (72 km/h), 60 mi/h (96 km/h). Two speeds were used to determine the effect of speed on the levels of splash and spray.

Table 10. Full-factorial experimental design matrix.

Driver Vehicle	Spray Vehicle	Maneuver	Rain Rate	Speed (mph)
Sedan	Dump Truck	Following	Moderate	45
				60
			Heavy	45
				60
		Passing	Moderate	45
				60
			Heavy	45
				60
	Tractor Trailer	Following	Moderate	45
				60
			Heavy	45
				60
		Passing	Moderate	45
				60
			Heavy	45
				60
SUV	Dump Truck	Following	Moderate	45
				60
			Heavy	45
				60
		Passing	Moderate	45
				60
			Heavy	45
				60
	Tractor Trailer	Following	Moderate	45
				60
			Heavy	45
				60
		Passing	Moderate	45
				60
			Heavy	45
				60

5.1.2 Presentation Order

Due to the large number of conditions, a partial Latin Square was used to create four balanced presentation orders. Each order was seen by 24 participants (12 female, 12 male) except order 4, which was seen by 28 participants (16 female, 12 male). Table 11 shows an example of one of the presentation orders. Each order started with two practice videos (P1 and P2), which always matched videos 16 and 17 so as to include as many different variables as possible.

Table 11. Example presentation order.

Video #	Maneuver	Spray Vehicle	Speed (mph)	Rain Rate	Driver Vehicle
P1	Following	Dump	60	Heavy	SUV
P2	Passing	Tractor	45	Moderate	Sedan
1	Following	Tractor	45	Moderate	Sedan
2	Following	Tractor	45	Moderate	SUV
3	Following	Tractor	45	Heavy	Sedan
4	Following	Tractor	45	Heavy	SUV
5	Following	Tractor	60	Moderate	Sedan
6	Following	Tractor	60	Moderate	SUV
7	Following	Tractor	60	Heavy	Sedan
8	Following	Tractor	60	Heavy	SUV
9	Following	Dump	45	Moderate	Sedan
10	Following	Dump	45	Moderate	SUV
11	Following	Dump	45	Heavy	Sedan
12	Following	Dump	45	Heavy	SUV
13	Following	Dump	60	Moderate	Sedan
14	Following	Dump	60	Moderate	SUV
15	Following	Dump	60	Heavy	Sedan
16	Following	Dump	60	Heavy	SUV
17	Passing	Tractor	45	Moderate	Sedan
18	Passing	Tractor	45	Moderate	SUV
19	Passing	Tractor	45	Heavy	Sedan
20	Passing	Tractor	45	Heavy	SUV
21	Passing	Tractor	60	Moderate	Sedan
22	Passing	Tractor	60	Moderate	SUV
23	Passing	Tractor	60	Heavy	Sedan
24	Passing	Tractor	60	Heavy	SUV
25	Passing	Dump	45	Moderate	Sedan
26	Passing	Dump	45	Moderate	SUV
27	Passing	Dump	45	Heavy	Sedan
28	Passing	Dump	45	Heavy	SUV
29	Passing	Dump	60	Moderate	Sedan
30	Passing	Dump	60	Moderate	SUV
31	Passing	Dump	60	Heavy	Sedan
32	Passing	Dump	60	Heavy	SUV

5.1.3 Participants

One hundred participants were selected to participate in this study. The age of participants ranged from 19 years old to 76 years old, with the mean age being 40. A total of 48 males and 52 females participated. Approval from the Virginia Tech Institutional Review Board (IRB) was obtained prior to recruiting subjects. Recruitment occurred through the Virginia Tech Transportation Institute (VTTI) participant database, a poster, and word of mouth. A general description of the study was provided to the subjects over the phone before they decided if they would like to participate. If they were interested, participants

were then screened with a verbal questionnaire to determine whether they were licensed drivers and whether they had any health concerns that should exclude them from participating in the study.

If participants were determined to be eligible for the study, they would then be scheduled to arrive at VTTI for participation. When subjects arrived at VTTI, they read and signed an informed consent form. Subjects were paid $20/h and were allowed to withdraw at any time, with compensation adjusted accordingly.

5.1.4 Facilities and Equipment

The videos participants were asked to rate were recorded on the Virginia Smart Road in Blacksburg, Virginia. The Smart Road is a 2.2-mile, two-lane controlled-access road. A weather-making system along a 0.75-mile section was used to create the different levels of rain.

The two vehicles from which the driver videos were recorded were a 2003 Chevy Malibu (sedan; Figure 39) and a 1999 Ford Explorer (SUV, Figure 40). Both vehicles were equipped with a luminance camera system that recorded the view in front of the vehicle. The resulting images provide information about how much light is reflected off the various surfaces in the images. These were used to determine the amount of occlusion caused by the splash and spray.

Figure 39. Photo. Driver vehicle: sedan.

Figure 40. Photo. Driver vehicle: SUV.

The two spray vehicles used were a GMC C7500 dump truck (Figure 41) and a 1997 Volvo VN series class 8 tractor with trailer (Figure 42). A large black and white checkered board was attached to the back of the spray vehicles. This was used to provide participants a consistent point of reference between the two vehicles, as well as a means for determining the amount of occlusion caused by the splash and spray.

Figure 41. Photo. Spray vehicle: dump truck.

Figure 42. Photo. Spray vehicle: tractor (trailer not shown).

Participants were initially screened over the telephone. If the participant was eligible for the study, a time was scheduled for testing. Participants were instructed to meet an experimenter at VTTI in Blacksburg, Virginia. Participants were scheduled in groups of up to 12. On arriving at VTTI, each participant was asked to read and sign the Informed Consent and answer a pre-drive questionnaire.

Once each participant had read and signed the Informed Consent and answered the questionnaire, the experimenter would orient the participants to the study by reading a script aloud. The script explained that the focus of the study was splash and spray and explained how participants should answer the questionnaire. Using the script, the experimenter walked the participants through two practice videos to make sure each participant understood the instructions. Participants were given an opportunity to ask questions after the completion of the practice videos. Once questions had been answered, the experimenter would then begin the study.

The videos were presented one at a time using a PowerPoint presentation projected onto a large screen. The experimenter would click to play each video. After a video had been played, the experimenter would advance to the next slide, which listed five questions along with the associated 7-point scales. Participants were also provided with a paper copy of the questions and scales that they could refer to if they wished. Figure 43 shows the questions that participants answered for each video. The underlined word in question 1 changed depending on the maneuver shown in the video. For *following* maneuvers it read "vehicle," and for *passing* maneuvers it read "roadway." The experimenter would wait until everyone had finished writing their answers before proceeding to the next slide. This continued until each participant had finished answering the questions for all 32 video clips.

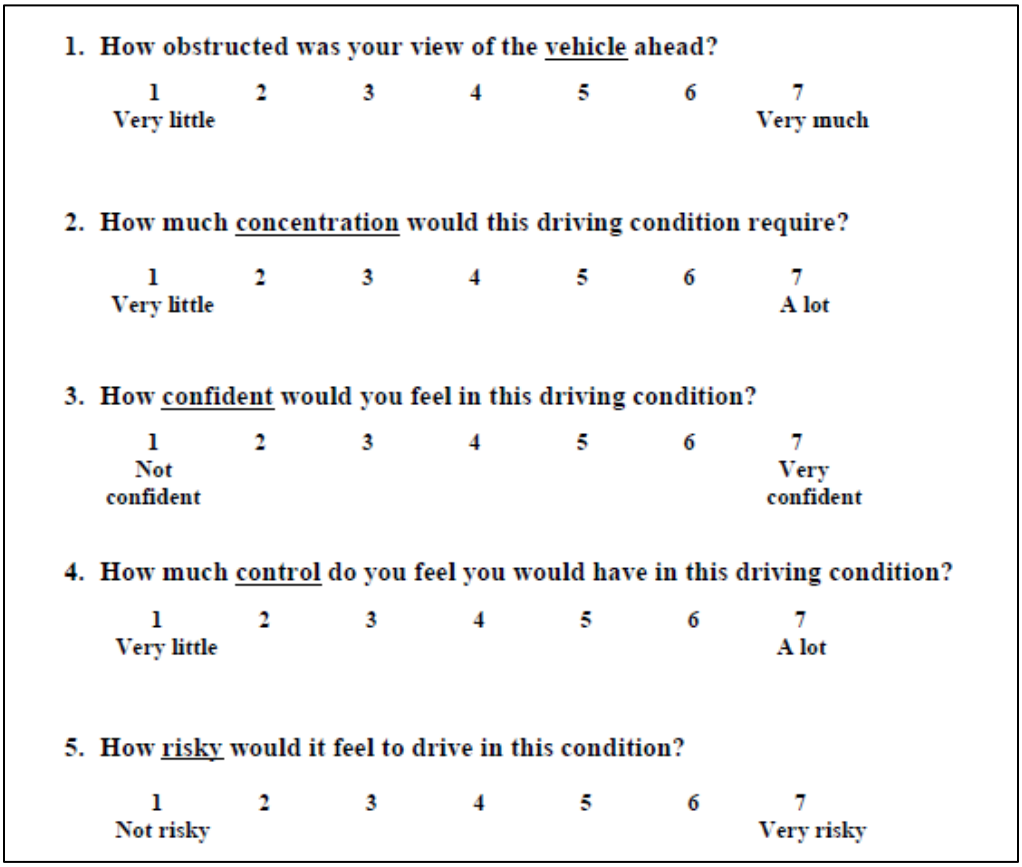

Figure 43. Screen shot. Questions answered for each video.

5.2 Data Analysis

5.2.1 Occlusion Factor

Five luminance camera images were analyzed for each video that showed the *following* maneuver. The occlusion factor was not computed for the *passing* maneuver because the checkerboard on the back of the spray vehicles was not clearly visible for the camera in those scenarios. The five images included one for each type of pavement to allow comparisons across pavement types.

The occlusion factor was defined as the ratio of the mean luminance of the black squares to the mean luminance of the white squares. A custom-written MATLAB program identified each of the squares, measured the luminance at the center of each square, and then created a mean value for the black squares and a mean value for the white squares. Figure 44 shows the original image, and Figure 45 shows the close-up image of the checkerboard with measurement locations.

This analysis works under the assumption that as splash and spray between the checkerboard and the camera increase, the luminance values for the black squares will increase (they will appear lighter in color) and values for the white squares will decrease (they will appear darker in color). At the point that splash and spray completely occludes the checkerboard, the values for black and white squares will be equal (ratio = 1). Figure 46 illustrates this concept by comparing an image of the checkerboard without splash or spray to an image with splash and spray.

Figure 44. Photo. Original luminance camera image.

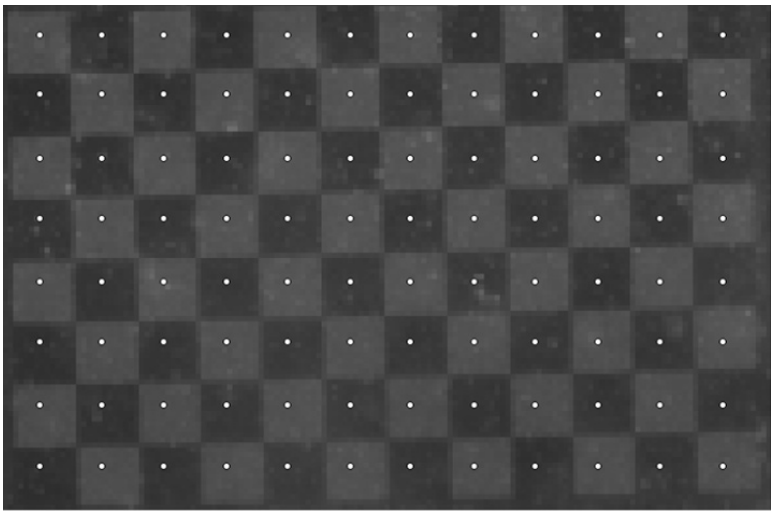

Figure 45. Photo. Close-up luminance camera image analysis to determine occlusion factor.

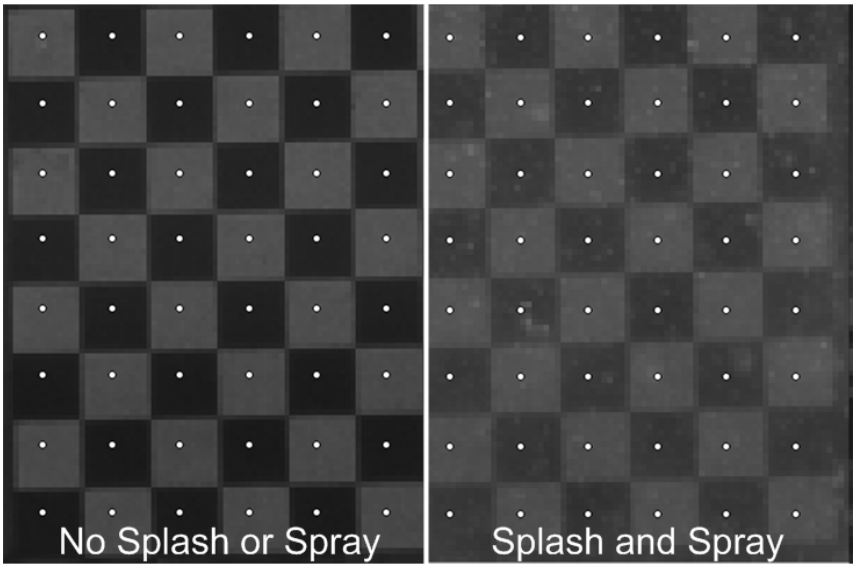

Figure 46. Photo. Comparison of checkerboard images under different levels of splash and spray.

The results of this analysis were originally intended to be used to determine any differences between pavement types, but this was not possible in this first set of experiments because the pavement sections were too short to differentiate in the videos. The results were correlated with the user perception data to determine the relationship between spray and splash and participants' ratings of obstruction, concentration, confidence, control, and risk. Because the videos participants rated involved all five pavement types, the mean occlusion factor was used for this comparison.

5.2.2 User Perception Analysis

A separate analysis was conducted for each dependent variable. An analysis of variance (ANOVA) with a significance level of 95 percent ($\alpha = 0.05$) was used in each case.

5.2.3 Results

A separate analysis was conducted for each dependent variable. As an example, the ANOVA results for the Obstruction variable are summarized in Table 12. Obstruction was considered a negative variable, that is, a higher rating indicated a less desirable situation, in this case, a higher level of visual obstruction. The independent variables have been abbreviated as follows: Maneuver (Man), Spray Vehicle (Spray), Speed (Speed), Rain Rate (Rain), and Driver Vehicle (Driver). The statistically significant factors are denoted by an asterisk, and the associated F values are shown.

Rain Rate was found to be a significant main effect. The interaction of Speed and Driver Vehicle was also found to be significant. Figure 47 shows the mean Obstruction rating for each Rain Rate. The participants' view was significantly more obstructed during heavy rain conditions. This is expected because the increased amount of water on the road surface contributes to more spray and splash.

The significant interaction of Speed and Driver Vehicle is shown in Figure 48. While the SUV and sedan did not have significantly different obstruction ratings for the 45-mi/h (72-km/h) condition, the sedan had slightly higher ratings in 60-mi/h (96-km/h) condition. This suggests that drivers of a higher profile vehicle may experience less obstruction at higher speeds.

Table 12. ANOVA results for Obstruction.

Source	DF	Type III SS	Mean Square	F Value	Pr>F
Man	1	146.8144	146.8144	74.76	0.0733
Spray	1	33.4089	33.4089	2.99	0.3339
Man×Spray	1	84.0779	84.0779	5.22	0.2626
Speed	1	429.5990	429.5990	14.98	0.1609
Man×Speed	1	10.9356	10.9356	0.66	0.5662
Spray×Speed	1	8.2602	8.2602	1.45	0.4407
Man×Spray×Speed	1	0.3417	0.3417	1.02	0.4964
*Rain	1	265.8991	265.8991	110355	0.0019
Man×Rain	1	12.3855	12.3855	3.13	0.3274
Spray×Rain	1	1.2700	1.2700	7.08	0.2289
Man×Spray×Rain	1	1.8472	1.8472	1.32	0.4563
Speed×Rain	1	3.6981	3.6981	1.90	0.3996
Man×Speed×Rain	1	14.3676	14.3676	5.34	0.2600
Spray×Speed×Rain	1	1.5538	1.5538	8.90	0.2059
Man×Spray×Speed×Rain	1	0.0216	0.0216	0.56	0.5910
Driver	1	0.6329	0.6329	0.21	0.7283
Man×Driver	1	8.8850	8.8850	14.15	0.1654
Spray×Driver	1	10.1782	10.1782	14.42	0.1639
Man×Spray×Driver	1	8.2984	8.2984	25.01	0.1256
*Speed×Driver	1	1.3023	1.3023	476.21	0.0292
Man×Speed×Driver	1	0.7673	0.7673	10.09	0.1942
Spray×Speed×Driver	1	0.2674	0.2674	0.79	0.5376
Man×Spray×Speed×Driver	1	0.5185	0.5185	0.41	0.6368
Rain×Driver	1	2.5691	2.5691	12.85	0.1732
Man×Rain×Driver	1	15.1268	15.1268	99.31	0.0637
Spray×Rain×Driver	1	24.0672	24.0672	25.08	0.1255
Man×Spray×Rain×Driver	1	0.0584	0.0584	0.25	0.7039
Speed×Rain×Driver	1	0.7491	0.7491	69.22	0.0762
Man×Speed×Rain×Driver	1	0.1080	0.1080	1.28	0.4612
Spray×Speed×Rain×Driver	1	8.5447	8.5447	59.96	0.0818
Man×Spray×Speed×Rain×Driver	1	0.1978	0.1978	62.45	0.0801
Total	31	1096.75			

** $p < 0.05$ (significant)*

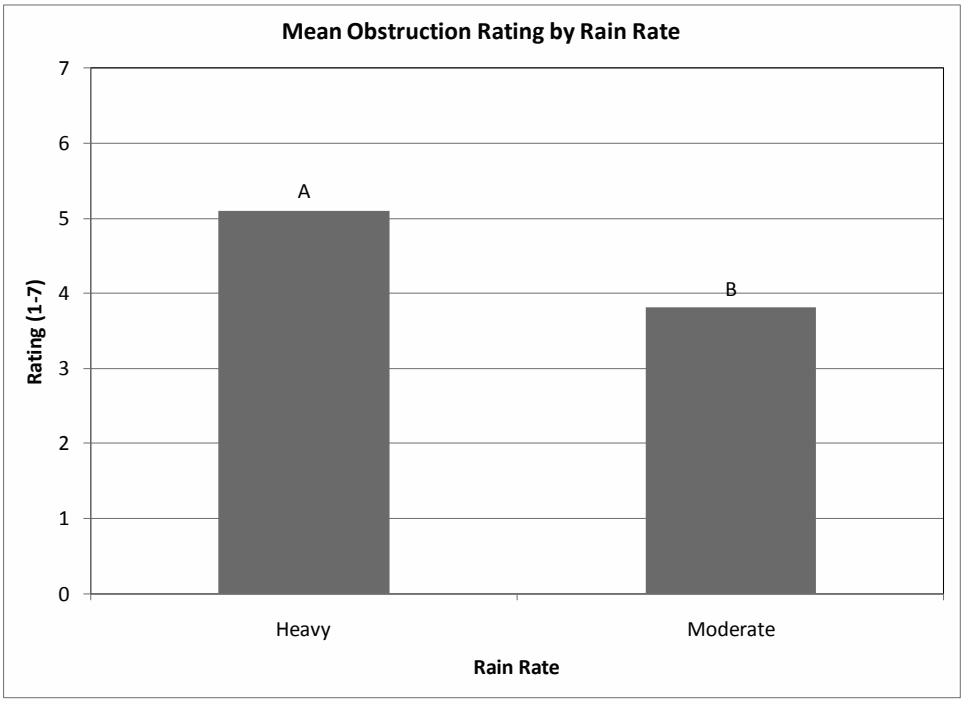

Figure 47. Chart. Mean Obstruction rating by Rain Rate
(1=very little obstructed, 7=very much obstructed).

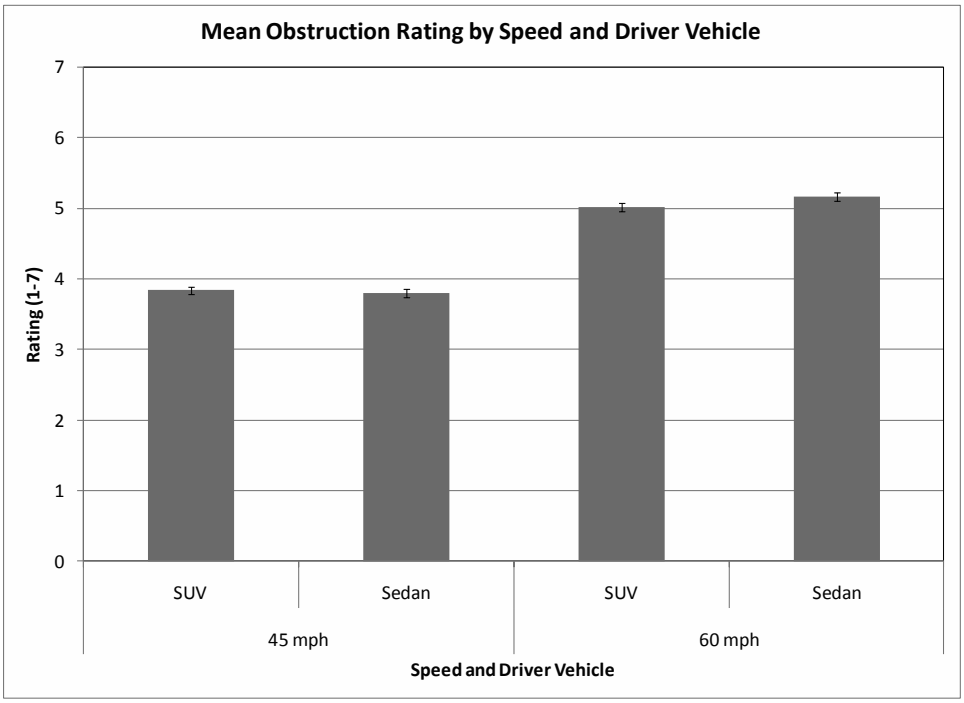

Figure 48. Chart. Mean Obstruction rating by Speed and Driver Vehicle
(1=very little obstructed, 7=very much obstructed).

Figure 49 shows the relationship between mean Obstruction rating and the mean Occlusion Factor with the associated linear relationship and coefficient of determination, R^2, value. Occlusion Factor is shown to have a strong positive correlation with Obstruction rating. This is expected because the two variables are different methods of measuring the same concept. Furthermore, Figure 50 through Figure 53 show that all the user perception variables are highly correlated with the objective occlusion variable, suggesting that occlusion may be a good measure of user perception of splash and spray nuisance.

Table 13 summarizes the results for the five subjective user perception variables. The table presents *p* values that were deemed significant ($p < 0.05$). The lowest values indicate the most significant variables or interactions. One interesting result is that concentration is the variable that is influenced by the greatest number of combinations.

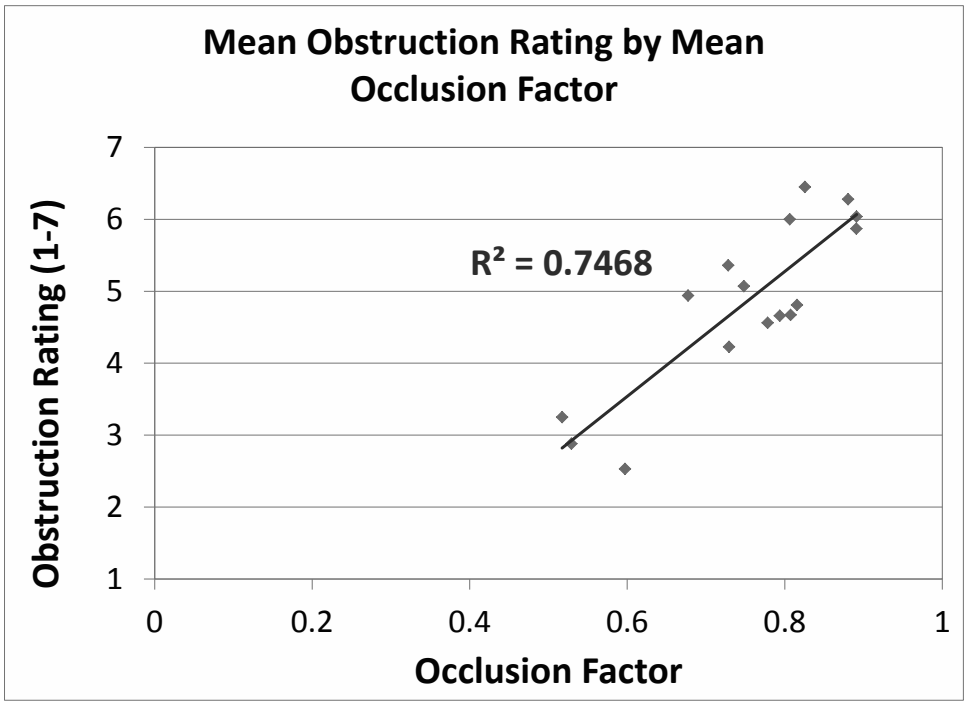

Figure 49. Graph. Mean Obstruction ratings by mean Occlusion Factor.

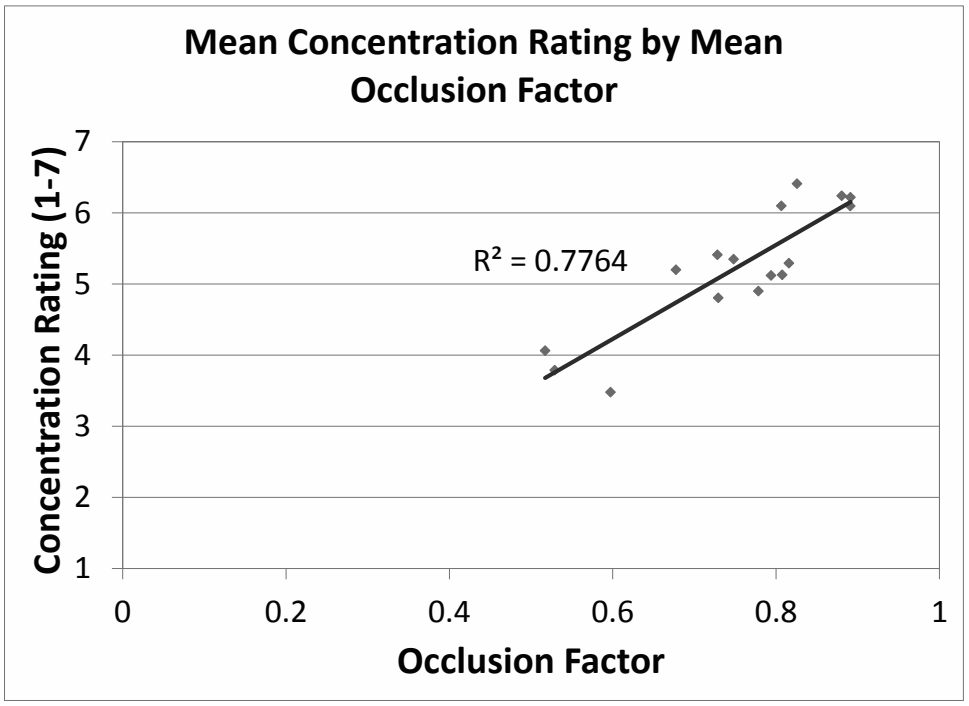

Figure 50. Graph. Mean Concentration ratings by mean Occlusion Factor.

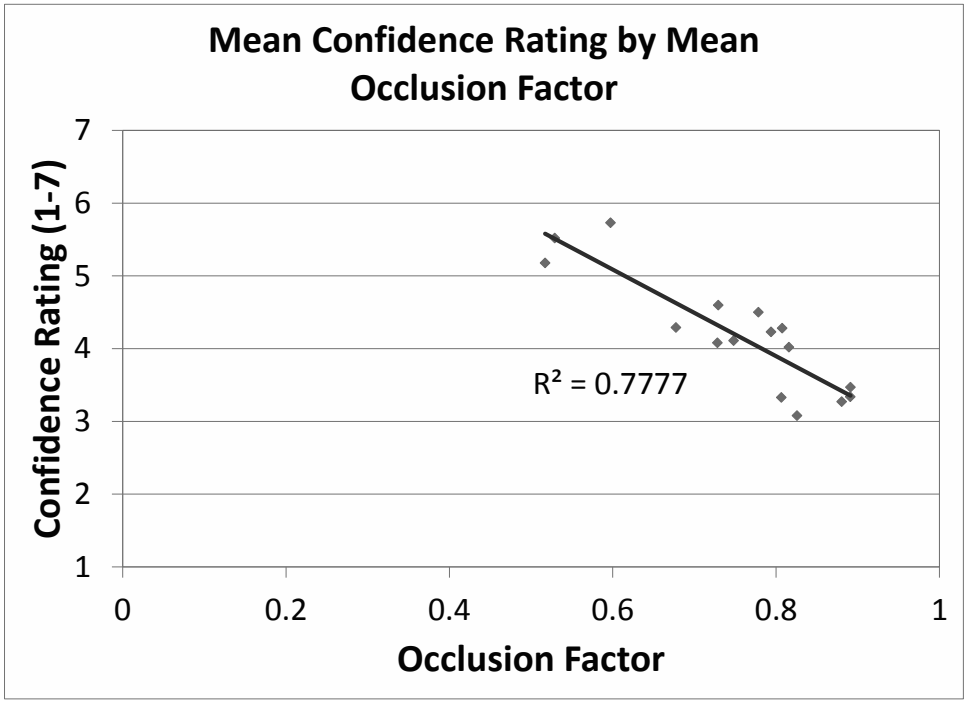

Figure 51. Graph. Mean Confidence ratings by mean Occlusion Factor.

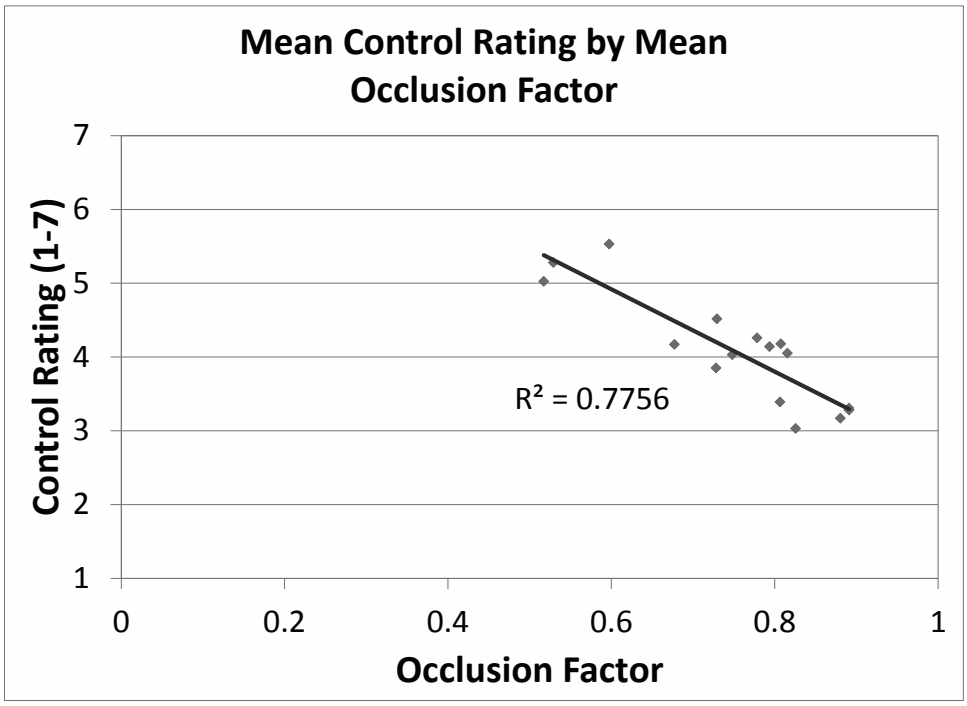

Figure 52. Graph. Mean Control ratings by mean Occlusion Factor.

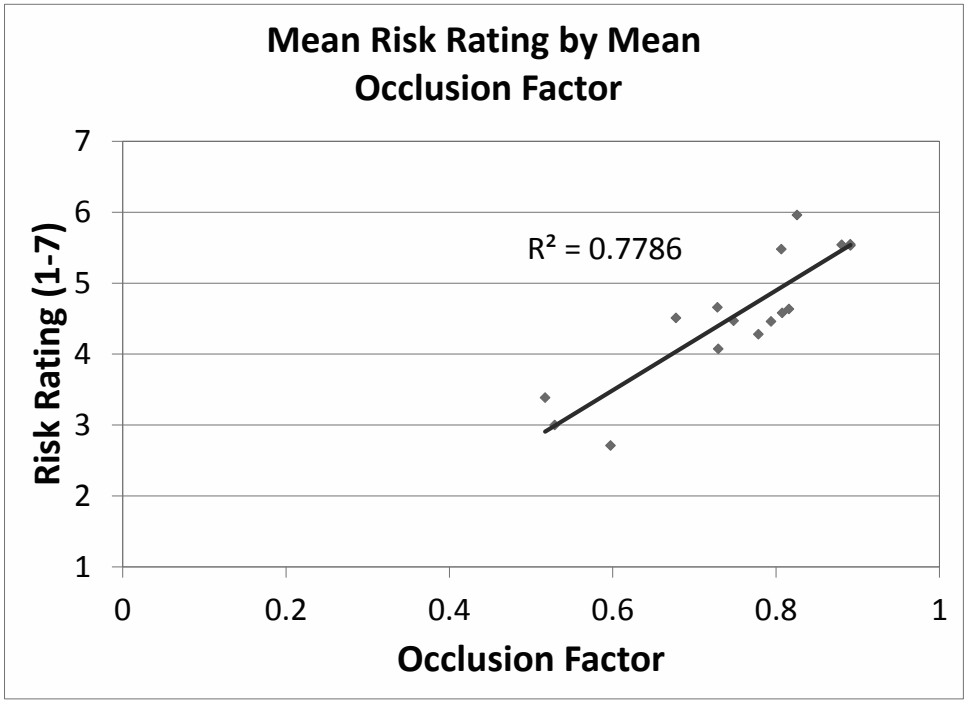

Figure 53. Graph. Mean Risk ratings by mean Occlusion Factor.

Table 13. Summary of ANOVA results (*p* values) for all user perception variables.

Source	Obstruction	Concentration	Confidence	Control	Risk
Man					
Spray					
Man×Spray					
Speed				0.0075	
Man×Speed					
Spray×Speed					
Man×Spray×Speed					
Rain	0.0019				
Man×Rain					
Spray×Rain		0.0159	0.0251		
Man×Spray×Rain					0.0161
Speed×Rain					
Man×Speed×Rain					
Spray×Speed×Rain		0.0367			
Man×Spray×Speed×Rain					
Driver					
Man×Driver					
Spray×Driver				0.0157	
Man×Spray×Driver				0.0111	
Speed×Driver	0.0292				
Man×Speed×Driver		0.0201			
Spray×Speed×Driver					0.0498
Man×Spray×Speed×Driver					
Rain×Driver					
Man×Rain×Driver					
Spray×Rain×Driver		0.0404			
Man×Spray×Rain×Driver					
Speed×Rain×Driver		0.0241			
Man×Speed×Rain×Driver					
Spray×Speed×Rain×Driver		0.0149		0.0211	
Man×Spray×Speed×Rain×Driver		0.0486			

5.3 Discussion

As mentioned in the previous section, user perception variables were considered either positive or negative, based on whether a high rating of the variable represented a more desirable (positive) or less desirable (negative) situation. Negative variables included Obstruction, Concentration, and Risk because a high rating for these variables indicated a situation with a high amount of visual obstruction, that required high levels of concentration, or was highly risky, respectively. Positive variables included Confidence and Control because high ratings for these variables indicated a situation in which the participant felt very confident or in a high degree of control, respectively.

With this dynamic in mind, all five variables are considered simultaneously to determine what factors or conditions may lead to more or less desirable splash-and-spray situations:

- Figure 54 shows the average rating for each variable by Maneuver. Though there was no significant main effect of Maneuver, the figure shows that the Following maneuver tended to be rated as a less desirable condition.

- Figure 55 shows the average rating by Speed. While Speed had a significant main effect only for Control, the 60-mi/h (96-km/h) condition tended to be seen as less desirable for all ratings.

- Figure 56 shows the average rating by Rain Rate. The heavy-rain condition tended to be rated as less desirable. The average ratings for each Rain Rate are also very similar to those for Speed. This indicates that increasing speed has similar effects on participants' perceptions as increasing rain.

- Figure 57 shows the average rating by Maneuver and Spray Vehicle. While this interaction was not found to be significant for any single variable, the figure does show that passing the dump truck tended to be rated as a more desirable situation than the other three conditions.

- Figure 58 shows the average rating by Speed and Maneuver. The Following maneuver at 60 mi/h (96 km/h) was rated the least desirable of these four conditions. There was very little variation between maneuvers in the 45-mi/h (72-km/h) condition, but Following was rated worse at higher speeds.

- A similar pattern was found for Rain Rate and Maneuver, as shown in Figure 59. The Following maneuver in heavy rain was rated the worst for these factors. There was also a slight difference between maneuvers in the Moderate rain condition, with Passing being rated slightly better than Following.

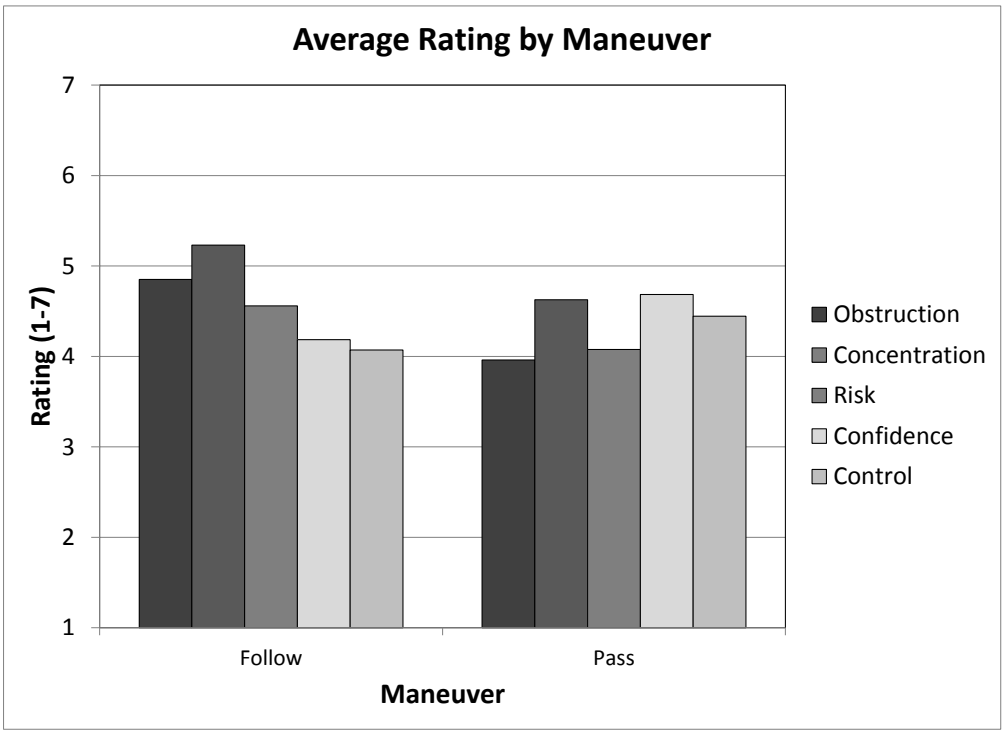

Figure 54. Chart. Average rating by Maneuver for all variables
(1=very little, 7=very much).

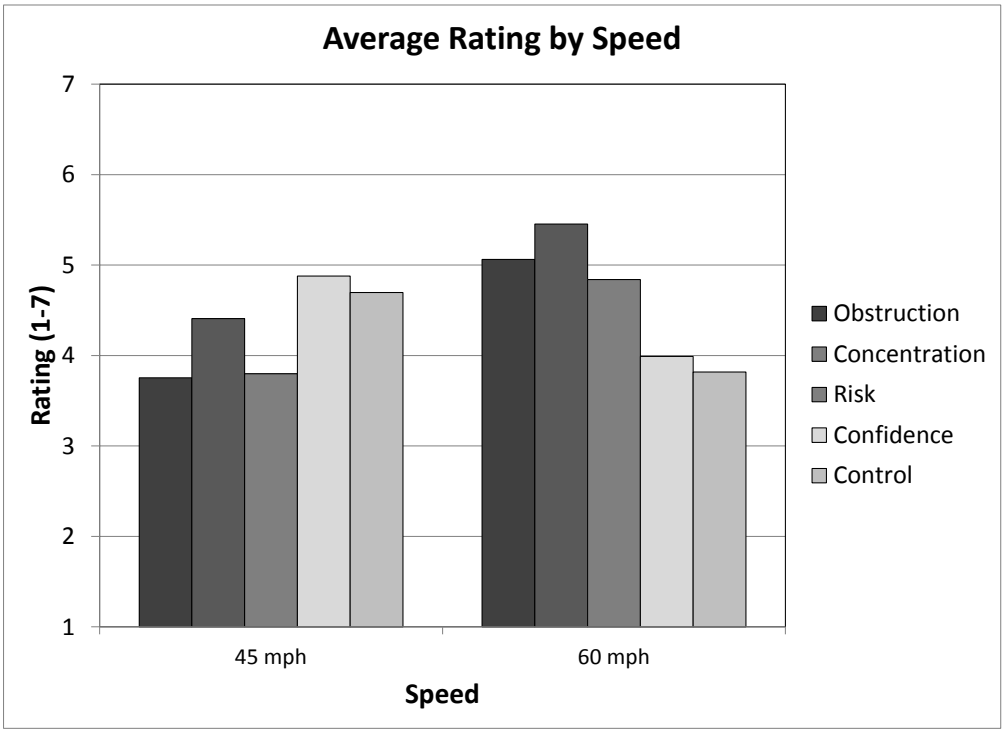

Figure 55. Chart. Average rating by Speed for all variables
(1=very little, 7=very much).

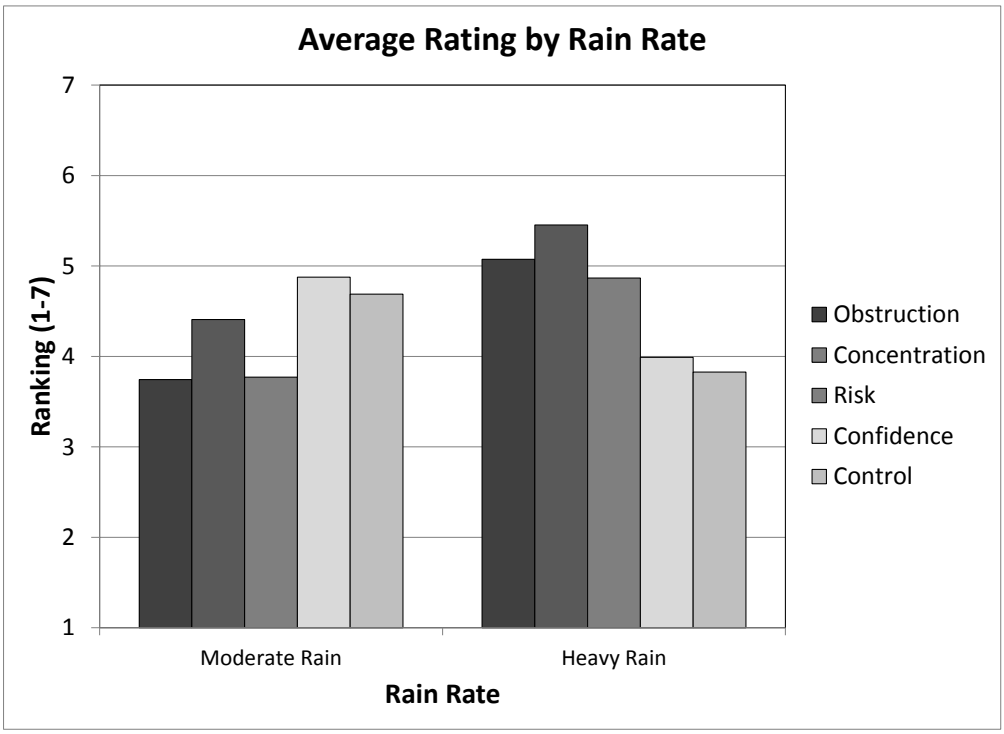

Figure 56. Chart. Average rating by Rain Rate for all variables
(1=very little, 7=very much).

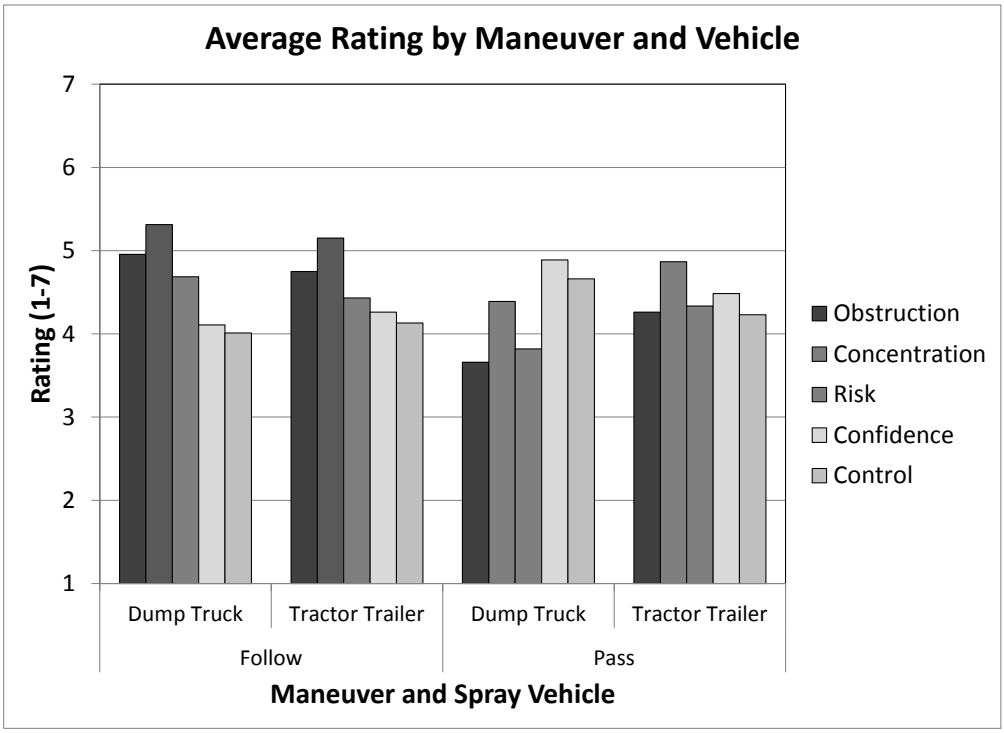

Figure 57. Chart. Average rating by Maneuver and Spray Vehicle for all variables
(1=very little, 7=very much).

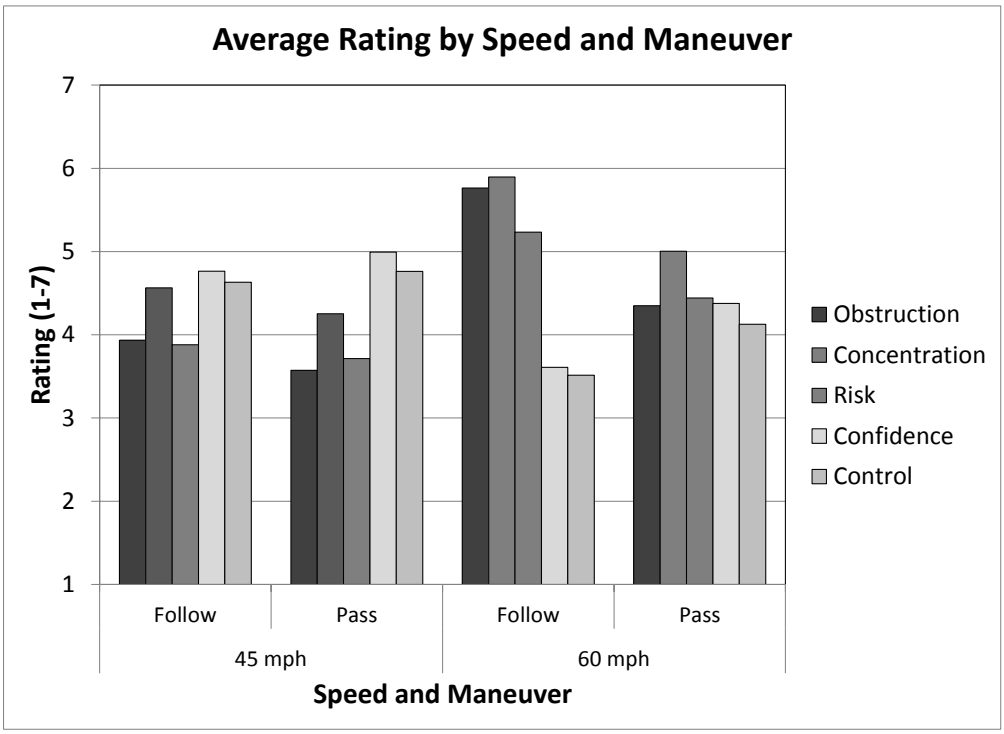

Figure 58. Chart. Average rating by Speed and Maneuver for all variables
(1=very little, 7=very much).

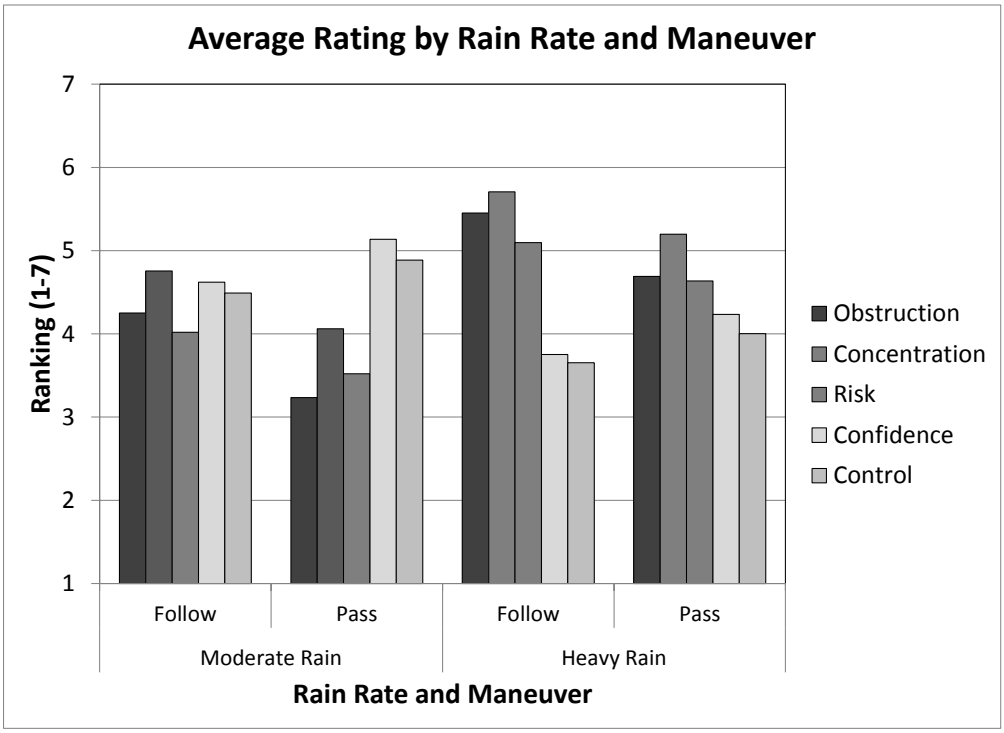

Figure 59. Chart. Average rating by Rain Rate and Maneuver for all variables
(1=very little, 7=very much).

5.4 Conclusions

This chapter described the methodology and results from a set of field tests assessing the impact of splash and spray on road users. The tests were conducted at the Virginia Smart Road, following a full-factorial experiment that considered four within-subjects independent variables—Driver Vehicle, Spray Vehicle, Maneuver, and Rain Rate—and defined five subjective user perception variables and an objective occlusion measure. The results of the experiment suggest that participants experience a greater degree of nuisance from splash and spray (i.e., higher ratings for obstruction, concentration, and risk and lower ratings for confidence and control) for the Following maneuver (particularly when following the dump truck) than for the Passing maneuver. In addition, they show that the occlusion factor correlated well with all of the perception variables and, thus, can be used as a measure of the nuisance produced by splash and spray.

6 Splash and Spray Assessment Tool Development[12]

This chapter covers the final stages of development of the splash and spray assessment tool. The chapter combines outcomes from project experiments and computational fluid dynamic (CFD) modeling of mechanisms of splash and spray generation, summarizes the CFD modeling techniques used, and amalgamates the results to propose a tool that can be used by highway engineers.

The flow chart in Figure 60 shows the model development stages, as they were conceived at the outset of the project. Experiments that have been reported to this point are denoted by an asterisk.

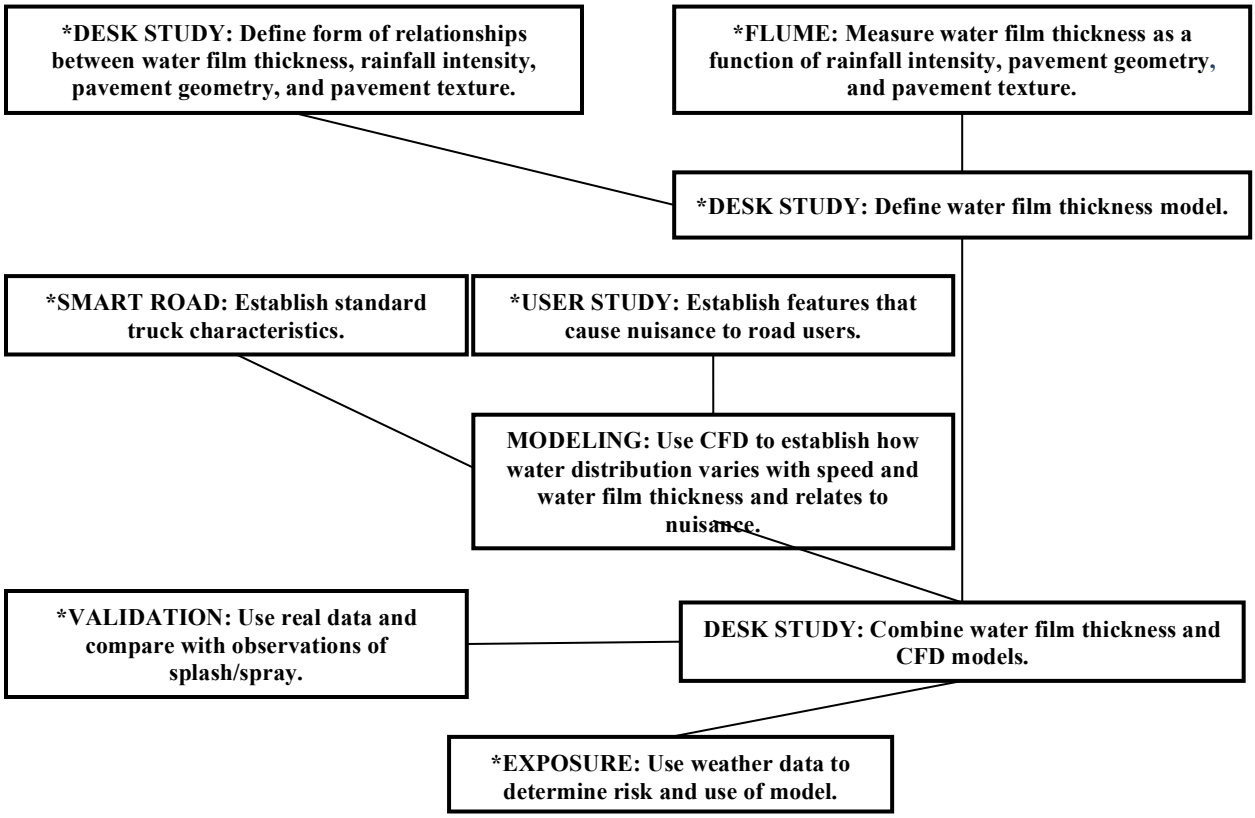

Figure 60. Diagram. Stages in the development of the splash and spray assessment tool.

6.1 Water film thickness

Results presented in Chapter 3 provided the following general formula for predicting water film thickness (Equation 31), given the rainfall intensity, the slope and texture depth of the pavement, and the length of pavement upstream of a given position:

$$WD = 6\times10^{-4}.T^{0.09}.(LI)^{0.6}.S^{-0.33} \quad (31)$$

[12] This chapter is an expanded version of the paper "Development of a Prediction Model for Splash and Spray," by H. Viner, D. Hargreaves, A. Dunford, K. Nesnas, T. Parry, and G.W. Flintsch, presented at the *7th International Symposium on Pavement Surface Characteristics* (SURF 2012), Sep. 18-21, 2012, Norfolk, VA.

where *WD* is water film thickness in meters, *T* is mean profile depth in millimeters, *L* is drainage length in meters, *I* is rainfall intensity in meters per hour, and *S* is slope as a fraction.

According to this formula:

1. Water film thickness increases as the slope decreases.
2. Water film thickness is lower for smooth surfaces, probably because the reduced turbulence results in a higher flow rate of water draining away.

6.1.1 Porous Asphalt

The flume experiment made measurements in steady-state conditions: saturated pavement surfaces and constant flow of water. The effect water film thickness of porous pavements, such as open-graded friction course (OGFC), on water film thickness was not considered. To further investigate the effect of porous pavements on water film thickness, measurements were made of the permeability of a sample of the pavement sections used in the flume.

The time taken for two liters (half a gallon) of water to dissipate from an annular area on each pavement section was measured. The apparatus used comprises a plastic tube of internal diameter 65 mm (2.5 inches) with an opening in its base of diameter 45 mm (1.8 inches) stopped by a rubber ball on a plunger. The tube was attached to a solid annular base with diameter 290 mm (11.5 inches) and that had a sponge-rubber ring fixed to its underside. The sponge-rubber base was compressed onto the test surface when the standing board (a sheet of plywood with a hole in its center and rubber feet at its corners) was positioned over the base and loaded equally on both sides, either by operators or by static mass. The tube was filled with water, and the time taken for the known volume of water, between two marks on the tube, to escape through the hole in the base after pulling the plunger to remove the rubber ball stopper, was recorded. The water could either travel into the surface (if it is porous), through gaps between the sponge rubber seal and the surface (if the surface texture is sufficiently large), or remain in the tube (if surface texture is sufficiently low that the sponge rubber forms a complete seal).

Later, to examine the impact on permeability of restricting the flow of water through the pavement (vertically and horizontally), the edges and then the base of the porous OGFC sections were sealed with latex before repeating the permeability test. Table 14 shows the results.

Table 14. Average time taken for water to dissipate.

Pavement material	Average time for water dissipation (seconds)
Open Graded Friction Course (OGFC)	4.5
Asphaltic concrete	647.8
Stone mastic asphalt	n/a
Tined concrete	10.7
OGFC (edges sealed)	4.5
OGFC (edges and base sealed)	11.4

Water dissipates through the OGFC surface very rapidly. Even when the edges and base of the pavement sections were sealed, the water was still able to drain from the permeameter tube, either because the surface's texture was sufficiently large to prevent a seal or because the water could be forced into the bulk of the material and then back out of the surface. The asphaltic concrete sections were impermeable but

allowed some water to drain through channels in the surface texture. The stone mastic asphalt sections were impermeable and had low enough texture that a seal between the permeameter apparatus and the surface prevented any water from escaping. The channels created by tining on the surface of the tined concrete sections were deep enough to allow water to drain away easily.

The speed at which water can travel through porous asphalt means that, even though its relatively high surface texture contributes to high water film thickness under steady-state conditions (as in the flume experiment), some of the water will drain thorough the pavement reducing the amount of water available to be displaced by the tire.

A literature review carried out by Stanard et al. (2007) suggests that the range of hydraulic conductivity that can be expected on a porous pavement is between 40 mm/h (1.6 inches/h) and 4,200 mm/h (165 inches/h) depending on factors such as age, layer thickness, and coarse aggregate size. The permeability of a porous pavement degrades with time unless its pores are cleaned during regular maintenance and, furthermore, the ability of the pavement to remove water from the surface depends on the design of the lower layers (i.e., there has to be some mechanism for storage or draining away of the water that permeates).

The research team decided that the final splash and spray tool should allow the engineer to account for the presence or absence of a porous pavement by accepting inputs for hydraulic conductivity, void content, and pavement depth. The values can then be used to attenuate the input rainfall intensity before calculation of water film thickness. Even if very high hydraulic conductivity can reduce the chance of standing water, there will probably still remain a thin film of water on the surface that might lead to generation of at least some spray.

Because the most robust use of the splash and spray tool is likely to be to judge the risk of nuisance at a given location, accounting for exposure and road geometry, the specification and use of a porous asphalt surface course could be a tool to be employed by the pavement designer when necessary.

6.2 Modeling the Vehicle and Its Surroundings

This section describes the development of a computational fluid dynamic (CFD) model to investigate how the water remaining on the road (calculated using the water film thickness model) is converted into splash and/or spray. Much of the approach presented is based on the findings of the Lawrence Livermore National Laboratories Heavy Vehicle Aerodynamics Project (Paschkewitz, 2006).

6.2.1 Splash Truck Model

In the user perception studies described in Chapter 5, participants were asked to rate their reactions to a series of video clips taken from within a vehicle either following or passing a truck in wet conditions. The responses showed that a greater degree of nuisance (inferred from higher ratings for obstruction, concentration, and risk and lower ratings for confidence and control) was experienced for the Following maneuver than for the Passing (overtaking) maneuver. Also, a greater degree of nuisance was found for the dump truck than for the articulated truck and when the following/passing vehicle was a sedan rather than an SUV. These observations determined the basis of the CFD model, which was created for a typical sedan car following the GMC dump truck used in the user study.

The CFD model was created using a combination of photographs and reference measurements. Figure 61 shows the side view of the dump truck, and Figure 62 shows the 3D solid model constructed. Working from photographs will inevitably introduce a number of inaccuracies, and smaller features such as wing mirrors, exhaust pipes, and door handles were deliberately ignored because including them would increase the computational effort required by perhaps an order of magnitude and have relatively little

effect on the outcome. The solid model preserves the bulk aerodynamic features of the body shell and the underside of the truck.

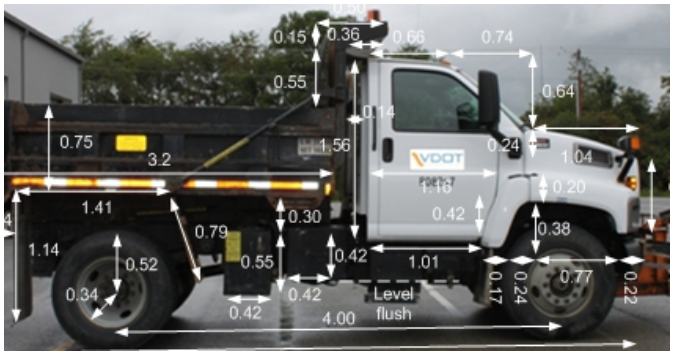

Figure 61. Photo. Digitized photograph of the dump truck, marked with measurements.

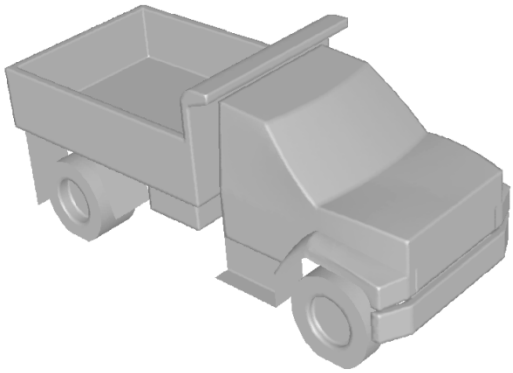

Figure 62. Rendering. Solid model of the dump truck.

The solid model was subtracted from a rectangular volume constructed around it, leaving a void. The volume, the region in which fluid flow can take place, was converted into a mesh by filling it with cells. The cells were largely tetrahedral, with smaller cells used close to the truck to increase detail in regions where large velocity and pressure gradients might be expected. Viewing the volume mesh is unhelpful; Figure 63 and Figure 64 show the surface mesh in the vicinity of the rear and front wheels, respectively. The total mesh comprises 4.2 million cells. This 3D model uses the GAMBIT CAD and meshing software, which is part of the ANSYS-FLUENT (hereafter referred to as Fluent) software suite.

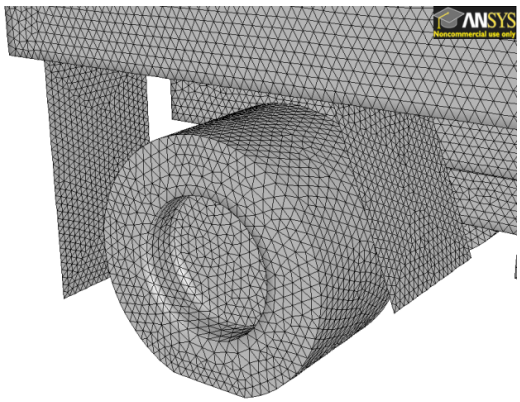

Figure 63. Rendering. Surface mesh on the rear wheels.

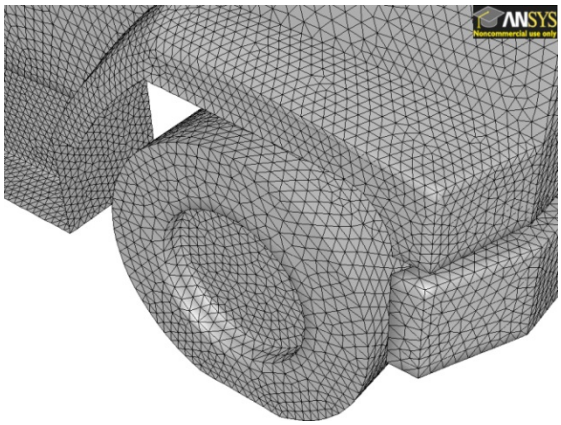

Figure 64. Rendering. Surface mesh on the front wheels.

6.2.2 Material Properties and Boundary Conditions

Because incompressible flow was being modeled, the two important material properties for the air were its density, 1.225 kg/m^3 (0.0765 lb/ft^3), and dynamic viscosity, 1.79×10^{-5} Pa·s.

In the CFD model, the truck was held stationary, and air enters the meshed domain at one end, passes around the truck, and leaves via the other end. This frame of reference corresponds to that of an observer in the driver's seat as opposed to an external observer watching the vehicle go past. The air speed normal to the inlet was fixed at a value that corresponds to the speed of the truck; for example if the truck is travelling at 72 km/h (45 mi/h), the air speed is 20.1 m/s (66 ft/s). Because the vehicle is traveling into still air, the turbulence intensity was set to 1 percent and the turbulence length scale to 1 m (3.3 ft) (Section 6.2.3). At the outlet, the relative pressure was set to 0.0 Pa. This does not correspond to a perfect vacuum, but rather is relative to atmospheric pressure. At this boundary, the air can leave unhindered.

The ground was modeled as a wall with a translational velocity aligned with and equal to the air velocity. Similarly, the wheels of the truck were rotated at a rate that is appropriate for the speed of the truck. For the 72-km/h (45-mi/h) case with wheel diameter 0.5025 m (20 inches), this equates to one revolution of the wheel every 0.1571 s, which means that the angular velocity of the wheel is 39.99 rad/s. The remaining boundaries—the sides and top of the domain—were modeled using symmetry boundary conditions. At these boundaries, the normal derivatives of the field variables are zero. Such boundary conditions are often used to model distant boundaries in these situations. Indeed, this is one difference between the virtual and the real wind tunnel, which does have side walls and a roof.

6.2.3 Turbulence and Particle Tracking

The Reynolds number, Re, of the flow for the 72-km/h (45-mi/h) case is 3.4×10^6, which means the flow is highly turbulent.[13] There are a variety of turbulence models available in Fluent, but here the RNG k-ε model was chosen because of its success in a previous project (Sterling et al., 2010). The simulation had to be run as unsteady because a steady-state solution would not converge due to the inherent unsteadiness of the wake behind the vehicle. Values of the field variables that are presented are therefore time-averages from a point where the simulation had reached a statistically stationary state.

[13] The Reynolds number was based on the vehicle speed and the width of the truck (2.5 m).

The Discrete Phase Model (DPM) in Fluent is a Lagrangian particle-tracking model, suitable for this application because the volume loading of the spray is small, except in the region immediately next to the wheels (Paschkewitz, 2006). The motion is described by Equation 32:

$$\boldsymbol{m_d \frac{du_d}{dt}} = F_d + \boldsymbol{m_d} g \tag{32}$$

where m_d is the mass of the droplet, u_d is the velocity of the droplet, g is the acceleration due to gravity, and F_d is the aerodynamic drag and

$$F_d = \frac{1}{2} C_d \rho A_d |u - u_d|(u - u_d) \tag{33}$$

where u is the air velocity, ρ is the air density, C_d is the drag coefficient, and A_d is the area of the droplet presented to the flow. The drag coefficient is for a spherical droplet and is typically a complex function of the Reynolds number, based on the particle diameter, d.

The density of the droplets was set to 1,000 kg/m^3 (62.5 lb/ft^3). Previous work (Paschkewitz, 2006) suggests that the range of droplet sizes should be between 10 µm (0.0004 inches) and 5,000 µm (0.2 inches). There are a number of fates for the droplets once they are in flight:

- They can be trapped on a wall and thereby removed from the simulation.
- They can reflect from a wall with an angle governed by restitution coefficients.
- They can escape from the domain via the outlet.

The trajectory of the droplets is governed by the turbulence model and a random walk imposed on the overall flight path, the magnitude of which is related to the turbulence level at the given point in space.

6.3 Mechanisms of Splash and Spray Generation

In the CFD process, water droplets are released into the air-flow model and their trajectories are predicted within the turbulent airstream around the truck. An overall model for splash and spray will be developed from an understanding of the quantity of water arriving at a location likely to give rise to user nuisance under different starting conditions (i.e., truck speeds and water film thicknesss).

Research by Weir et al. (1978) established four primary mechanisms by which the tire displaces the water in its path: bow wave, side wave, tread pickup, and capillary adhesion. Figure 1 showed the approximate trajectory expected for water droplets following each mechanism.

The bulk of splash will come from the side of the tire (side wave) and the front of the tire (bow wave). The initial trajectory of the side wave ranges between 10° and 15° in the plane parallel to the direction of travel and between 15° and 20° on the horizontal plane; the inclination of the side wave in the plane perpendicular to the direction of travel is 45°. The bow wave trajectory has an initial inclination ranging between 30° and 40° in the plane parallel to the direction of travel; the inclination of the trajectory in the plane perpendicular to the direction of travel is 90°.

The third mechanism encountered when the tire shifts water is tread pickup, in which the water from within the grooves forming the tread comes out as spray behind the tire due to turbulent flow in the grooves.

The fourth and last mechanism is the capillary adhesion of the water to the tire. This mechanism starts at the contact patch between the tire and the ground, where water is attracted to the tire by surface tension. At some stage, water shifted by capillary adhesion will detach from the tire surface due to outward forces along the tire perimeter.

In reality, the hydrodynamic circulation of the air around the body of the vehicle causes splash generated by bow and side wave mechanisms to become a spray of water droplets that will, in turn, disintegrate to smaller sizes when they are caught in air vortices or impact a surface. However, to properly model this effect would require a significant increase in computational resource, so it is not considered in this study.

6.3.1 Introducing Water to the Model

The CFD model will be used to calculate the spray generated by a truck travelling at a speed V, based on the mechanisms identified by Weir et al. (1978). This chapter first considers the location for release of water droplets, then presents a methodology for calculating flow rates, and discusses the approach for defining the initial droplet velocities.

The water droplets are released from the tires of the truck. The truck has two single front tires and two dual rear tires. The required modeling characteristics of the tires are given in Table 15. The mesh of the tires is used to define the surfaces from which the water droplets are released.

Table 15. Tire geometry.

	Tire width (mm)	**Radius** (mm)	**Non-grooved area** (percent)	**Tread depth** (mm)
Front wheel	280	502	75	10
Rear wheel	560	502	75	10

Figure 65 depicts the zones S_{BW}, S_{SW}, S_{TP}, and S_{CA}, from which the droplets are released to simulate the splash or spray generation mechanisms associated with the bow wave, side wave, tread pickup, and capillary adhesion, respectively.

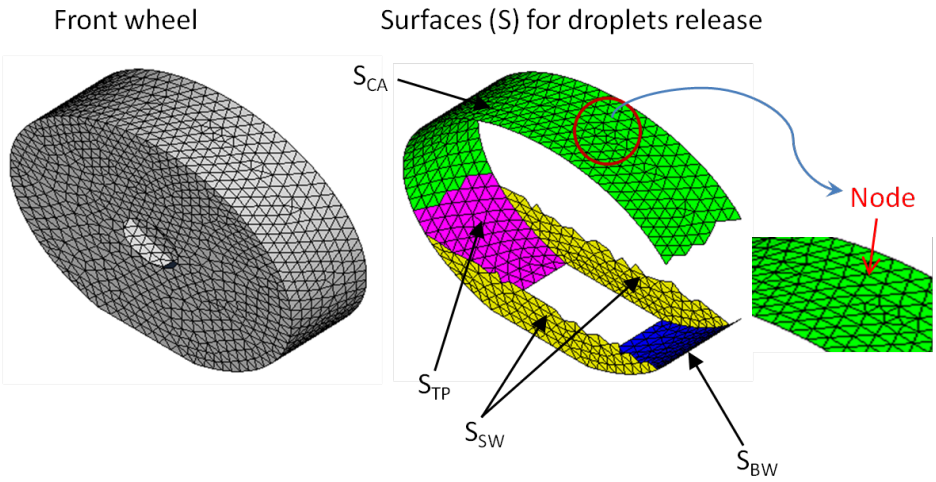

Figure 65. Rendering. Surfaces from which water droplets are released to simulate splash or spray.

6.3.2 Mass Flow Rate

The mass flow rate of water (MR_w) that could be displaced by a single tire along its path is estimated as:

$$MR_W = \gamma_W \cdot V \cdot WD \cdot b \quad (34)$$

where γ_w is the density of water, V is the speed of travel, WD is water film thickness in the road, and b is the tire width.

Using a water film thickness range between 0 mm and 5 mm (0 inches and 0.2 inches), a speed range between 48 km/h (30 mi/h) and 96 km/h (60 mi/h), and a tire tread width of 280 mm (11 inches), the mass flow rate of water shifted by the tire calculated using Equation (34) is depicted in Figure 66. It is observed that the mass flow rate of water shifted by the tire increases with vehicle speed and water film thickness.

The mass of water attributed to each of the mechanisms described by Weir et al. (1978) (capillary action [CA], tread pickup [TP], bow wave [BW], and side wave [SW]) is described in the following sections, and their sum should equal the total mass flow rate (MR_W):

$$MR_W = MR_{CA} + MR_{TP} + MR_{BW} + MR_{SW} \quad (35)$$

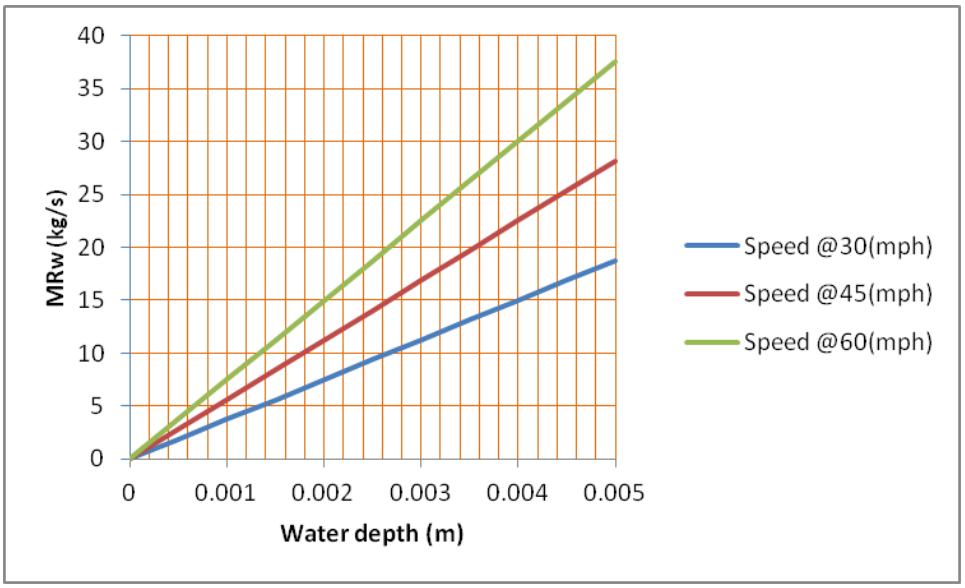

Figure 66. Graph. Estimated mass flow rate of water shifted by a single tire for different vehicle speeds.

6.3.3 Capillary Adhesion

Assuming the tire is not hydroplaning, it will remove the bulk of the surface water it contacts, such that only a small depth of water remains in the contact area between the tire and the road. Some of this small amount of water will be attracted by the tire rubber, picked up at the contact interface, and later flung off by the wheel rotation. It is not known what mass flow rate this accounts for in practice, so we have assumed that, on each tire rotation, up to 0.1 mm depth of water can be picked up by the tire and is later flung off. The maximum mass flow rate associated with capillary adhesion (MR_{CA}) is therefore estimated as the number of tire rotations per second multiplied by the volume of water dispersed on each tire rotation multiplied by the density of water, or

$$MR_{CA} = \left[\frac{V}{2\pi R}\right] \cdot \left[2\pi R \cdot b \cdot K \cdot h_{film}\right] \cdot \gamma_W = \left[V.b \cdot K \cdot h_{film}\right] \cdot \gamma_W \quad (36)$$

where V is the truck speed; R is the tire radius; b is the tire width; K is a factor that indicates the proportion of the tire width that is not a groove; h_{film} is the depth of the water film picked up on each

rotation, assumed to be 0.1 mm (0.004 inches) or the depth of water if lower; and γ_w is the density of water.

6.3.4 Tread Pickup

After capillary action, the tire is able to displace a volume of water within its tread. The maximum flow rate for this mechanism (MR_{TP}) will occur when all the water contained in the tread volume is flung out of the tread during each tire rotation. Thus, it can be computed as the number of tire rotations per second multiplied by the capacity of tire's tread on each rotation multiplied by the density of water:

$$MR_{TP} = V \cdot b \cdot (1 - K) \cdot h_{groove} \cdot \gamma_W \tag{37}$$

where the variables are the same as in Equation 36 except that now the proportion of the tire that does have grooves is important, and h_{groove} is the depth of water in the tire tread.

It is assumed that the tread depth, and therefore the maximum depth of water in the tread, is 10 mm (0.4 inches), which is representative of a worn tire. Because MR_{TP} is directly proportional to the tread depth, there is an implied significant difference between new and worn tires.

6.3.5 Bow Wave and Side Wave

Any remaining water for which there is no capacity either underneath the tire contact area or within the tire tread must be displaced to the front of the tire or to the side, causing the bow wave and side wave, respectively. For varying amounts of water, it is assumed that the ratio between bow and side waves will be constant, although it may be related to the tire geometry and tread pattern.

Combining Equations 35, 36, and 37, the total mass flow rate that can be attributed to bow and side wave mechanisms can be written as:

$$MR_{BW} + MR_{SW} = \gamma_W \cdot b \cdot V \cdot \left(WD - K \cdot h_{film} - (1 - K) \cdot h_{groove}\right) \tag{38}$$

so that MR_{BW} and MR_{SW} can be estimated separately as:

$$MR_{BW} = \alpha \cdot \gamma_W \cdot b \cdot V \cdot \left(WD - K \cdot h_{film} - (1 - K) \cdot h_{groove}\right) \tag{39}$$

$$MR_{SW} = \beta \cdot \gamma_W \cdot b \cdot V \cdot \left(WD - K \cdot h_{film} - (1 - K) \cdot h_{groove}\right) \tag{40}$$

where α and β are calibration factors that satisfy $\alpha + \beta = 1$. Until other evidence is available, it will be assumed that $\alpha = \beta = 0.5$.

Equations 36, 37, 38, and 39 are used to calculate the total mass flow rate and the flow rates attributed to each splash and spray generation mechanism. The available water (Equation 34) is allocated first to capillary adhesion, then to tread pickup, and finally to bow and side wave mechanisms.

6.3.6 Droplet Size and Mass Flow Rate at Individual Nodes

Droplets of different diameter can be released into the model from the nodes on each surface. The size of water droplets introduced into the model were altered for the different generation mechanisms: diameters of 100 µm, 200 µm, 500 µm, 1000 µm, 2000 µm, and 5000 µm (4 mil, 8 mil, 20 mil, 40 mil, 80 mil, and 200 mil) were used for droplets released into the model as a result of bow wave and side wave mechanisms; diameters of 100 µm, 200 µm, 500 µm, and 1000 µm (4 mil, 8 mil, 20 mil, 40 mil, and 80 mil) were used for droplets released as a result of capillary adhesion and tread pickup. This assumption could be verified by detailed experimentation.

Droplets are released from individual nodes. For a single node (i) in a given surface (S), the mass flow rate for each droplet diameter will be:

$$MR_i^S = \frac{MR_S}{N_d \cdot N_n} \quad (41)$$

where MR_S is the total mass flow rate for a particular surface (e.g., the mass flow rate MR_{CA}, leaving surface S_{CA} for capillary adhesion), N_n is the number of nodes on that surface, and N_d is the number of droplet diameters used.

6.4 Initial Velocities

The CFD model requires an injection file in the format (x y z v_x v_y v_z d T MR), where (x, y, z) are the coordinates of the nodes from which droplets will be released; (v_x, v_y, v_z) are the x, y, and z components of the velocity of droplets when they are released into the model; d is the diameter of a droplet; T is temperature; and MR is the mass flow rate of droplets being released. This section describes the methodology for calculating initial velocities of water droplets released from the mesh representing each tire. As before, the four assumed splash and spray mechanisms are discussed in turn.

6.4.1 Capillary Adhesion

Figure 67 depicts the setup of the CFD model, where the truck is stationary and the ground is moving at the speed V in the direction of the x negative axis and the reference frame (X, Y, Z) is attached to the truck.

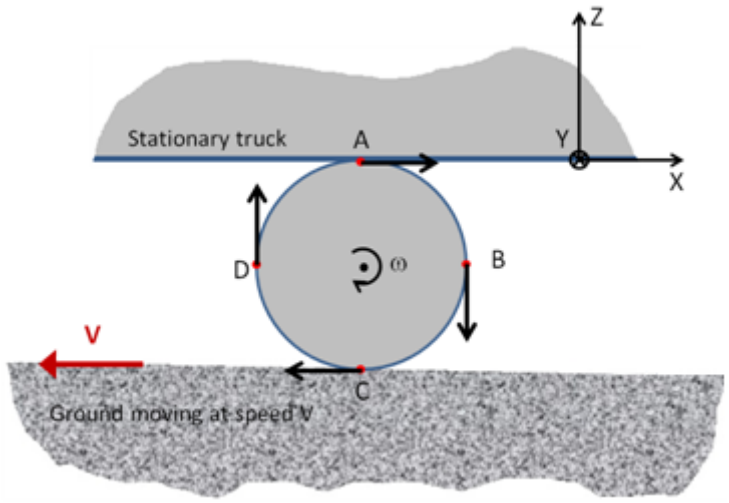

Figure 67. Diagram. Kinematic condition of a tire in the CFD model.

In this reference frame, the tire, with radius R, is rotating with an angular velocity of ω defined as:

$$\omega = \frac{V}{R} \quad (42)$$

and, for example, the velocities at points A, B, C, and D on the surface of the tread are:

$$V_A = (V, 0, 0)$$
$$V_B = (0, 0, -V)$$
$$V_A = (-V, 0, 0)$$
$$V_A = (0, 0, V)$$

Water droplets entering the model must be injected with the correct velocity, which, in the case of capillary adhesion, will be tangential to the tire surface. The model requires velocities to be specified in Cartesian components which, for a point M on the surface (remembering that the surface in question has been defined in Figure 65), may be calculated as follows (refer to Figure 68):

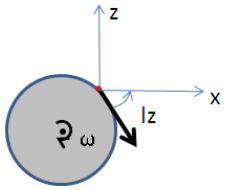

Figure 68. **Diagram. Cartesian axles used for modeling water droplets .**

- Let (u, w) be coordinates of a point M on the tire surface with respect to its center. Note that there is no velocity in the y-axis.
- Calculate $A = \frac{u}{\sqrt{u^2+w^2}}$ and $B = \frac{w}{\sqrt{u^2+w^2}}$
- Calculate $a = \cos^{-1}(A) \cdot \frac{180}{\pi}$ and $b = \sin^{-1}(B) \cdot \frac{180}{\pi}$
- The angular directions l_x and l_z of the initial velocity v_M satisfy
  - If $B \geq 0$ then $l_x = A$
  - If ($A < 0$ and $B < 0$) then $l_x = a - 2b$
  - If ($A > 0$ and $B < 0$) then $l_x = 360 - a$
  - $l_z = l_x - 90$
- So the components of the initial velocity are:
  - $v_x = \omega \cdot \sqrt{u^2 + w^2} \cdot \cos\left(l_z \cdot \frac{\pi}{180}\right)$
  - $v_y = 0$
  - $v_z = \omega \cdot \sqrt{u^2 + w^2} \cdot \sin\left(l_z \cdot \frac{\pi}{180}\right)$

The droplets released into the CFD model due to capillary adhesion are shown in Figure 69; the lines depict the direction of droplets travel, and the color coding shows the amount of time they have existed in the model, with the blue lines representing newer droplets.

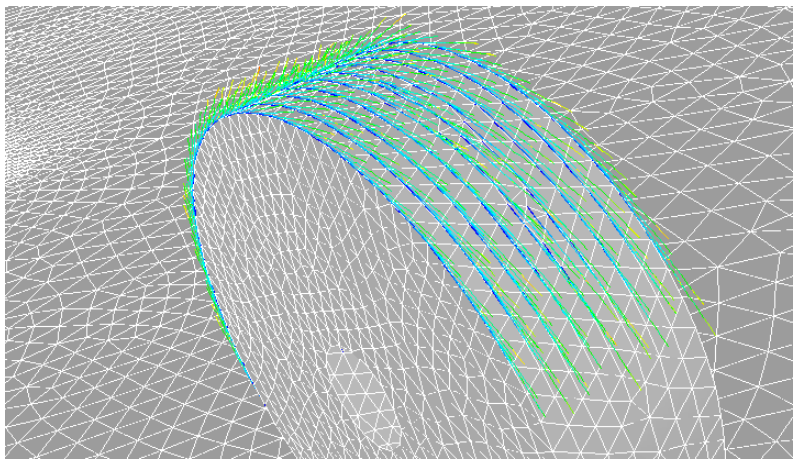

Figure 69. Rendering. Simulation of droplets entering the CFD model from surface S_{CA} due to capillary adhesion.

6.4.2 Tread Pickup

Figure 70 shows a representation of the initial velocities of droplets entering the CFD model due to the tread pickup mechanism, ejected from zone S_{TP} behind the tire at an angle of l = 10 °. The initial velocity $\vec{V}_{TP}$ is coplanar with plane XZ and is equal to the truck speed V.

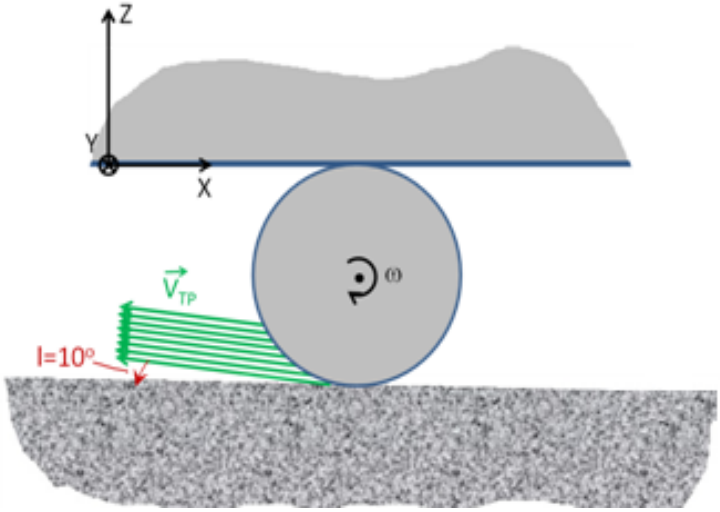

Figure 70. Diagram. Representation of the initial velocity for droplets released from zone S_{TP}.

The components of the initial velocity are calculated as:

- $v_x = -V \cos\left(\frac{\pi l}{180}\right)$
- $v_y = 0$
- $v_z = V \sin\left(\frac{\pi l}{180}\right)$

Figure 71 shows the initial direction of droplets being released into the CFD model from the back of the tire.

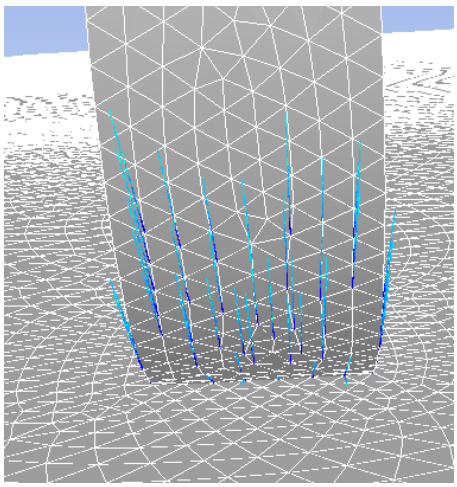

Figure 71. Rendering. Simulation of droplets entering the CFD model from surface S_{TP} due to tread pickup.

6.4.3 Bow Wave

In the frame of reference attached to the truck, a body of water on the road will impact the tire at a speed V, equal to the truck speed. It is assumed that the bow wave emerges at an angle *l* with respect to the x axis, as depicted in Figure 72, and the speed of the wave is V_{BW}, defined as:

$$\boldsymbol{V_{BW} = \zeta \cdot V} \tag{43}$$

where V is the truck speed and ζ is a constant satisfying the inequality $0 < \zeta \leq 1$ (i.e., the speed of the bow wave will not exceed the speed of the truck, but the case of $V_{BW} = V$ can happen under the condition of an elastic impact). The case $V_{BW} < V$ is more realistic because it is likely that the impact generates energy losses that could be attributed, for example, to generated heat or water turbulence.

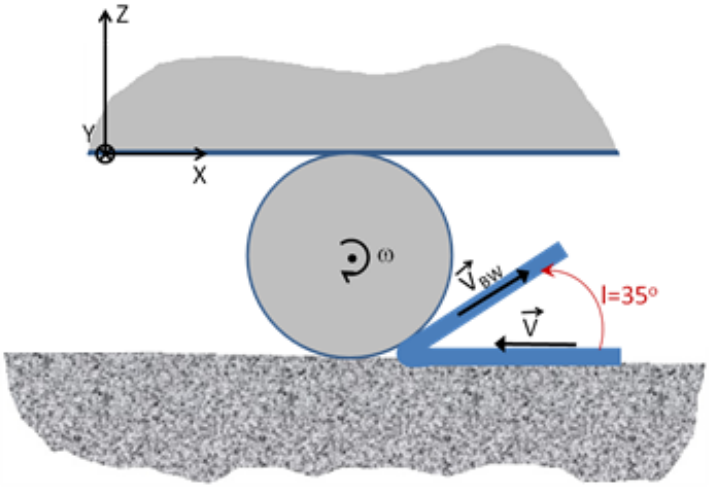

Figure 72. Diagram. Representation of the initial velocity for droplets released from zone S_{BW}.

Assuming that the bow wave occurs only in the plane (x,z), the components of the initial velocity $\vec{V}_{BW}$ are:

- $v_x = \zeta \cdot V \cdot \cos\left(\frac{\pi l}{180}\right)$
- $v_y = 0$
- $v_z = \zeta \cdot V \cdot \sin\left(\frac{\pi l}{180}\right)$

Figure 73 shows the initial direction of droplets being released into the CFD model from the front of the tire.

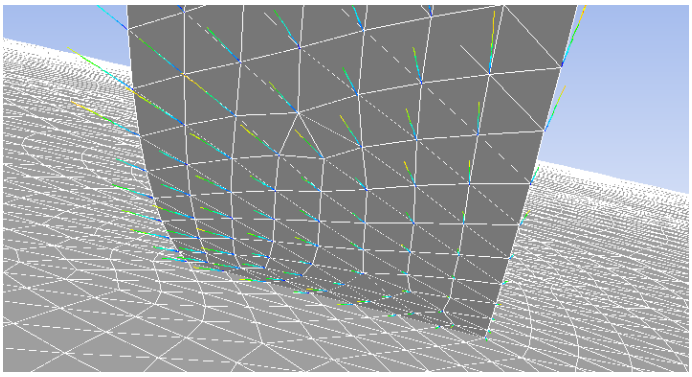

Figure 73. Rendering. Simulation of droplets entering the CFD model from surface S_{BW} for the bow wave.

To subjectively judge the effect of the parameter ζ, which controls the magnitude of the initial droplet velocities, the CFD model was allowed to run with just those droplets entering from a bow wave with ζ equal to 0.1, 0.2, 0.5, and 0.75. Figure 74 depicts the trajectories of the droplets released from zone S_{BW} for these values of ζ. The effect of increasing the value of ζ is to increase the distance traveled by the droplets; more droplets will make it into the wake behind the truck, reaching as far as where the car is positioned, 10 m behind. The cases with ζ = 0.1 and ζ = 0.2 were judged to be more realistic, and a value of ζ = 0.2 has been used.

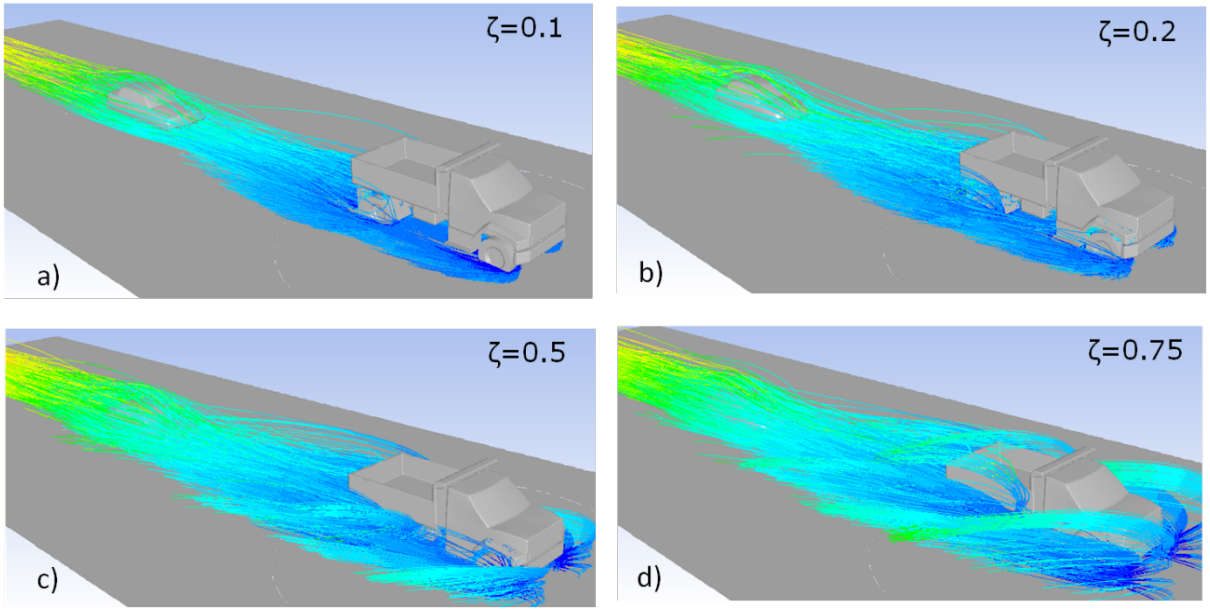

Figure 74. Rendering. Effect of the parameter ζ on the shape of the bow wave.

6.4.4 *Side Wave*

The initial velocity of the side is defined by the vector $\vec{V}_{SW}$, depicted in Figure 75 and Figure 76; it is assumed that its horizontal component, v_x, is equal to the speed of the vehicle, so that the magnitude of the initial velocity, V_{SW}, is:

$$V_{SW} = V\sqrt{\left(1 + tan^2\left(\frac{\pi l}{180}\right) + tan^2\left(\frac{\pi n}{180}\right)\right)} \tag{44}$$

where *n* and *l* are the angles shown in Figure 76 and the vector components required for the injection file are:

$$v_x = -V$$
$$v_y = \pm V \cdot \tan\left(\frac{\pi n}{180}\right)$$
$$v_z = V \cdot \tan\left(\frac{\pi l}{180}\right)$$

The range of the angles *l* and *n* have already been defined as 10° to 15° and 15° to 20°, respectively.

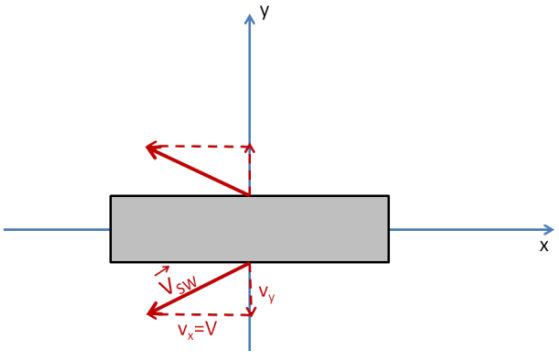

Figure 75. Diagram. Representation of the initial velocity of droplets entering the CF model from zone S_{SW}.

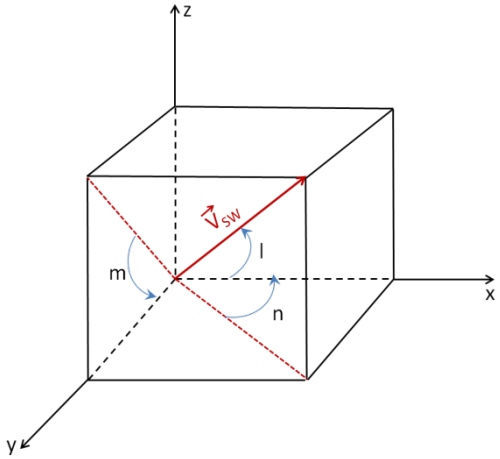

Figure 76. Diagram. Cartesian components of velocity for side wave droplets.

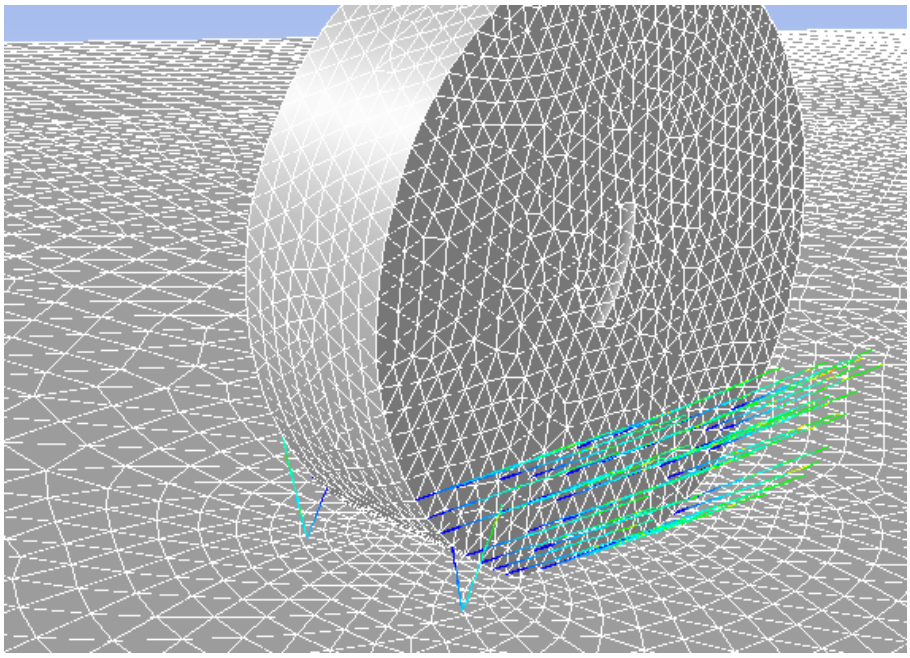

Figure 77. Rendering. Simulation of droplets entering the CFD model from surface S_{SW} for the side wave.

6.5 Characterizing Splash and Spray

This section presents three different methods for examining the amount of spray[14] generated by the truck, via the four mechanisms described above. To provide a single value representing the amount of spray, the final method allows demonstration of a relationship between the mass of spray behind the truck, M_{spray}, water film thickness, WD, and the speed of the truck, V.

6.5.1 Visualizing Droplet Trajectories

Figure 78 through Figure 81 show how the trajectories of droplets, introduced to the model via the four theoretical mechanisms, develop during the CFD modeling. The differences between the mechanisms appear to be in line with expectations. Capillary adhesion results in rather high trajectories that take a significant proportion of droplets directly onto the windscreen of the following vehicle.

In contrast, trajectories arising from tread pickup remain closer to ground level, and the droplets ejected from the rear tires appear to fall quickly to ground level; the trajectories end just behind and to the side of the truck, where they impact on the road surface.

[14] In the simulation model, *spray* refers to both splash and spray.

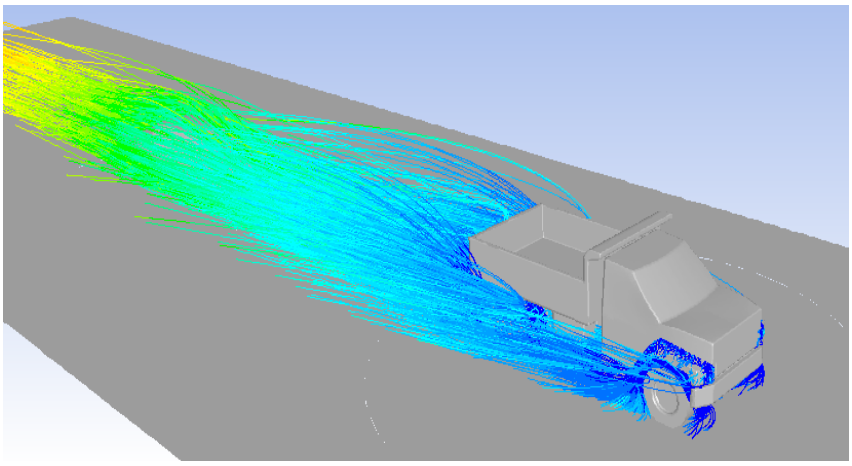

Figure 78. Rendering. Simulated droplet trajectories resulting from capillary adhesion at 30 mi/h (48 km/h).

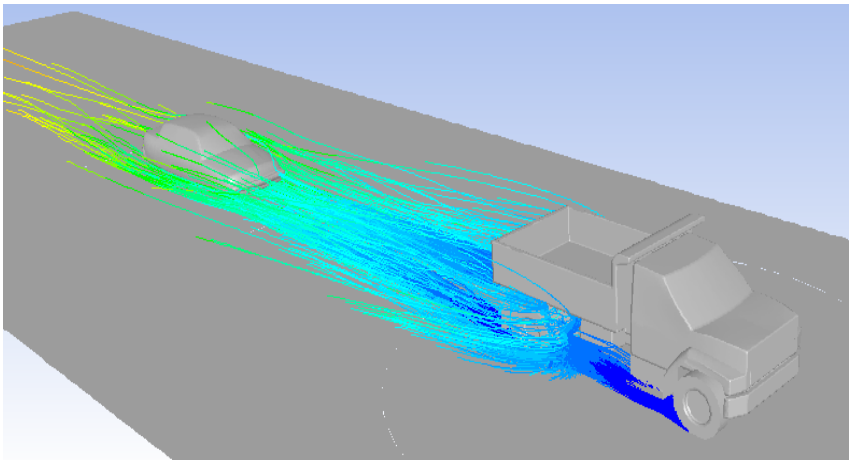

Figure 79. Rendering. Simulated droplet trajectories resulting from tread pickup at 30 mi/h (48 km/h).

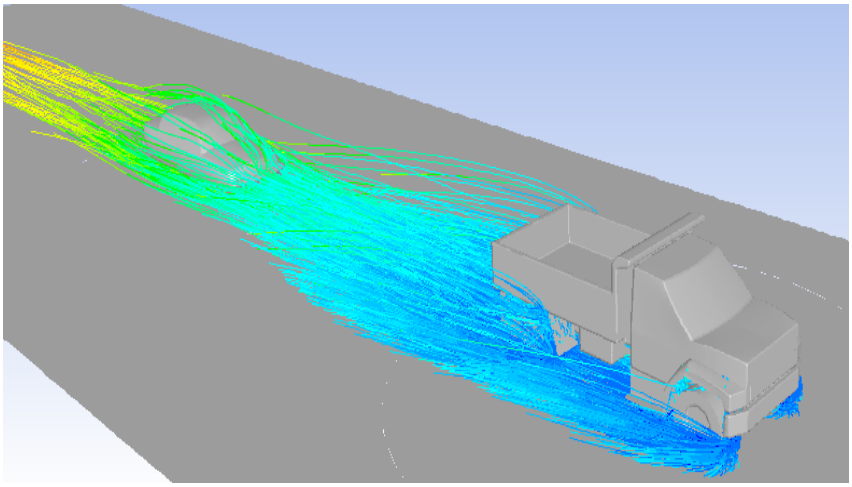

Figure 80. Rendering. Simulated droplet trajectories resulting from bow wave at 30 mi/h (48 km/h).

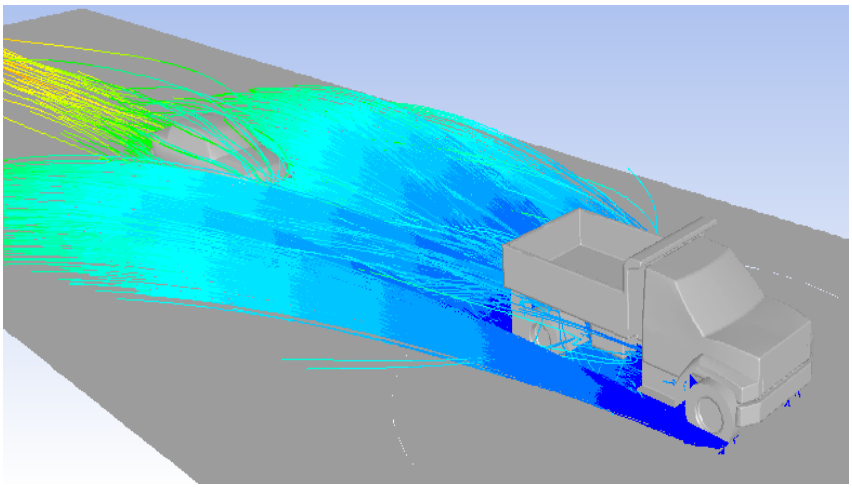

Figure 81. Rendering. Simulated droplet trajectories resulting from side wave at 30 mi/h (48 km/h).

Of all the mechanisms, tread pickup appears to result in the least nuisance to the following vehicle. The bow wave droplets begin by traveling forward and are rapidly displaced to the side of the vehicle by the airstream; these droplets also tend to remain close to the ground. Trajectories of droplets in the side wave are higher, and this may cause nuisance to a vehicle overtaking the truck. A vehicle following the truck, as shown, appears to be relatively unaffected by either the bow wave or side wave. Figure 82, which combines the spray from all four mechanisms, shows that the sensitivity to increasing vehicle speed appears to be convincing.

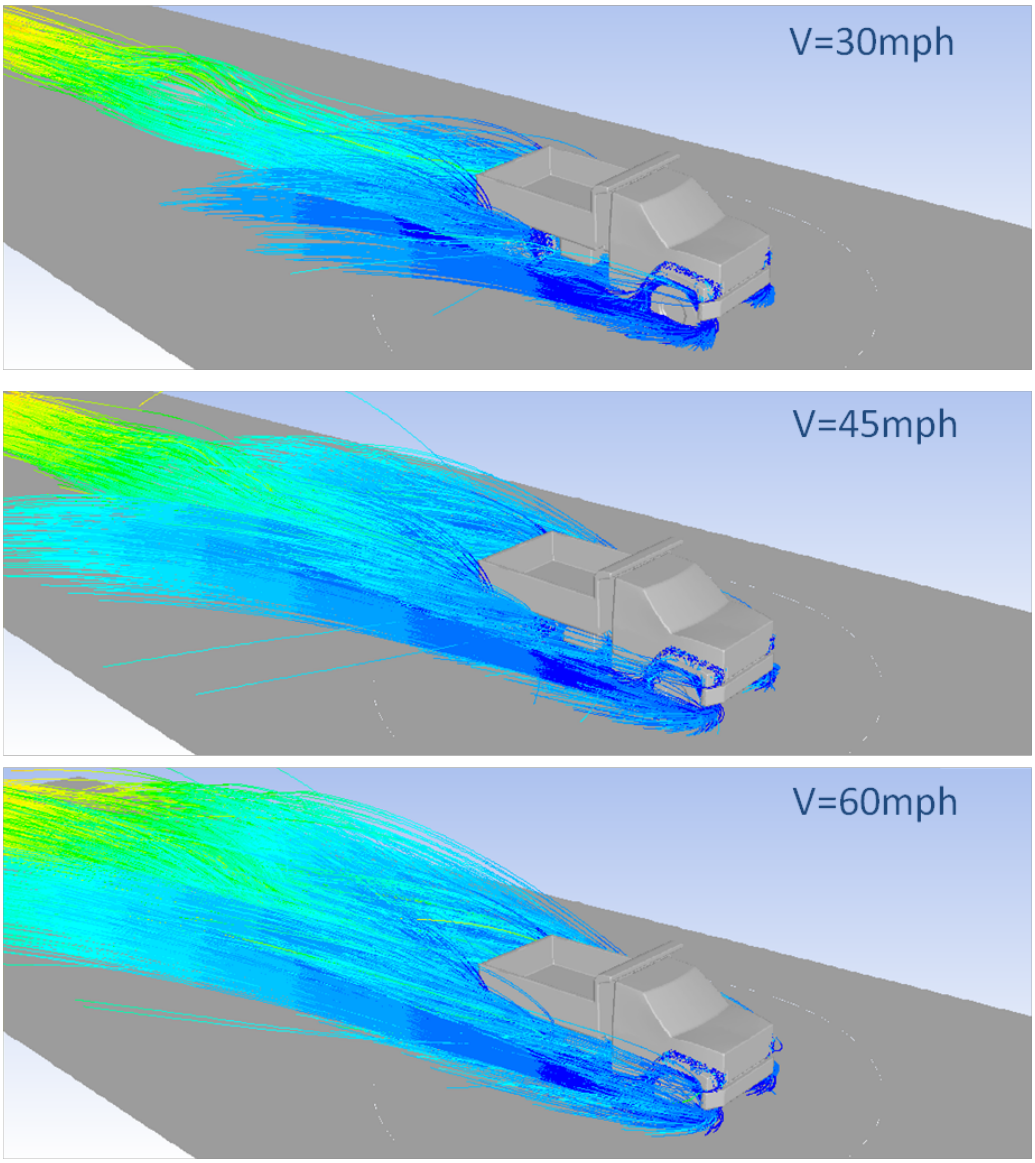

Figure 82. Rendering. Trajectories of water droplets from all four splash/spray mechanisms for different truck speeds.

6.5.2 Spray Concentration

Figure 83 depicts two vertical planes positioned 2.88 m (9.45 ft) and 12.9 m (42.3 ft) from the center of the dump truck. These distances approximately correspond to the rear of the truck and the front of the following car, respectively.

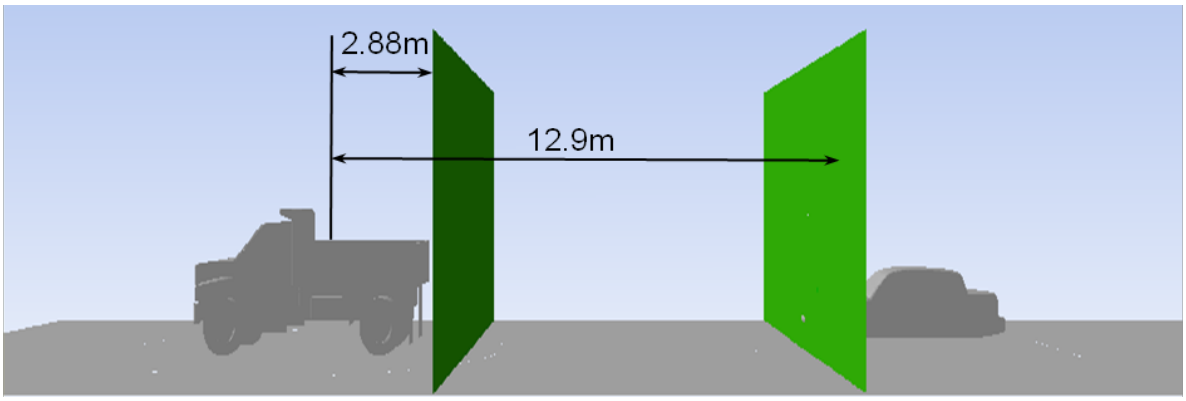

Figure 83. Diagram. Vertical planes used to output contour plots of spray concentration.

The spray concentration in these vertical planes is plotted as contours in Figure 84 and Figure 85 for truck speeds of 30 mi/h (48 km/h), 45 mi/h (72 km/h), and 60 mi/h (96 km/h). The highest spray concentrations, greater than 0.035 kg/m^3 (0.0022 lb/ft^3), are depicted in red, and the lowest spray concentrations, less than 0.0035 kg/m^3 (0.00022 lb/ft^3), are depicted in blue.

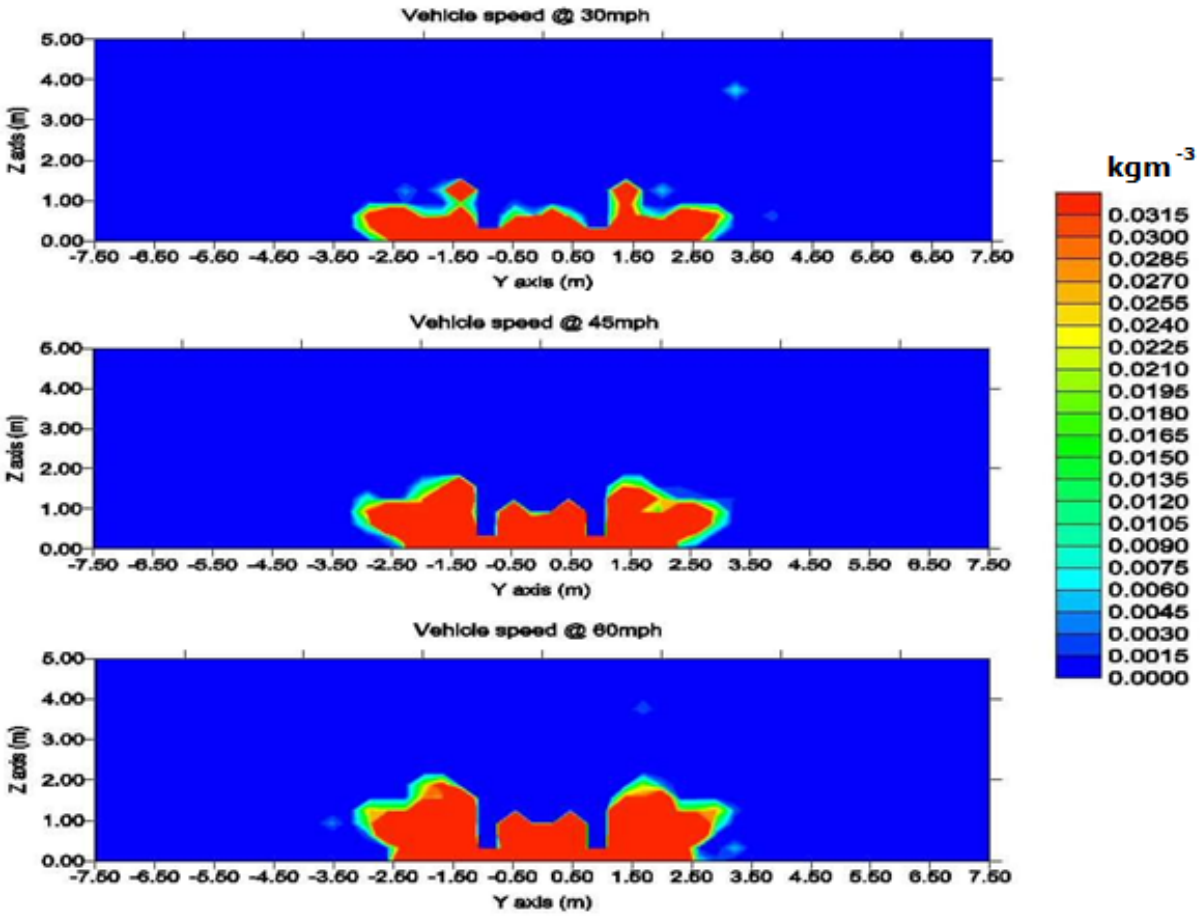

Figure 84. Graphs. Spray concentration in the vertical plane at 2.88 m (9.45 ft) at (top to bottom) 30 mi/h (48 km/h), 45 mi/h (72 km/h), and 60 mi/h (96 km/h).

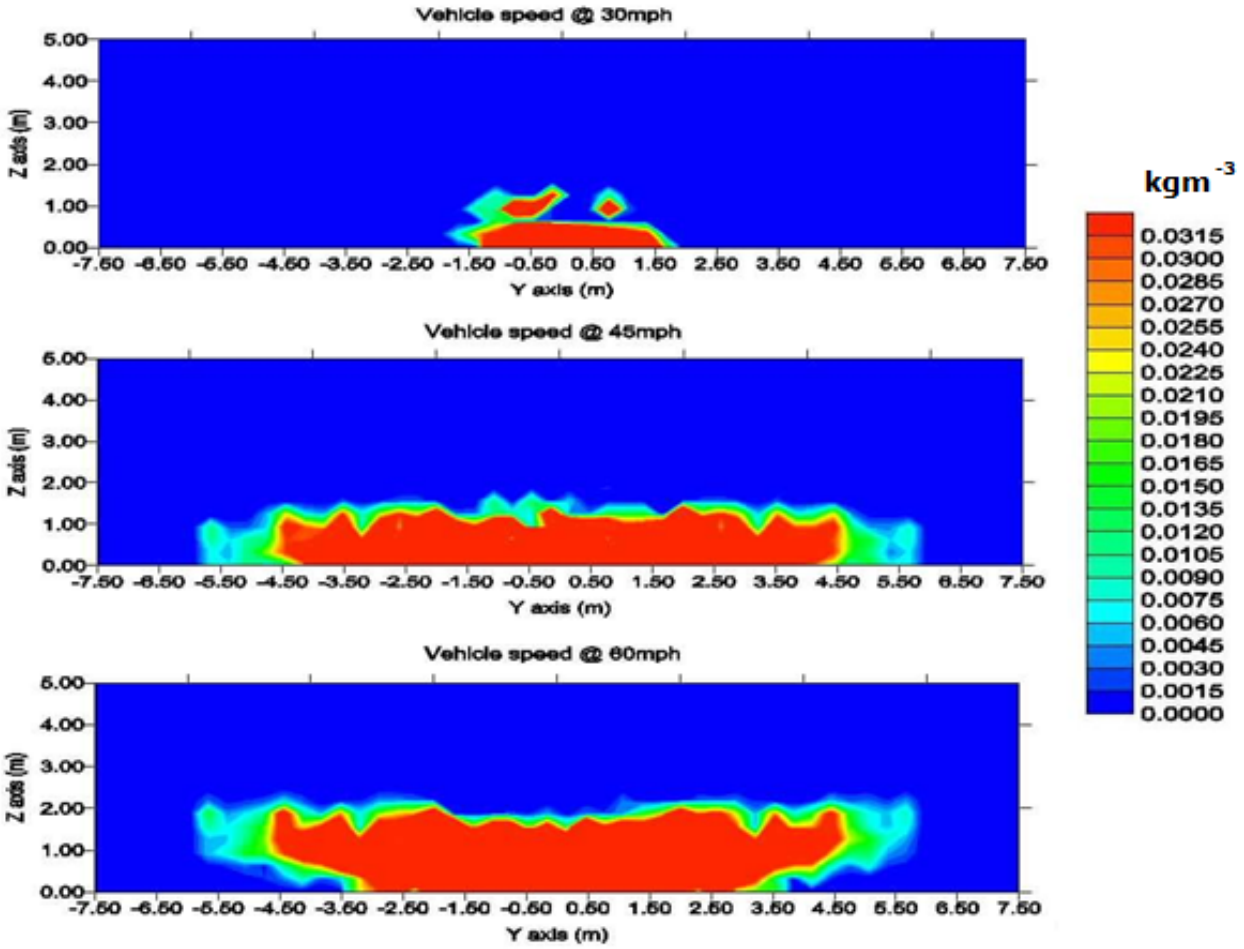

Figure 85. Graphs. Spray concentration in the vertical plane at 12.9 m (42.3 ft) at (top to bottom) 30 mi/h (48 km/h), 45 mi/h (72 km/h), and 60 mi/h (96 km/h).

The results show that both the distance from the rear of the truck and the speed of the truck have an effect on the spray concentration. The horizontal extent of the spray increases with distance from the truck, and the vertical extent of the spray increases with speed.

6.5.3 Quantifying the Amount of Spray

To attempt to characterize different conditions using a single measurement, the mass of spray collected in a volume of space between the truck and a following car was investigated. The volume is defined by the green box shown in Figure 86; the box is situated between 1 m (3.3 ft) and 2 m (6.6 ft) from the ground (at approximately the height of the following car's windscreen), and it extends to a distance of 8 m (26 ft) behind the truck; the width of the box is 2 m (6.6 ft), approximately the width of the truck.

To calculate the mass of spray in the volume, several analyses were run using different levels of two parameters: three truck speeds, 30 mi/h (48 km/h), 45 mi/h (72 km/h), and 60 mi/h (96 km/h), and four water film thickness (WD), 0.5 mm (20 mil), 1 mm (39 mil), 2.5 mm (98 mil), and 5 mm (196 mil).

The mass of spray generated by all four mechanisms at those speeds and water film thickness is shown in the graph in Figure 87. Each point on the graph was calculated as an average of three model runs. The mass of spray increases with speed and with water film thickness, and the rate of increase with speed is greater for deeper water film thickness.

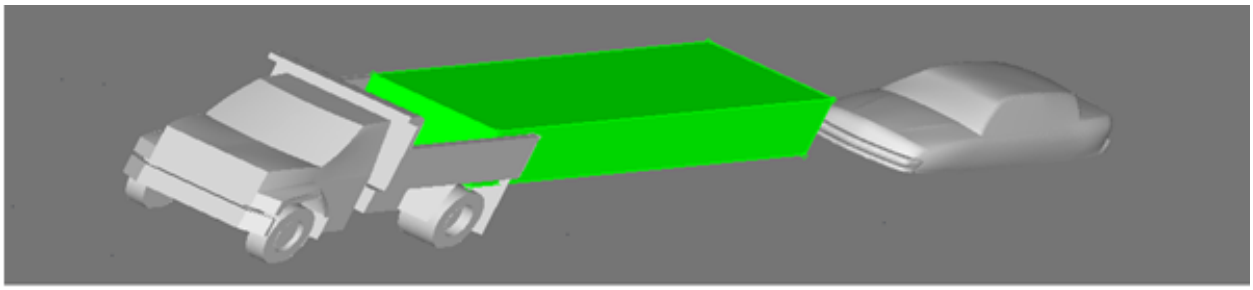

Figure 86. Rendering. A representation of the volume used to calculate mass of spray generated by the truck.

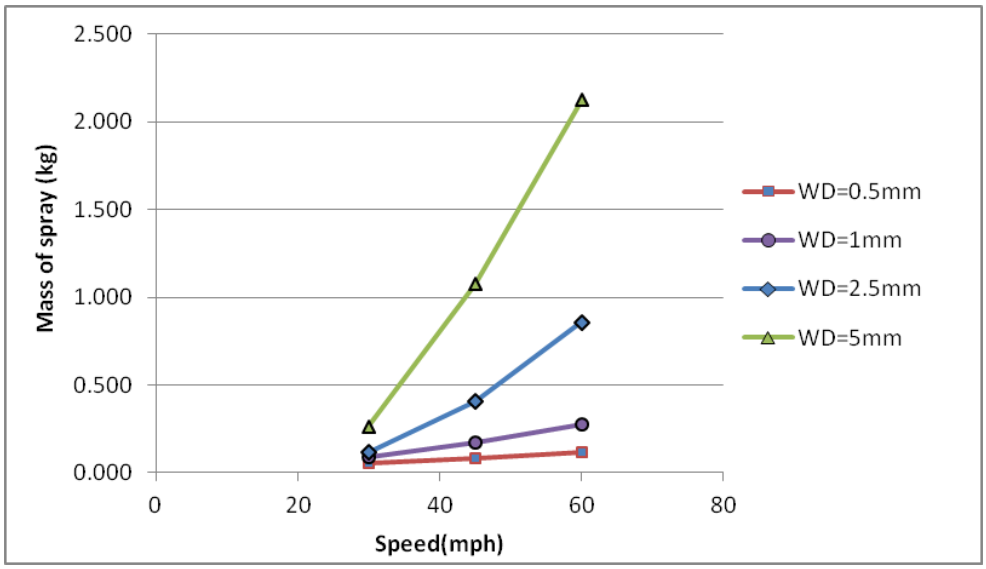

Figure 87. Graph. Effect of truck speed and water film thickness on total mass of spray in a region behind the truck.

6.6 Use of Modeling Results to Develop Simple Prediction Tools

This chapter describes the development of two simple tools that make use of the complex CFD modeling to compute density of splash and spray. Primarily, the tools enable a pavement engineer to make straightforward comparisons of the amount of splash and spray that is likely to be associated with various design or construction characteristics.

6.6.1 Distillation of CFD Results

CFD modeling is a time consuming process, so the simple tool used by pavement engineers should make use of average results rather than require further running of the model. To simplify the calculations, individual relationships for the mass of spray per unit mass flow rate, for different vehicle speeds, and for

each of the four individual mechanisms were determined. This makes calculation of the total mass flow rate more flexible in the assessment tool. Later validation may find that more realistic assumptions can be made about the way spray is generated by the four mechanisms or that their relative contributions are different. If so, the tool's summation can be amended without needing to carry out more CFD modeling because the four mechanisms' contributions to the total spray amount are separated.

The CFD model was used to calculate the mass and density of spray in the defined volume and to determine the maximum mass flow rates for the three speeds (30 mi/h, 45 mi/h, and 60 mi/h). The maximum mass flow rate was based on the theoretical mass flow rate calculated using Equations 36, 37, 38, and 39, and the model was used to determine the subsequent effect of vehicle speed given those rates. For each speed, the average density of spray calculated using the CFD model for three runs was normalized by dividing by the flow rate to give a density of spray per mass flow rate.

The graph in Figure 88 shows the average spray density, in the volume of air behind the truck, per unit of mass flow rate input to the model (per wheel), for each of the four splash- or spray-generating mechanisms.

Spray generated by capillary adhesion appears to decrease with increasing speed, which is somewhat counter-intuitive given that spray generated by the other mechanisms increases with speed. This effect probably results from a change in the trajectory of water droplets generated by capillary adhesion once they are influenced by the turbulent air flow. It is possible that the water droplets are either thrown sufficiently high and to the side of the following vehicle that they do not linger in the volume of space defined behind the truck, or that the they do not escape the air vortices generated in the vicinity of the tires but strike the surface of the truck or road and so do not enter into the volume behind the truck. These phenomena could be investigated by real-world experimental validation.

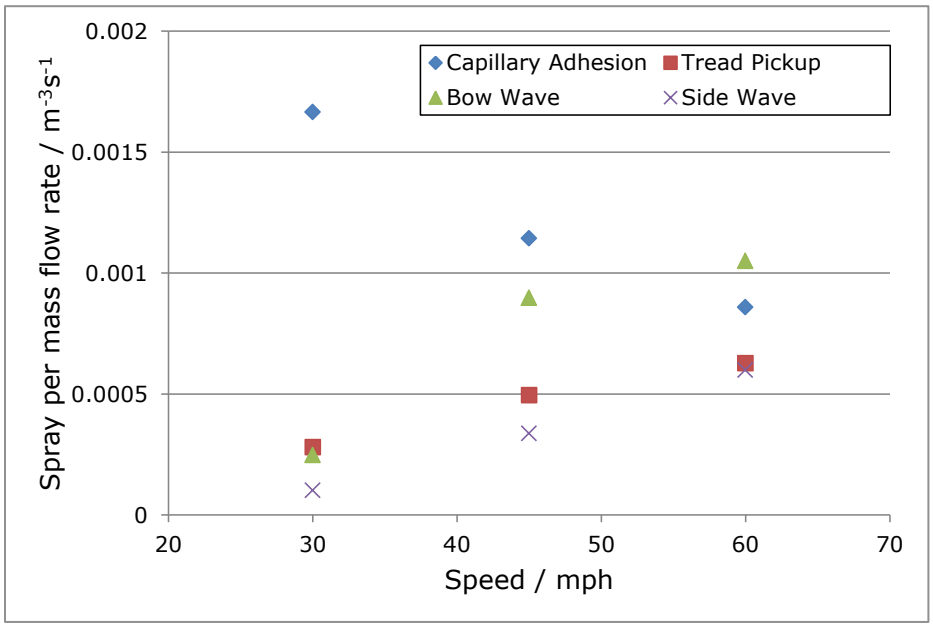

Figure 88. Graph. Mass of spray per unit mass flow rate for each of the four splash- or spray-generating mechanisms.

The spray densities generated using the CFD model appear to approximately follow a linear trend with speed for all but the bow wave mechanism. There are only three data points, but a linear fit to the data in

each case may be sufficiently robust, provided it is only applied between those speeds modeled (i.e., between 30mph (48 km/h) and 60mph (96 km/h)). Therefore, the following equations 45, 46, 47 and 48 were determined using linear regression:

Capillary Adhesion

$$\frac{SD_{CA}}{MR_{CA}} = -2.69 \cdot 10^{-5} \cdot V + 2.43 \cdot 10^{-3} \quad (45)$$

Tread Pickup

$$\frac{SD_{TP}}{MR_{TP}} = 1.16 \cdot 10^{-5} \cdot V - 5.25 \cdot 10^{-5} \quad (46)$$

Bow Wave

$$\frac{SD_{BW}}{MR_{BW}} = 2.67 \cdot 10^{-5} \cdot V - 4.71 \cdot 10^{-4} \quad (47)$$

Side Wave

$$\frac{SD_{SW}}{MR_{SW}} = 1.65 \cdot 10^{-5} \cdot V - 3.99 \cdot 10^{-4} \quad (48)$$

where SD is total spray density, MR is input mass flow rate per wheel and V is the speed of the truck (mph).

6.6.2 Splash and Spray Tools

To facilitate the implementation of the results, the model has been implemented in two prototype tools:

1. A standalone Excel spreadsheet that requires the user to input the rainfall intensity and duration in addition to the pavement surface characteristics.
2. A MATLAB script that automatically uploads the rainfall information based from the wet-hour database on the location selected by the user.

6.6.2.1 Excel Worksheet

The results from the various analyses have been used to create a basic calculation spreadsheet that allows input of the following parameters:

- Gradient, g
- Cross-slope, c
- Pavement width, w (all lanes)

} Pavement geometry

- Rainfall intensity, I
- Rainfall duration, D

} Rainfall information

- Pavement type (porous or non-porous)
- Pavement hydraulic conductivity, κ (if porous)
- Pavement layer depth, δ (if porous)
- Pavement void content, ε (if porous)
- Pavement texture, T

} Pavement material

- Speed limit

The user interface for input these parameters and instructions for the Excel assessment tool is shown in Figure 89.

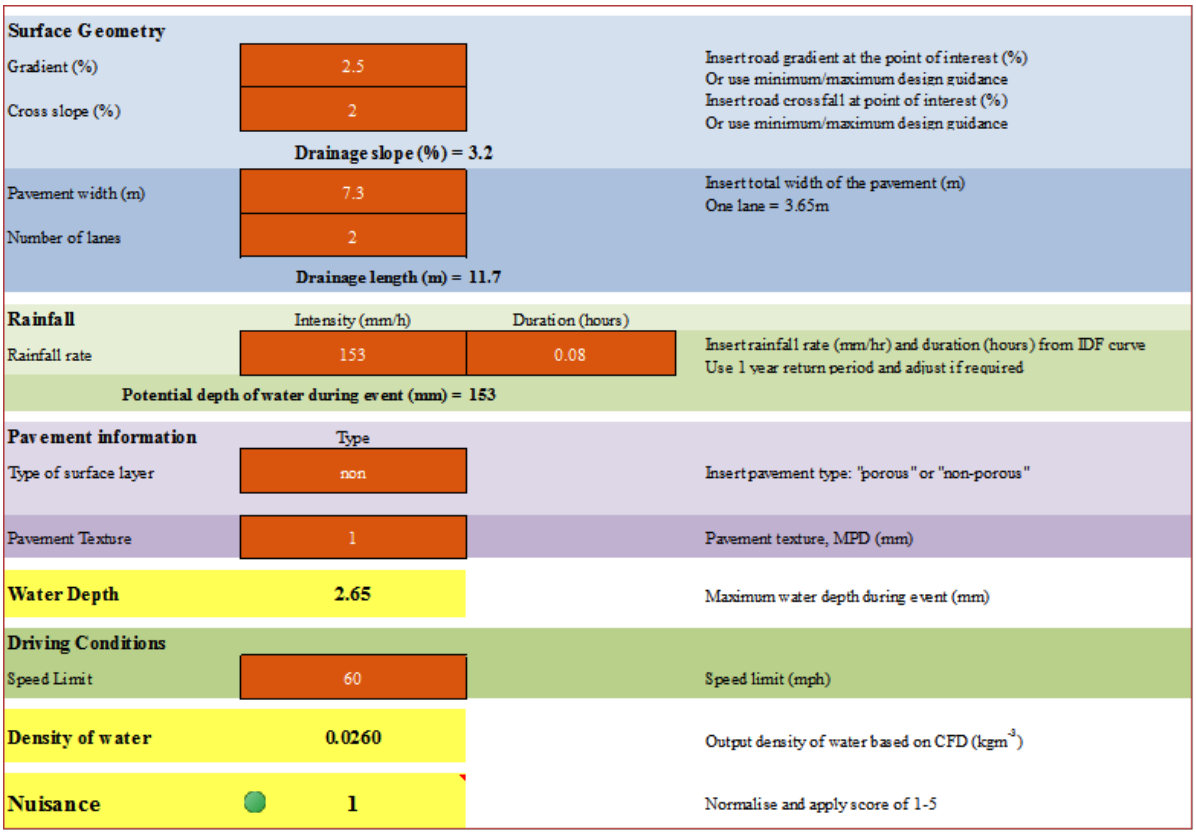

Figure 89. Screen shot. Appearance of the splash and spray assessment tool.

The first three sets of input data (pavement geometry, rainfall information, and pavement material) are all used to calculate water film thickness, using Equation (31), reproduced below:

$$d = 6\times10^{-4}.T^{0.09}.(LI)^{0.6}.S^{-0.33} \tag{31}$$

The slope, S, is calculated using the input values for gradient and cross-slope:

$$S = \sqrt{g^2 + c^2} \tag{49}$$

Drainage length, L, is calculated using the input values for gradient, cross-slope, and carriageway width:

$$L = w \cdot \sqrt{1 + \frac{g^2}{c^2}} \tag{50}$$

Rainfall intensity, I, is either taken directly from the input value or attenuated by the effects of a porous pavement. If a porous pavement is specified, and values for rainfall duration, pavement conductivity, depth, and void content are given, then the resulting intensity can be calculated.

The potential depth of water during a specified rainfall event is the input intensity multiplied by rainfall duration. The depth of water that can be removed by the porous pavement is the sum of its conductivity over the rainfall duration and the capacity of the pavement layer. Finally, the attenuated rainfall intensity, I_{atten}, is the potential depth of water during the rainfall event less the depth of water that can be removed by the pavement, all divided again by the duration of the rainfall event:

$$\boldsymbol{I_{atten} = \frac{I \cdot D - (\delta.\varepsilon + \kappa \cdot D)}{D}} \tag{51}$$

The final output from the tool is the density of water in the volume defined behind the truck. This is calculated by combining the equation for theoretical mass flow rate for each splash- or spray-generation mechanism (Equations 36, 37, 38, and 39) with the appropriate equation for the density of spray per unit of mass flow rate (Equations 45, 46, 47, and 48) associated with the same generation mechanism, using the input vehicle speed, V, and then summing all four values. An assumption is made about the distribution of water between the generation mechanisms: The available water film thickness is allocated first to capillary adhesion, then to the tread depth, and any remaining water is then split evenly between the bow and side wave mechanisms, as discussed in Section 6.3.5.

The density of water could, through practical validation, be linked to the amount of nuisance perceived by a road user (in the following sedan, for example) and the splash and spray potential of the site could be rated on this basis. For engineering purposes, it may be sufficient to see the relative effect on the density of water from adjustment of input parameters that can be controlled or designed.

6.6.3 MATLAB Script

The second tool allows the user to extract the rainfall rate input from the intensity, duration, and frequency curves, discussed in Section 4, by selecting a specific geographical location. By integrating this wet-exposure information with the splash and spray assessment tool, the user can estimate the potential nuisance to users of roads, with given properties, anywhere in the country. This software includes a simple graphical interface developed using the MATLAB Graphic User Interface (GUI) tool as shown in Figure 90.

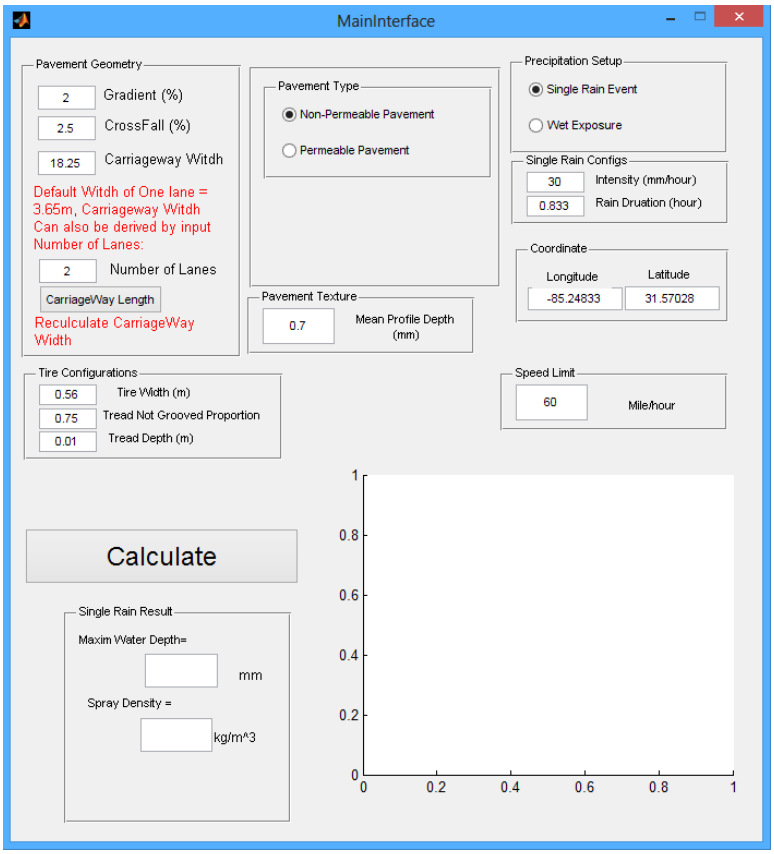

Figure 90. Screen Shot. Main input screen of Matlab splash and spray tool.

The first group of required input corresponds to the pavement geometry (top left of Figure 90). The user must input the gradient, cross slope, and pavement width. The tool also allows the user to enter the number of lanes instead of the total pavement width and assumes a default lane width value of 12 ft (3.65 m).

The user can also change some of the other values provided by default:

- The tire configuration, including width, tread depth, and percentage or surface not grooved.
- The pavement macrotexture (mean profile depth [MPD]).
- Permeable versus non-permeable surface layer. Selecting a permeable pavement requires the user to enter the conductivity, depth, and void content of the porous layer.

Finally, the user can choose to calculate the splash and spray density for a single rain event of a specific intensity and duration or for various average intensities in a specific location. The user can enter the latitude and longitude, and the software selects and displays the wet exposure for the corresponding county.

6.7 Discussion

This section presented the development of the final splash and spray model by combining outcomes from project experiments with CFD modeling of mechanisms of splash and spray generation. The CFD modeling was used to predict splash and spray generation by the four prevailing mechanisms—bow wave, side wave, tread pickup, and capillary adhesion—for different vehicle speeds and water film thicknesses. The outcome was synthesized in a set of simple equations.

These equations were then used to develop two simple tools to facilitate the implementation of the results: (1) a standalone Excel spreadsheet that requires the user to input the rainfall intensity and duration in addition to the pavement surface characteristics and (2) a MATLAB script that automatically uploads the rainfall information from the wet-hour database for the location selected by the user. These tools could be integrated into AASHTO's PaveSuite technologies (AASHTO, 2013); they complement the Automated Cross-Slope and Drainage Path Method, which allows pavement engineers to efficiently and effectively identify roadway areas with a high likelihood of hydroplaning.

7 Validation Experiments[15]

This chapter presents a second set of experiments conducted under controlled condition at the Virginia Smart Road to validate the splash and spray model. The original plan was to run the experiments under regular precipitation on actual roads, but this was not possible due to time constraints, weather changes, and availability of equipment. The chapter also expands on the calculation of the occlusion factor defined in Chapter 5 and presents the application of the model to an actual road segment to illustrate the practicality of the tools and methods proposed.

7.1 Controlled Experiments

7.1.1 Experimental Design

The controlled experiments were conducted using the most severe maneuver, the vehicle following the truck, and at two speeds, 45 mi/h (72 km/h) and 60 mi/h (96 km/h). The same level of precipitation (approximately 0.4 inches/h (10 mm/h)) was used in all the experiments. The available rain setup overlapped with four of the flexible pavement sections with the following surfaces:

- Two Superpave mixes (Sections I and J), with average texture of 0.99 mm and 1.15 mm MPD, respectively.
- An open graded friction course (OGFC, Section K), with an average texture of 1.75 mm MPD and an as-built porosity of approximately 20 percent.
- A stone mastic asphalt (SMA) mix (Section L), with an average texture of 1.1 mm MPD.

7.1.2 Facilities and Equipment

In this test, the black-and-white grid was attached to the tailgate of a Virginia Department of Transportation (VDOT) dump truck, which was then driven through simulated rain on the Smart Road. The following vehicle (a 1999 Ford Explorer, used because an instrumented sedan was not available) followed approximately 30 m (100 ft) behind the dump truck and recorded images of the spray and splash. The truck and following vehicles are shown in Figure 91 and Figure 92.

Figure 91. Photo. Splash- and spray-generating truck.

[15] This chapter was prepared by L. Tang, B. Williams, G. Flintsch, R. Gibbons, and S. Katicha from the Virginia Tech Transportation Institute.

Figure 92. Photo. Following driver vehicle.

The following vehicle was equipped with a luminance camera system as discussed in Chapter 5. A large black-and-white checkered board was attached to the back of the spray vehicle. The resulting images provide information about how much light is reflected off the various surfaces in the images. This was used to determine the amount of occlusion caused by the splash and spray.

7.2 Data Analysis

7.2.1 Occlusion Factor Calculation

As defined in Chapter 5, the occlusion factor is a measure of the amount of spray and splash created by a vehicle driving on a wet surface. It refers to the level at which a black-and-white, 12x8 grid attached to the back of a vehicle is occluded by the spray and splash the vehicle creates.

The occlusion factor was defined as the ratio of the mean luminance of the black squares to the mean luminance of the white squares. A custom MATLAB program identified each of the squares, measured the luminance at the center of each square, and then created a mean value for the black squares and a mean value for the white squares.

This analysis works under the assumption that as splash and spray between the checkerboard and the camera increase, the difference in luminance values between the black squares and white squares decreases. At the point that splash and spray completely occlude the checkerboard, the luminance values for black squares and white squares would be equal (ratio = 1). Figure 93 illustrates this concept by comparing an image of the checkerboard without splash or spray to an image with splash and spray.

Three to five images were analyzed for each pavement section at the two speeds. Images that were analyzed included only those taken just after the windshield wipers cleared the windshield of the following vehicle, in order to minimize the effect of water droplets on the windshield. The three to five images for each pavement section and speed were averaged. Figure 94 shows the results.

As shown, the baseline occlusion factor—when no splash or spray is present—is approximately 0.35. This is because the white squares have about three times as much luminance as the black squares. At 45 mph (72 km/h), section I had an occlusion factor (0.61) significantly less than the other sections which were not significantly different from one another (0.75 to 0.79). At 60 mph (96 km/h), section J had an occlusion factor significantly lower than sections I and K; however, there was no practical difference because all sections ranged from 0.88 to 0.93. Table 16 summarizes the rain intensities recorded during the experiment.

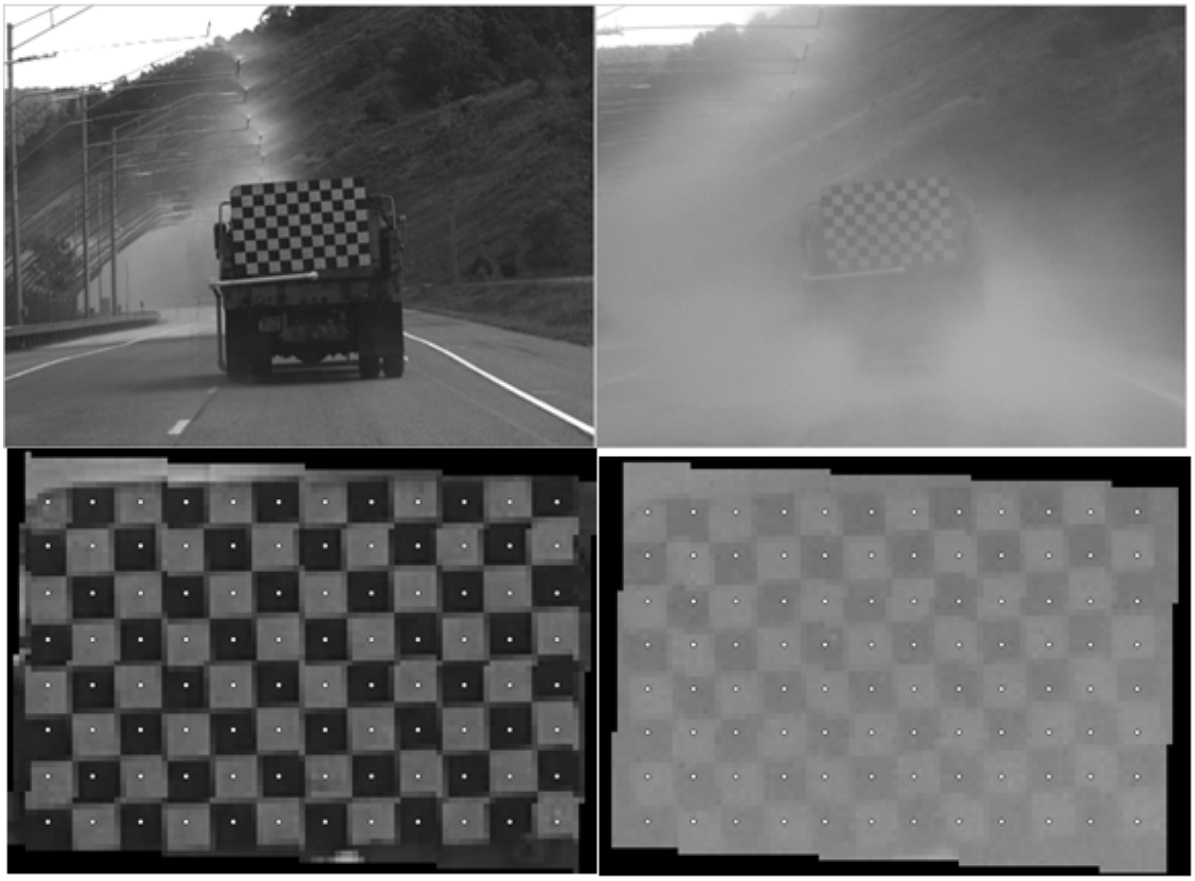

Figure 93. Photo. Comparison of checkerboard images with and without splash and spray.

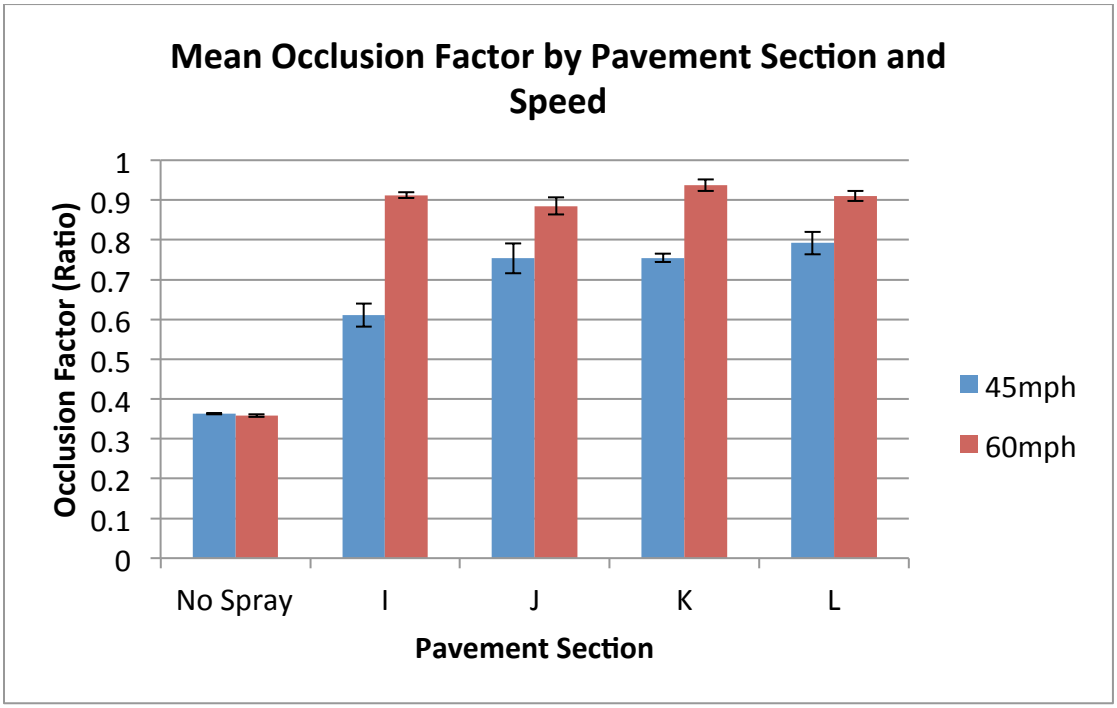

Figure 94. Chart. Mean Occlusion Factor by Pavement Section and Speed.

Table 16. Rain gauge measurements during the validation experiments.

Inches of Rain	Duration of Measurement (min)	(hours)	Section	Rain Intensity (inches/h)
0.09	9	0.15	I	0.60
0.29	25.5	0.43	J	0.68
0.33	23.5	0.39	K	0.84
.	.	.	L	Instrument error

These values were based on an overall average of the luminance of all 48 white squares and all 48 black squares. To determine if the occlusion factor was uniform across the grid, or if some areas of the grid were more occluded than others, a "heat map" table was created for each section and speed. This was done by creating an occlusion factor for each pair of white and black squares on the grid, creating a 6x2 grid. Figure 95 presents how the squares were paired and the mean occlusion factor for each of those pairs. The lowest values are highlighted in green, the highest in red. As shown, the occlusion factor was generally very consistent across the grid.

7.2.2 Discussion

The change in texture among the various sections is not very pronounced, so these occlusion factor results were in line with expectations. At slow speeds, the lower rain intensity recorded in Section I resulted in a lower occlusion. An unexpected result is that the OGFC apparently did not show any benefits with respect to splash and spray; however, the short length of the section may have masked its benefits.

7.3 Nuisance Levels

The last step in the validation was to define a preliminary scale to assess the effect of the splash density (SD) on the users. The results for the limited tests conducted as part of the user perception study were used to illustrate how this can be done. The splash density was computed for the most and least severe of the conditions experienced by the users during the experiments. The most severe condition corresponded to the truck traveling at 60 mi/h (96 km/h) and the heavy rainfall intensity, 64 mm/h (2.5 inches/h). These conditions produced, using the developed spreadsheet, a spray density of 0.019 kg/m^3. In the least severe condition, the truck traveled at 45 mi/h (72 km/h) under moderate rainfall intensity, 20 mm/h (0.8 inches/h) and produced a splash density of 0.006 kg/m^3.

Based on these observations, the following splash density scale was developed:

- very low: $SD \leq 0.006$ kg/m^3
- low: 0.006 kg/m^3 $< SD \leq 0.010$ kg/m^3
- medium: 0.010 kg/m^3 $< SD \leq 0.014$ kg/m^3
- high: 0.014 kg/m^3 $< SD \leq 0.018$ kg/m^3
- very high: $SD \geq 0.018$ kg/m^3

These values were based on a very limited number of experiments, so they are presented as an example only.

Figure 95. Illustration Heat maps of the mean occlusion factors.

7.4 Pavement Management Applications

To test the practicality of the proposed approach, the splash and spray prediction model was applied to an actual segment of road using data provided by the Florida DOT. The road segment chosen for this calculation is a state route located in Alachua County, Florida. This section of road was evaluated as part of the Florida DOT's research "Automated Cross-Slope and Drainage Path Method."

7.4.1 Pavement Data

Figure 96 and Figure 97 show the transversal and longitudinal slope measurements for the segment of road studied. Figure 96 shows that the area from milepost 10 to 10.8 features a section with super-elevation, and the cross slope is higher than for the rest of the road. The grade of the road varies along with the terrain, with a maximum grade of approximately 5 percent. The road has two lanes in each direction; given that the width of each lane is 12 ft (3.6 m), the total pavement drainage width is 24 ft (7.2 m). The road surface is relatively impermeable, and the average texture depth was assumed to be 0.7 mm.

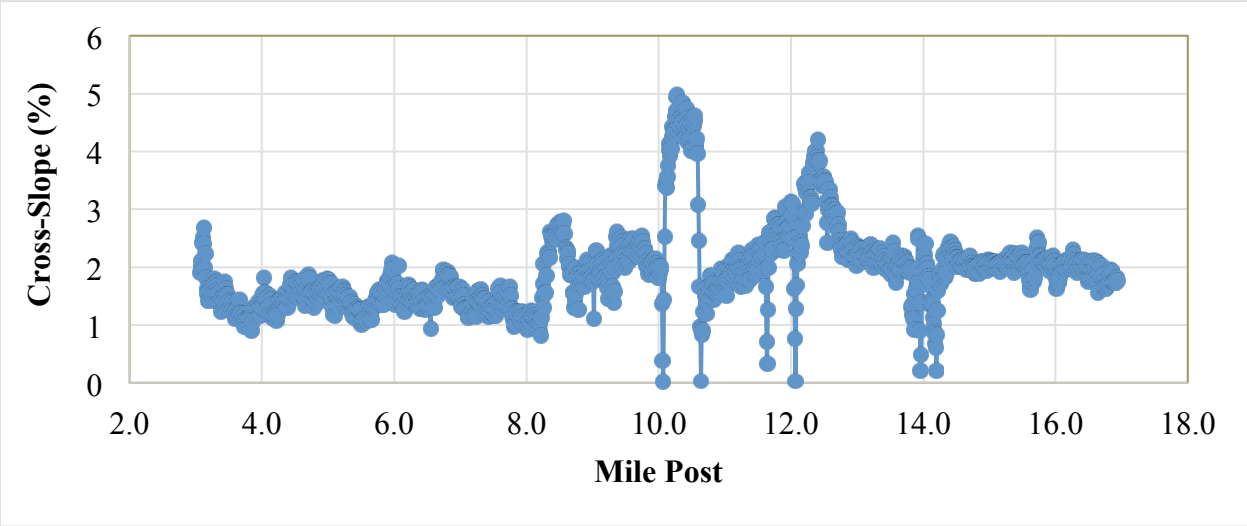

Figure 96. Graph. Pavement surface cross slope.

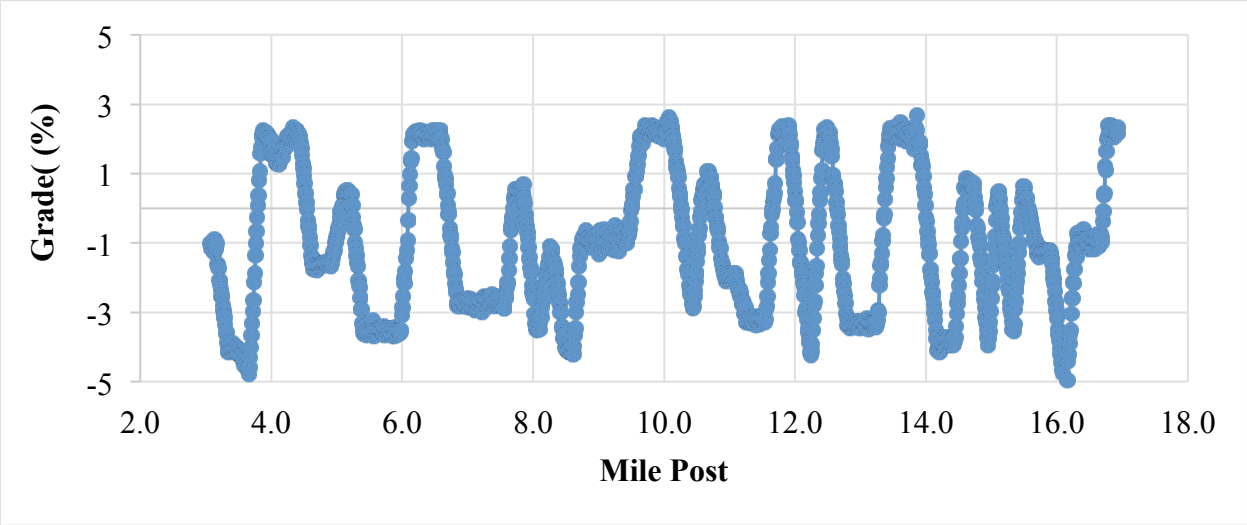

Figure 97. Graph. Longitudinal grade.

7.4.2 Drainage Path Calculation

The splash and spray tool was used to first calculate the length of the drainage path for each location along the road (Figure 98).

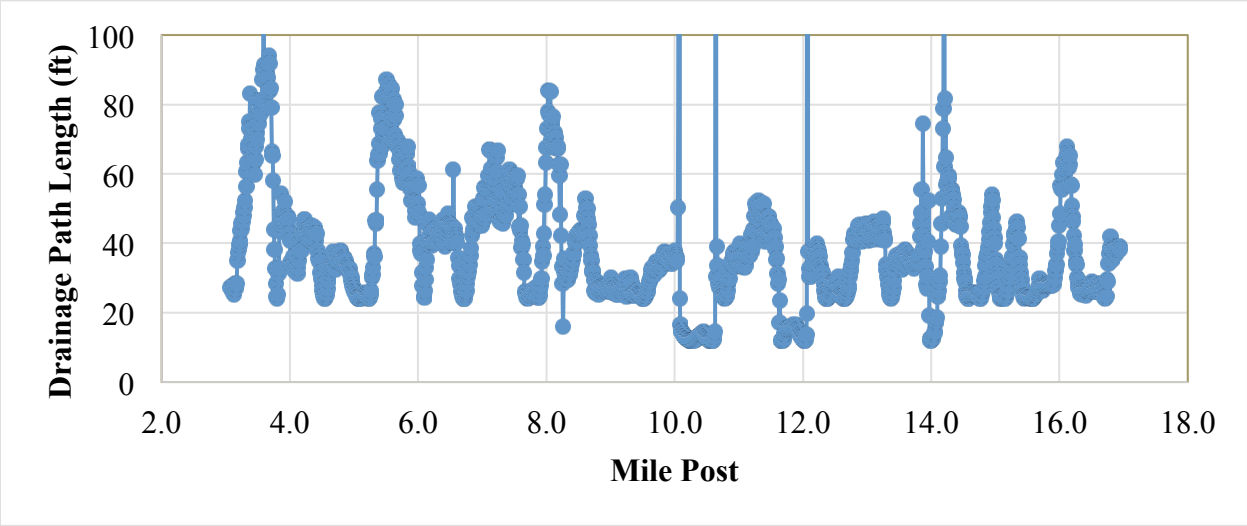

Figure 98. Graph. Calculated drainage path length (ft).

The graph shows that when the cross-slope is very small (close to 0, e.g., at the transitions), the equation gives extreme drainage path lengths. Though a lack of cross slope leading to bigger drainage path is expected, it also shows that the equation is not accurate for extreme conditions; rather, it assumes that the transversal slope is maintained for a relatively long section of road.

7.4.3 Rainfall Intensity (Wet Exposure)

The weather database integrated in the splash and spray MATLAB tool was used to estimate the wet-pavement exposure for different rainfall durations in Alachua County. Figure 99 shows that, for example, in a year this county will have 10 hours of rain with an intensity higher than 0.68 inches/h (17 mm/h).

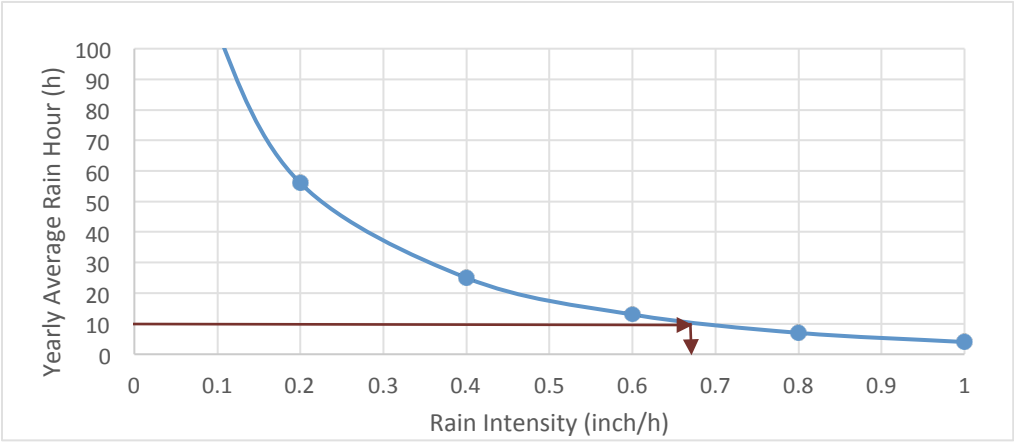

Figure 99. Graph. Average annual wet exposure for Alachua County, Florida.

7.4.4 Splash and Spray Density Calculation

Using the intensity of 0.68 inches/h (17 mm/h), the tool calculated the splash and spray density along the road, as shown in Figure 100. The super-elevated section, which has higher cross-slope than other sections, has the least splash and spray density. This implies that, on average, for 10 hours per year, users will encounter values of splash and spray that equal or exceed the level indicated.

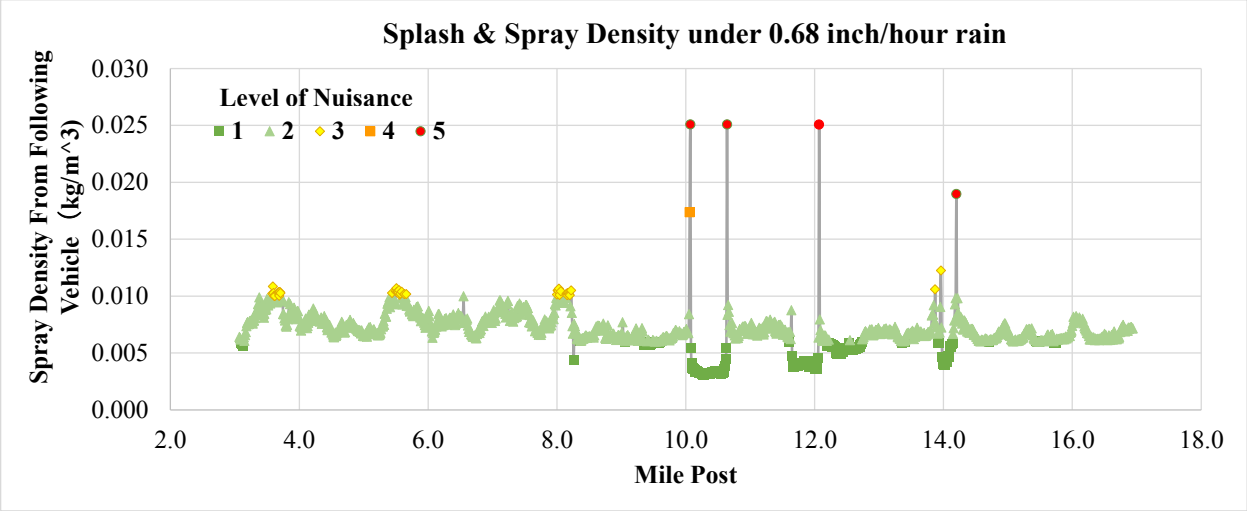

Figure 100. Graph. Splash and spray density for a 0.68-inch/h (17-mm/h) rainfall (10-hour level).

Similarly, an engineer designing a road surface can estimate the level of splash and spray that the user would experience for any time duration. For example, Figure 101 shows the level that would be exceeded, on average, for four hours each year, which correspond to a rainfall intensity of 1 in/h (25 mm/h). The engineer could also use the tool to estimate how many hours in the year the users will experience a critical splash and spray level, e.g., 1 in/h (25 mm/h).

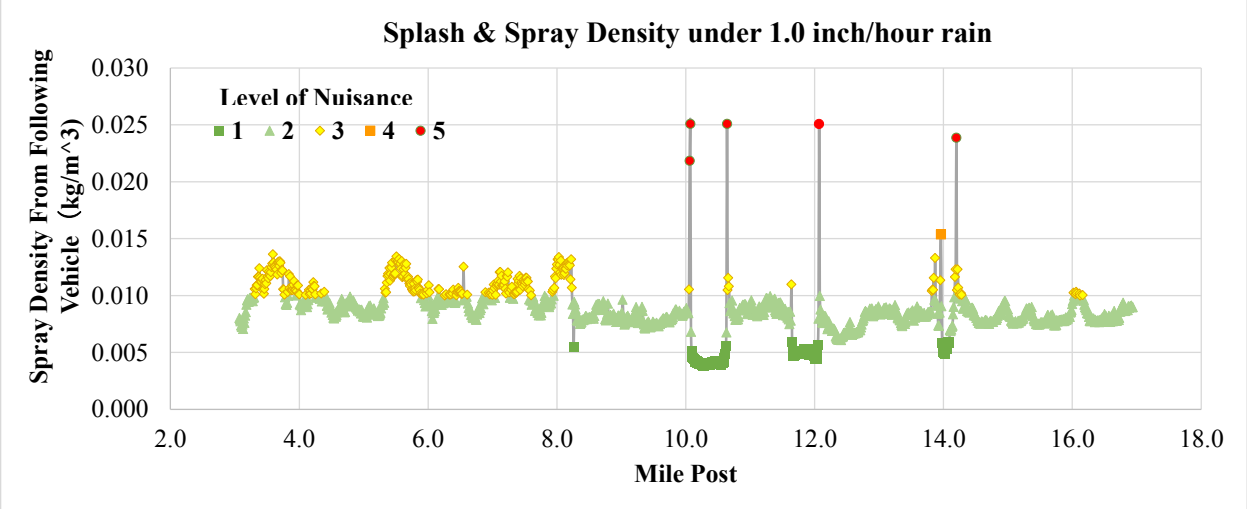

Figure 101. Graph. Splash and spray density for a 1-inch/h (25-mm/h) rain (4-hour level).

8 Findings and Conclusions

This report describes the development of an assessment tool to characterize the propensity of highway sections to generate splash and spray during rainfall and the impact of splash and spray on road users. The project started with an evaluation of prior work in the area of splash and spray mechanisms. It then followed with the development of the three sub-modules that comprise the splash and spray assessment tool:

1. A water film thickness model that predicts water film thickness on pavement surfaces based on pavement surface properties and rain intensity.
2. An exposure model for estimating the amount of water that is going to be projected by the tire given the water film thickness, pavement characteristics, and vehicle speed.
3. A splash and spray model that predicts the likelihood of splash and spray occurrence based on the other two models.

This report also proposes a new method of measuring splash and spray, by computing an *occlusion factor*. The occlusion calculation measures the loss of visibility because of the splash and spray produced, and the report links it with various user perceptions. Finally, the models were implemented in simple prototype tools and validated through field experiments and pilot implementations using existing data. These experiments showed that the developed splash and spray assessment model was practical and can be used to support highway engineers' decisions regarding highway design and maintenance.

8.1 Findings

The main findings of the research project can be summarized as follows:

- A review of available literature showed that there has been a considerable amount of research into the problem of splash and spray, but results have often been inconclusive and contradictory.
    - Considering the mechanisms of splash and spray generation, the literature showed that a number of factors affect splash and spray, including water film thickness, vehicle speed, tire geometry, tire tread depth, vehicle aerodynamics, and vehicle spray suppression devices.
    - Although there are several techniques that have been used to measure splash and spray (collection, contrast change, light attenuation, and subjective observation), none of them is widely accepted and readily available for routine pavement surface evaluations.
    - No conclusive link had been demonstrated between water film thickness and splash and spray generation, and there was little knowledge of the effect of splash and spray on motorists' safety and comfort.
- An in-depth analysis of previous water film thickness models allowed the development of a generic formula to compute the water film thickness as a function the texture of the surface, length of the drainage path, intensity of the rainfall, and slope of the drainage path.
    - Values for the constants in this generic formula were then found, using the results from the flume experiments to develop a calibrated formula for predicting the water film thickness (Equation 31).
    - This formula showed that the water film thickness is higher with lower slopes and higher macrotexture surfaces, as well as longer drainage path and rainfall intensities.
- Processing of the rainfall data available nationwide from the NCDC allowed the creation of an inventory of the expected percentage of time that the precipitation intensity will exceed various precipitation levels.

- A GIS-based spatial interpolation process was developed to estimate wet exposure for the counties that have no precipitation station available and to compute the county's average wet exposure for those in which more than one station was available.
- One limitation in the calculation process is the quality of raw data. There were many hours of recordings missing, which impacted the accuracy of the predictions. However, the inventory of wet hours does provide enough information to predict user exposure to different levels of potential splash and spray.

- Field tests, conducted under controlled precipitation conditions, assessing the impact of splash and spray on road users allowed the definition of a new measure of splash and spray: the occlusion factor. The occlusion factor was defined as the ratio of the mean luminance of the black squares to the mean luminance of the white squares on a large checkerboard placed on the splash- and spray-generating vehicle, as captured by a camera placed on the following vehicle and pointing toward the board.
  - The experiment also suggested that participants experience a greater degree of nuisance (i.e., higher ratings for obstruction, concentration, and risk and lower ratings for confidence and control) for the Following maneuver (particularly when following the dump truck) than for the Passing maneuver.
  - A statistical analysis of the collected data showed that the occlusion factor correlated well with the five subjective user perception variables studied (obstruction, concentration, risk, confidence, and control) and, thus, can be used as a measure of the nuisance produced by splash and spray.
- The four prevailing splash and spray mechanisms—bow wave, side wave, tread pickup, and capillary adhesion—for different vehicle speeds and water film thicknesses were successfully modeled using a computational fluid dynamic (CFD) model of splash and spray generation. This was done simulating in a virtual wind tunnel the most critical maneuver and vehicle combination identified in the field experiments.
  - The simulations showed that while capillary adhesion was the prevalent mechanism at low speeds, the other mechanisms became dominant as speed increased.
  - The outcomes of the various simulation runs were synthesized in a set of simple equations that model the mechanisms and combine them into a simple equation to model pavement splash and spray.
  - The equation was used to develop two simple prototype tools to illustrate the practicality and ease of implementation of the developed approach.
- Pilot applications of the model showed that the predicted values approximately follow the trends observed in the field and that the approach can be easily implemented using available pavement-surface data.

8.2 The Splash and Spray Assessment Tool

The main product of the study is a model that can be used to predict splash and spray based on pavement surface characteristics and climatic conditions. The model can provide useful information for supporting highway design and maintenance business processes. The following steps summarize the process that should be followed to calculate the splash and spray, according to the developed assessment tool:

1. Compute the water film thickness based on the rainfall intensity and pavement surface properties:

   $$WD = 6x10^{-4}\, T^{0.09}\, (LI)^{0.6}\, S^{-0.33}$$

   where:

   WD = water depth (m)

T = texture (mm)

L = drainage length (m)

I = rainfall intensity (m/h), modified for considering the drainage ability if the surface is a porous layer

S = slope (ratio)

2. Compute the maximum amount of water available for splash and spray, MR_W, based on the computed water film thickness:

$$MR_w = V \cdot b \cdot WD \cdot \gamma_W$$

3. Compute the contribution of each splash and spray mechanism, using the following equations in the order presented until the total amount of available water is exhausted. The tread pickup will be activated only if there is water remaining after the capillarity adhesion, and the bow and side waves will be activated only if there is water remaining after the capillary adhesion and tread pickup.

$$MR_{CA} = V \cdot b \cdot K \cdot h_{film} \cdot \gamma_W$$

$$MR_{TP} = V \cdot b \cdot (1 - K) \cdot h_{groove} \cdot \gamma_W$$

$$MR_{BW} = \alpha \cdot \gamma_W \cdot b \cdot V \cdot \left(WD - K \cdot h_{film} - (1 - K) \cdot h_{groove}\right)$$

$$MR_{SW} = (1 - \alpha) \cdot \gamma_W \cdot b \cdot V \cdot \left(WD - K \cdot h_{film} - (1 - K) \cdot h_{groove}\right)$$

where:

MR_i = input mass flow rate per wheel for mechanism i (kgs^{-1})

V = truck speed (m/s)

b = tire width (m)

K = factor that indicates the proportion of the tire width that is not a groove (ratio)

h_{film} = depth of the water film (m) picked up on each rotation; assumed to be 0.0001 m (0.004 inches) or the depth of water if lower

α = proportion of water (ratio) for the wave mechanisms (MR_w - MR_{CA} - MR_{TP}) that corresponds to the bow wave

h_{groove} = depth of water (m) in the tire tread; assumed to be 0.01 m (0.4 inches) or the depth of water if lower

γ_w = density of water

4. Compute the spray density corresponding to each mechanism based on the corresponding mass flow and the speed of the truck:

$$SD_{CA} = (-2.69 \cdot 10^{-5} \cdot V' + 2.43 \cdot 10^{-3}) MR_{CA}$$

$$SD_{TP} = (1.16 \cdot 10^{-5} \cdot V' - 5.25 \cdot 10^{-5}) MR_{TP}$$

$$SD_{BW} = (2.67 \cdot 10^{-5} \cdot V' - 4.71 \cdot 10^{-4}) MR_{BW}$$

$$SD_{SW} = (1.65 \cdot 10^{-5} \cdot V' - 3.99 \cdot 10^{-4}) MR_{SW}$$

where:

SD_i = total spray density for mechanism I (kgs^{-3})

V' = speed of the truck (mi/h).

5. Compute the total spray density:

$$SD_W = SD_{CA} + SD_{TP} + SD_{BW} + SD_{SW}$$

6. Convert the spray density level to a subjective nuisance index, for example, as presented in Section 7.3.

The splash and spray assessment tools can be used to support decisions about the selection of pavement surfaces for a new construction or pavement preservation and renewal projects. For example, the model developed could be used to develop practical guidance that that can be incorporated into a new section in the pavement deign guide dealing with pavement surface section. The tools can be also useful for pavement evaluation and it is recommended to explore the integration of the excel tool with the AASHTO PaveSuite technologies (AASHTO 2013). In particular, the splash and assessment tools complement the Automated Cross-Slope and Drainage Path Method developed to help pavement engineers of identify roadway areas with a high likelihood of hydroplaning and evaluate mitigation strategies.

8.3 Limitations and Areas for Improvement

The model developed provides a practical tool for assessing splash and spray potential based on pavement surface properties and expected precipitation. However, the research team has identified some potential limitations that could be addressed in future improvements of the model; these are described following.

Water Depth Model

1. Water depth model was better for asphalt surfaces than for smooth concrete and Perspex surfaces. This might suggest that the mean texture depth is not the only texture parameter that should be taken into account when calculating water depth.
2. Although the range of flow used in the flume experiments varied from 20 L/min to 140 L/min at 20 L/min increments, all these rates are relatively high especially when compared to the validation experiment performed at the Virginia Smart Road. Additional filed experiments could yield some light about the accuracy of the model for lower rates of precipitation.

Water Exposure Model

1. There were many hours of precipitation recordings missing, which may have impacted the accuracy of the predictions.

Assessment of the Impact of Splash and Spray on Road Users

1. The study was performed under controlled conditions. In general, it was shown that passing was rated as more desirable than following the vehicle. However only one vehicle (other than the subject vehicle) was on the road. Therefore, the passing maneuver is much less complicated than in real driving conditions (example when many trucks are on the road) and possible much less stressful. Furthermore, in real driving conditions users might be confronted with another vehicle while passing which increases splash and spray.
2. Users experienced both rain and splash and spray. Therefore, the study could not completely isolate the effect of splash and spray from that of rain. However, this is not a mayor limitation, since it simulates what is experienced by regular users.

Mechanism of Splash and Spray Generation

1. The mechanism modeled using CFD was only partially verified experimentally. The experiment verified that increasing speed increases splash and spray which is in accordance with the model;

however, the distribution of water droplets was not captured by the validation experiments. Additional experimentation with high-resolution high-speed cameras under controlled conditions could be used to fine tune the model.

2. The experimental sections with different textures are relatively short sections (about 100 m (300 ft)). This could be a reason why the effect of texture on splash and spray could not be experimentally verified.

8.4 Acknowledgements

The research team acknowledges the guidance and contributions at the various stages of the project of Mark Swanlund and Larry Wiser from FHWA that supervised the technical aspects of the project.

9 References

AASHTO. (2004). *A Policy on Geometric Design of Highway and Streets*, American Association of State Highway and Transportation Officials, Washington, D.C.

AASHTO. (2013). PaveSuite website, http://tig.transportation.org/Pages/PaveSuite.aspx, accessed 12-13-13.

Abdul Ghani, S., Aroussi, A., & Rice, E. (2001). Simulation of road vehicle natural environment in a climatic wind tunnel. *Simulation Practice and Theory, Volume 8, Issues 6-7*, 359-375.

Anderson, D. A., Huebner, S. R., Reed, J. R., Warner, J. C., & Henry, J. J. (1998). *Improved Surface Drainage of Pavements.* State College, Pennsylvania: The Pennsylvania Transportation Institute.

Anderson, J. A. (1995). Depth of rain water on road surfaces. *Highways and Transportation*, 45-49.

Baughan, C. J., Hedges, B., & Field, J. (1983). *A National Survey of Lorry Nuisance.* Wokingham, United Kingdom: Transport and Road Research Laboratory.

Baughan, C. J., & Hart, P. K. (1988). *Water Spray from Road Vehicles: Transmittance Analysis Method.* Wokingham, United Kingdom: Transport and Road Research Laboratory.

Baughan, C. J., & Byard, N. G. (1997). *Spray from Road Vehicles: A Test Method, and Results for a Range of Vehicle Types (Draft).* Unpublished report.

Best, A. C. (1950). The size distribution of raindrops. *Quarterly Journal of the Royal Meteorological Society*, 16-36.

Blocken, B., & Carmeliet, J. (2004). A review of wind-driven rain research in building research. *Journal of Wind Engineering and Industrial Aerodynamics*, 1079-1130.

Botes, J. A., & Fourie, F. l. (2002). *Determining the Effectiveness of Wheel Mudguards, Flaps and Valances to Reduce the Effect of Splash and Spray Generated by Heavy Vehicles when Travelling on Wet Surfaces.* Pretoria, South Africa: Technikon.

Button, J. W., Fernando, E. G., & Middleton, D. R. (2004). *Synthesis of Pavement Issues Related to High-Speed Corridors.* College Station, Texas: Texas Transportation Institute.

Chatfield, A. G., Reynolds, A. K., & Foot, D. J. (1979). *Water Spray from Heavy Goods Vehicles: An Assessment of Some Vehicle Modifications.* London: Department of Transport.

Choi, E. (1997). Numerical modelling of gust effect on wind-driven rain. *Journal of Wind Engineering and Industrial Aerodynamics*, 107-116.

Coiret, A. (2005). *Spectroscopic Evaluation of Pavement Wetting States: Influence on Tire/Road Friction.* Nantes, France: LCPC.

Consano, L., Lucarelli, D., & Lupo, F. (2007). Fuel reduction on a tractor-trailer truck at IVECO. *3rd European Automotive Conference* (pp. 45-56). Frankfurt, Germany.

Corin, R. J., He, L., & Dominy, R. G. (2008). A CFD investigation into the transient aerodynamic forces on overtaking road vehicle models. *Journal of Wind Engineering and Industrial Aerodynamics*, 1390-1411.

Daines, M. E. (1992). *Trials of Porous Asphalt on the A38 at Burton.* Wokingham, U.K.: Transport and Road Research Laboratory.

Design Manual for Roads and Bridges. (1999, February). *Volume 4 Section 2, TA 80/99, Surface Drainage of Wide Carriageways*. London, United Kingdom: The Stationery Office.

Design Manual for Roads and Bridges. (2000, November). *Volume 4 Section 2, HA 102/00 Spacing of Road Gullies*. London: The Stationery Office.

Forrest, M., Lindsay, I., Hallmark, S. L., & Humpherys, J. (2009, May). Accident data relationships. *Transportation Research Circular Number E-C134 - Influence of Roadway Surface Discontinuities on Safety*, May 2009, pp. 3-11.

Fuller, R. (2005). Towards a general theory of driver behaviour. *Accident Analysis and Prevention, 37(3)*, pp. 461-472.

Fuller, R. Towards a general theory of driver behaviour. (2005). *Accident Analysis and Prevention*, *37(3)*, pp. 461-472.

Gallaway, B. M., Schiller, R. E., & Rose, J. G. (1971). *The Effects of Rainfall Intensity, Pavement Cross Slope, Surface Texture and Drainage Length on Pavement Water Depths.* College Station, Texas: Texas Transportation Institute.

Gough, V. (1974). A tire engineer looks critically at current traction physics. In D. F. Hays, & A. L. Browne, *The Physics of Tire-Traction and Practice.* New York: Plenum Press.

Hargreaves, D. M., & Morvan, H. P. (2008). Initial validation of crosswind effects on a high-sided vehicle. *NAFEMS International Journal of CFD Case Studies*, 17-31.

Harwood, D. W., Blackburn, R. R., & Kibler, D. F. (1987). *Users' Guide for the Wettime Exposure Estimation Model. Users Guide FHWA/RD-87/106.* McLean, Virginia: Federal Highway Administration.

Harwood, D. W., Blackburn, R. T., Kulakowski, & Kibler, D. E. (1987). *Wet Weather Exposure Measures. Final Report FHWA/RD-87/105.* McLean, Virginia: Federal Highway Administration.

Harwood, D. W., R. R. Blackburn, D. F. Kibler, & Kulakowski, B. T. (1988). Estimation of wet pavement exposure from available weather records. *Transportation Research Record: Journal of the Transportation Research Board*, No. 1172. Transportation Research Board of the National Academies, National Research Council, Washington D.C., pp. 32-41.

Horne, W. B., Yager, T. J., & Ivey, D. L. (1986). Recent studies to investigate effects of tire footprint aspect ratio on dynamic hydroplaning speed. *The Tire Pavement Interface,* Edited by Pottinger, M.G. and Yager, T.J., ASTM STP 929, West Conshohocken, PA. 26-47.

Huang, J., Wang, S., & Shi, X. (2008). *Estimating the Wet-Pavement Exposure with Historical Precipitation Data in the State of California.* Washington, D.C.: Transportation Research Board.

Huebner, R. S., Anderson, D. A., Warner, J. C., & Reed, J. R. (1997). PAVDRN Computer Model for Predicting Water Film Thickness and Potential for Hydroplaning on New and Reconditioned Pavements. *Journal of the Transportation Research Board*. TRR 1599, 128-131.

Kalantari, D., & Tropea, C. (2006). Considerations in phase Doppler measurements of spray/wall interaction. *13th International Symposium on Applied Laser Techniques to Fluid Mechanics.* Lisbon, Portugal.

Knight, I., Dodd, M., Bowes, D., Donaldson, W., Smith, T., Neale, M., et al. (2005). *Integrated Safety Guards and Spray Suppression - Final Summary Report.* Wokingham, United Kingdom: TRL Limited.

Koppa, R. J., Pendleton, O., Zimmer, R. A., Pezoldt, V., & Ronald, B. (1985). *Heavy Truck Splash and Spray Testing: Phase II.* Detroit, Michigan: Motor Vehicle Manufacturers Association.

Koppa, R. J., Pezoldt, V. J., Zimmer, R. A., Deliman, M. N., & Flowers, R. (1990). *Development of a Recommended Practice for Heavy Truck Splash and Spray Evaluation.* Texas Transportation Institute, Texas A&M University.

Kulakowski, B. T., & Douglas, H. W. (1990). Effect of water-film thickness on tire pavement friction. *Surface Characteristics of Roadways: International Research and Technologies*, Edited by Meyer, W.E. and Reichert, J., West Conshohocken, PA: ASTM STP 1031. 50-60.

Manser, M. P., Koppa, R., & Moulsey, P. (2003). *Evaluation of Splash and Spray Suppression Devices on Large Trucks During Wet Weather.* Washington: AAA Foundation for Traffic Safety,

Maycock, G. (1966). *The problem of Water Thrown Up by Vehicles on Wet Roads.* Wokingham, United Kingdom: Road Research Laboratory.

McCallen, R. C., Salari, K., Ortega, J., Castellucci, P., Eastwood, C., Paschkewitz, J., et al. (2005). *Project on Heavy Vehicle Aerodynamic Drag.* Livermore, California: Lawrence Livermore National Laboratory.

Moore, D. F. (1970). The Measurement of Surface Texture and Drainage Capacity of Pavements. *International Colloquium on the Interrelation of Skidding Resistance and Traffic Safety on Wet Roads*. Berlin, Germany.

Moore, D. (1975). *The Friction of Pneumatic Tires.* Amsterdam: Elsevier Scientific Publishing Company.

National Highway Traffic Safety Administration. (2000). *Update on the Status of Splash and Spray Suppression Technology for Large Trucks - Report to Congress.* Washington, D.C.: U.S. Department of Transportation.

Ong, G. P., & Fwa, T. F. (2007). Prediction of wet-pavement skid resistance and hydroplaning potential. *Journal of the Transportation Research Board*, TRR 2005, 160-171.

Parry, A. R. (1999). *Macrotexture and Road Safety: Final Report.* Crowthorne, United Kingdom: Transport Research Laboratory.

Paschekewithz, J. S. (2006). *Simulation of Spray Dispersion in a Simplified Heavy Vehicle Wake*. Livermore, California: Lawrence Livermore National Laboratory.

Pérez-Jiménez, F., Martínez, A. Sánchez-Domínguez, F., & Ramos-García, J. A., (2011), "System for Measuring Splash on Wet Pavements," *Journal of the Transportation Research Board*, TRR 2227, 171-179.

Pilkington, G. B. (1990). *Splash and Spray.* Philadelphia: American Society for Testing and Materials.

Pilkington, G. B. (1990). Splash and Spray. *Surface Characteristics of Roadways: International Research and Technologies*, Edited by Meyer, W.E. and Reichert, J., West Conshohocken, PA: ASTM STP 1031. 528-541.

Pruyost, M., & Gothie, M. (1998). *Influence of Water Thickness on Friction Available.* Nantes, France: LCPC.

Qiu, L., & Nixon, W. A. (2008). Effects of adverse weather on traffic crashes: Systematic review and meta-analysis. *Transportation Research Record: Journal of the Transportation Research Board*, No. 2055. Transportation Research Board of the National Academies, National Research Council, Washington, D.C., pp. 139-146.

Resendez, Y. A., Sandberg, U., Rasmussen, R. O., & Garber, S. (2007). *Characterizing the Splash and Spray Potential of Pavements.* Austin, Texas: The Transtec Group, Inc.

Ritter, T. E. (1974). *The Development of Techniques to Measure Vehicle Spray on Wet Roads.* Chicago, Illinois: Society of Automotive Engineers.

Roe, P. G., Hewitt, A. P., Parry, A. R., May, R. W., & Cheetham, R. J. (1997). *Water Depths on Wide Carriageways - A Laboratory Study.* Crowthorne, United Kingdom: Transport Research Foundation.

Ross, N. F., & Russam, K. (1968). *The Depth of Rain Water on Road Surfaces.* Wokingham, United Kingdom: Road Research Laboratory.

Salles, C., & Poesen, J. (1999). Performance of an optical spectro pluviometer in measuring basic rain erosivity characteristics. *Journal of Hydrology, 218(3-4)*, pp. 142-156.

Sanders, P. D., Dunford A., Viner, H., Flintsch, G. W., & Larson, R. (2009). *Splash–Spray Assessment Tool Development Program (DTFH61-08-R-00029), First Interim Report: Revised Synthesis Report Submitted to FHWA.* Crowthorne, United Kingdom: Transport Research Laboratory.

Smith, R. (2008). *Analyzing Friction in the Design of Rubber Products and Their Paired Surfaces.* London: CRC Press.

Sterling, M., Quinn, A. D., Hargreaves, D. M., Sabbioni, E., & Tomasini, G. (2010). A comparison of different methods to evaluate the wind induced forces on a high sided lorry. *Journal of Wind Engineering & Industrial Aerodynamics, 98*, pp. 10-20.

Unrau, D., & Andrey, J. (2006). Driver response to rainfall on urban expressways. *Transportation Research Record: Journal of the Transportation Research Board*, No. 1980. Transportation Research Board of the National Academies, National Research Council, Washington D.C., pp. 24-30.

Veneziano, D., Wang, S., & Shi, X. (2009). Precipitation variation and identification of high-risk wet accident locations in California. *Journal of the Transportation Research Board*, TRR 2107. Transportation Research Board of the National Academies, National Research Council, Washington, D.C., pp. 123-133.

Wang, S., Veneziano, D., Huang, J., & Shi, X. (2008). *Estimating Wet Pavement Exposure with Precipitation Data: Final Report*. Sacramento, California: California Department of Transportation.

Weir, D. H., Strange, J. F., & Heffley, R. K. (1978). *Reduction of Adverse Aerodynamic Effects of Large Trucks - FHWA-RD-79-84.* Washington, D.C.: FHWA.

Yager, T., Gallaway, B., Ivey, D., & Mounce, J. (2009). Water accumulations. *Transportation Research Circular Number E-C134 - Influence of Roadway Surface Discontinuities on Safety*, Washington, District of Columbia: Transportation Research Board. 51-60.